

Experimental Study of Sea Salt Particles (SSP) Filtration Performance for On-Board SOFCs

by

Pengfei Zhao

A dissertation submitted to the Graduate Faculty of
Auburn University
in partial fulfillment of the
requirements for the Degree of
Doctor of Philosophy

Auburn, Alabama
May 07, 2016

Keywords: sea salt particles (SSP), SOFCs, filtration efficiency, pressure drop, particles loading capacity, woven and wet-laid nonwoven, relative humidity (RH), nanofiber entrapped media

Copyright 2016 by Pengfei Zhao

Approved by

Bruce J. Tatarchuk, Chair, Professor of Chemical Engineering
W. Robert Ashurst, Associate Professor of Chemical Engineering
Allan E. David, Assistant Professor of Chemical Engineering
Bart Prorok, Professor of Materials Engineering

Abstract

This work described in the dissertation mainly focuses on the filtration of sea salt particles (SSP), which flow into the cathode side of Solid Oxide Fuel Cells (SOFCs) on the ships. Currently, SOFCs are being considered as power source for ships due to their high energy efficiency and low waste emissions. However, different types of air contaminants existed in the air could cause harmful effects on the performance of those SOFCs and decrease their useful life time. The impurities contain gaseous contaminants, such as sulfur compounds and particulates, like sea salt particles and smokes. Salt particles are all over around the sea because of the wake and bow spray. They could lead to corrosions and fouling of fuel cell systems and clog the finely divided and highly tortuous flow channels in fuel cell stacks as well. Therefore, it is significantly important to remove them from air stream before entering SOFCs. Usually, filtration is the most commonly applied approach due to the high efficiency and low cost.

As for filtration system design, there are mainly two aspects. One is filter packaging configuration design and the other one is filter media design. Filter media is the most basic component of filter which does the filtration work. Depending on the type of filter media and how the filters are packaged, filter system could be designed to show different filtration performances for sea salt particles and meanwhile, an optimization could be achieved according to different air conditions and specifications.

Chapter I mainly describes the background, history and motivation of sea salt particles filtration. Three important filtration parameters are introduced briefly, including pressure drop, filtration efficiency and particles loading capacity. These three parameters are highly significant

during filter design that needs to be considered as main criteria. Moreover, in Chapter I, filter media manufacturing is described, which contains two main different processes, dry formed and wet laid process. In my work, all filter media tested are made using wet laid method due to its convenience and low cost.

Sea salt particles filtration using pleated filters in novel packaging configurations is described in Chapter II. Commercial filters (24'' by 24'') are tested for all the experiments. For single filter, the effects of filter depth and filter pleat count on three filtration parameters mentioned in Chapter I are discussed, including pressure drop across the filter, particles removal efficiency and loading capacity and compressor parasitic power. Meanwhile, MESA, which stands for Multi-Element Structured Array, is introduced and tested for salt particles filtration. MESA is a novel filter packaging configuration invented by Center of Microfibrous Materials Manufacturing (CM³), Auburn University, which integrates several single filters in one single filtration system to become a three dimensional array of filters and could extend the filtration area and reduce the pressure drop. The experiment results of MESAs are compared with single filters under same air conditions and conclude that MESAs are able to increase both particles removal efficiency and loading capacity and lower filter pressure drop and compressor parasitic power simultaneously, which results in much better filtration performance for salt particles.

In Chapter III, filter media is the major concern. Comparison of filtration performance for sea salt particles between nonwoven and woven activated carbon fiber media is described in this chapter. Activated carbon fiber is applied in this part of work because it can remove particulates and gas contaminants, such as VOCs simultaneously, which can lower filtration costs. Woven and nonwoven media are currently two most widely applied types of filter media. Due to their different structures, they can show different filtration performances for salt particles.

And to evaluate the advantages and disadvantages of each type of media is of high significance when the media are applied in real circumstances. Therefore, experiments of pressure drop, filtration efficiency and particles loading capacity are conducted for both nonwoven and woven filter media. The results have shown that nonwoven ACF media are much better for salt particles filtration due to the homogeneous structure. Moreover, since relative humidity (RH) during the sea environment is much higher, it is very necessary to investigate the effect of RH on filter media performance for salt particles. Activated carbon fiber belongs to hydrophilic material, which can absorb water into fiber pores. Experiment results show that higher RH is able to enhance filtration efficiency due to the improved capillary tension between particles and fiber surface.

Besides experimental study, theoretical study is also of highly importance during filtration system design. Since what we conclude from Chapter III is that nonwoven filter media is superior compared to woven filter media when applied in salt particles filtration, Chapter IV mainly describes theoretical analysis of various nonwoven microfibrinous filter media, including pressure drop across the filter media, filtration efficiency and particles loading capacity. Several different filter media are tested using bench scale setup and the experiment results are compared with estimation results in order to verify if the estimation equations are correct. Further modified PMP (Porous media permeability) and filtration efficiency equations according to various filter media type are used for pressure drop and particles removal efficiency estimation separately. Moreover, a new estimation approach for particles loading capacity is developed and verified with experiment results. From comparisons, what we can see is that estimation results match quite well with experiment results.

Chapter V mainly describes sea salt particles filtration of various nonwoven filter media. A new type of nonwoven filter media, VGCF (carbon nanofiber) entrapped nonwoven polymer media is evaluated in terms of the filtration performance, including pressure drop, filtration efficiency, particles loading capacity and compressor parasitic power. This media is manufactured using wet-laid approach, which could lead to uniform three dimensional nanofiber nonwoven filter media with high filtration efficiency and low pressure drop. Besides, particles loading performance is compared between different types of nonwoven filter media, including surface media and depth media. The results show that surface media is better for initial filtration application and depth filter media is more suitable for long term particles filtration and loading. In the end, effect of relative humidity on hydrophobic filter media is discussed and what can be concluded is higher RH is able to lower filtration efficiency due to the occupation of interstitial fiber space by water droplets.

Acknowledgements

I would like to express his sincere gratitude to Dr. Bruce J. Tatarchuk for his guidance and support throughout the course of this research. His tremendous experience and knowledge have been the cornerstones of my both technical and non-technical learning. I have learned a lot from Dr. Tatarchuk, not only in research skills, but also in how to be a successful person in the future. I would also like to express my sincere appreciation to Office of Naval research (ONR) for funding this research presented in this dissertation. I would also like to thank Dr. Mario Eden and Dr. Christopher Roberts for all his efforts in enhancing our department and making it a better place for students.

I would like to acknowledge my committee members, Dr. W. Robert Ashurst, Dr. Allan E. David and Dr. Bart Prorok for their guidance and support during my study. I am very thankful to Dr. Abhijeet Phalle for his help in schoolwork when I just joined the group and Dr. Yanli (Joyce) Chen for her assistance with laboratory work when I started my research. My appreciation goes to Dr. Michael Miller from Chemistry Department for his help with Scanning Electron Microscopy (SEM). I am also thankful to Mr. Brian Schwieker (chemical engineering shop) and Mr. Matt Montgomery (Auburn glass shop, Chemistry Department) for helping me in building my experimental setup. Special thanks are for all of my past and present Center for Microfibrous Materials Manufacturing (CM³) colleagues. In particular, I would like acknowledge the members of the filtration group for their helpful discussions and ideas.

I would also like to thank the following members of the staff in our department for their help during my research: Dr. Donald Cahela, Dr. Hongyun Yang, Dr. Wenhua Zhu, Dr. Amogh Karwa, Achintya Sujana, Mr. Dwight Cahela, Ms. Kimberly Dennis, Ms. Sue Ellen Abner, Ms. Karen Cochran, and Ms. Elaine Jimmerson. I am thankful to the Graduate School and the Office of International Programs at Auburn University for their efforts to ensure the well-being of international students.

I would like to thank all my friends in Auburn for making my study and stay exciting and meaningful. Also, I would like to express my gratitude to all my family members for their love and support during my study in Auburn. This dissertation would not have been possible without the unwarranted love and support of my parents.

Table of Contents

Abstract.....	ii
Acknowledgements.....	vi
List of Figures.....	xiv
List of Tables.....	xix
Chapter I Introduction and background.....	1
I.1 Introduction to air filtration for on-board SOFCs.....	1
I.2 Background.....	1
I.3 Use of filtration.....	3
I.4 History of particulate filtration.....	4
I.5 Fibrous filter design.....	4
I.5.1 Filtration efficiency.....	5
I.5.2 Pressure drop across filter.....	10
I.5.3 Particles loading capacity.....	11
I.5.4 Two main aspects of filter design.....	13
I.6 Filter media manufacturing.....	15
I.6.1 Dry formed processes.....	16
I.7 Laser airborne particle spectrometer (LAS-XII).....	19

I.7.1	Introduction	19
I.7.2	Theory of operations.....	20
I.8	Large particle generator (TSI 8108).....	23
I.9	Characterization techniques	25
I.9.1	Scanning Electron Microscopy (SEM)	25
I.9.2	Capillary flow porometry.....	26
I.9.3	Mercury intrusion porosimetry.....	26
I.9.4	Surface area measurement	27
I.10	Research goal.....	28
I.11	References	29
Chapter II	Sea salt particles filtration for SOFCs using pleated filters in novel packaging configurations	31
II.1	Abstract	31
II.2	Introduction.....	32
II.2	Theoretical study.....	34
II.2.1	Filter efficiency.....	34
II.2.2	Pressure drop.....	35
II.2.3	Loading of salt particles.....	36
II.3	Experimental.....	37
II.4	Results and discussion.....	40
II.4.1	Pressure drop of single filters	40

II.4.2	Filtration efficiency of single filters.....	41
II.4.3	Quality factor of single filters	44
II.4.4	Comparison of single filters in different depths	46
II.4.5	Pressure drop of MESAs	48
II.4.6	Filtration efficiency of MESAs	49
II.4.7	Quality factors of MESAs	50
II.4.8	Results and discussion of loading of salt particles.....	51
II.4.9	Comparison of compressor parasitic power of different filters	57
II.5	Conclusion	61
II.6	References	63
Chapter III Comparison of filtration performance for sea salt particles between nonwoven and woven activated carbon fiber media..... 66		
III.1	Abstract.....	66
III.2	Introduction	67
III.3	Experimental	68
III.3.1	Materials.....	68
III.3.2	Nonwoven activated carbon fiber media preparation (Wet-laid method)	68
III.3.3	Structures of ACF filter media	70
III.3.4	Filtration efficiency and pressure drop testing setup.....	71
III.4	Results and discussion	75
III.4.1	Filtration efficiency of ACF filter media	75

III.4.2	Pressure drop across ACF filter media.....	81
III.4.3	Quality factor of nonwoven and woven ACF filter media	86
III.4.4	Loading of salt particles using nonwoven and woven ACF media	88
III.4.5	Comparison of compressor parasitic power between nonwoven and woven ACF media.....	94
III.4.6	Effect of relative humidity (RH) on ACF media filtration for salt particles	97
III.5	Conclusion.....	100
III.6	References.....	102
Chapter IV	Theoretical study of various nonwoven microfibrinous filter media: Pressure drop, filtration efficiency and particles loading capacity.....	106
IV.1	Introduction.....	106
IV.2	Experimental.....	106
IV.2.1	Materials.....	106
IV.2.2	Nonwoven media preparation	107
IV.2.3	Experimental setup	108
IV.3	Results and discussions	110
IV.3.1	Pressure drop analysis (laminar flow region).....	110
IV.3.2	Pressure drop analysis (turbulent flow region)	113
IV.3.3	Filtration efficiency analysis	115
IV.3.4	Particles loading analysis.....	118
IV.4	Conclusion.....	121

IV.5 References	123
Chapter V Study of sea salt particles (SSP) filtration using various nonwoven filter media.....	126
V.1 Introduction	126
V.2 Experimental	127
V.2.1 Materials	127
V.2.2 Nonwoven media preparation (wet-laid method).....	127
V.2.3 Experimental setup.....	129
V.3 Discussions and results	131
V.3.1 VGCF enhanced microfibrrous filter media.....	131
V.3.2 Carbon nanotube (CNT) enhanced nonwoven filter media	136
V.3.3 Particles loading performance of various nonwoven filter media	142
V.3.4 Comparison of compressor parasitic power among various nonwoven filter media	147
V.3.5 Effect of relative humidity (RH) on hydrophobic filter media performance for salt particles	150
V.4 Conclusion	154
V.5 References:	157
Chapter VI Conclusions and Recommendations for Future Work	161
VI.1 Conclusions	161
VI.2 Recommendations for Future work.....	162
VI.2.1 Carbon nanofiber synthesized within woven ACF filter media via CCVD method	163
VI.2.2 VGCF entrapped nonwoven ACF filter media via ultra-sonication	164

VI.2.3 CFD (Computational fluid dynamics) modeling of filtration performance of pleated filters	165
Appendix : Nomenclature	166

List of Figures

Figure I-1 Example of SOFC system and a ship in the ocean with large wake and bow spray	2
Figure I-2 Typical particle size distribution of corrosion and fouling range	3
Figure I-3 Inertial impaction, diffusion and interception mechanisms of particles capture	6
Figure I-4 Typical filtration curve for varying particle sizes.....	8
Figure I-5 Most penetrating particle size (MPPS) at different face velocities	9
Figure I-6 Effect of electrostatic charge on filtration efficiency	10
Figure I-7 Typical profile of pressure drop across filter.....	11
Figure I-8 Schematic of particles loading by filter media	12
Figure I-9 Typical particles loading curve of filter.....	13
Figure I-10 Typical single pleated filter and V-shape pleated filter	14
Figure I-11 Typical “U” pleating curve for optimum pressure drop	14
Figure I-12 Microfibrous media (polymer, metal and ceramic)	15
Figure I-13 Schematic of meltblown process	17
Figure I-14 Typical diagram of an inclined wire wet lay process	19
Figure I-15 LAS-X II Spectrometer.....	20
Figure I-16 Block diagram of optical spectrometer	21
Figure I-17 LAS-X II spectrometer optical block.....	22
Figure I-18 Picture (A) and schematic (B) of TSI 8108 Large Particle Generator.....	24
Figure II-1 Different configurations of MESA units: (A) V-shaped MESA, (B) W-shaped MESA, (C) VW-shaped MESA	33

Figure II-2 Experimental setup (Upstream and downstream duct) for filtration performance study of salt particles, including pressure drop, filtration efficiency and particles loading capacity testing	39
Figure II-3 Size distribution of NaCl particles generated by TSI 8108	40
Figure II-4 Pressure drop across different pleat counts filters with respect to face velocity: (A) 2 inch deep pleated filter, (B) 1 inch deep pleated filter	41
Figure II-5 Comparison of upstream and downstream counting probes.....	42
Figure II-6 Salt particles filtration efficiency with respect to particle diameter at different filtration velocities for (A) 2 inch deep pleated filter, (B) 1 inch deep pleated filter	43
Figure II-7 Salt particles filtration efficiency with respect to particle diameter for different pleat counts filters: (A) 2 inch deep pleated filter, (B) 1 inch deep pleated filter (550 fpm)	44
Figure II-8 Quality factor (cal.) with respect to particle diameter for different pleat counts filters: (A) 2 inch deep pleated filter, (B) 1 inch deep pleated filter (550 fpm).....	46
Figure II-9 Comparisons of filtration performance for salt particles between filters of different depths (2 inch deep and 1 inch deep): (A) pressure drop with respect to face velocity, (B) filtration efficiency with respect to particle diameter and (C) quality factor (cal.) with respect to particle diameter.....	47
Figure II-10 Pressure drop across single filter and MESAs (V-shaped and W-shaped) with respect to face velocity.....	48
Figure II-11 Pressure drop across V-shape MESA in different pleat counts filters with respect to face velocity	49
Figure II-12 Salt particles filtration efficiency with respect to particle diameter for single filter and MESAs (V-shaped and W-shaped) at (A) 550 fpm, (B) 350 fpm	50
Figure II-13 Quality factor (cal.) with respect to particle diameter for single filter and MESAs (V-shaped and W-shaped) at (A) 550 fpm, (B) 350 fpm.....	51
Figure II-14 Nominal pressure drop increase with respect to deposited mass of salt particles for single filter at different filtration velocities	52
Figure II-15 Evolution of $\Delta P/U$ during loading of salt particles at different filtration velocities	52
Figure II-16 Nominal pressure drop increase with respect to deposited mass of salt particles for single filters with different pleat counts: (A) 2 inch deep pleated filter, (B) 1 inch deep pleated filter	53

Figure II-17 Nominal pressure drop increase with respect to deposited mass of salt particles for single filters of different depths	55
Figure II-18 Nominal pressure drop increase with respect to deposited mass of salt particles for single filter and MESAs (V-shaped and W-shaped): (A) 2 inch deep pleated filter, (B) 1 inch deep pleated filter.....	56
Figure II-19 SOFC energy balance showing the flow of air and power through the system	58
Figure II-20 Compressor parasitic power of single filters in different depths (A) and in different pleats (B).....	60
Figure II-21 Comparison of compressor parasitic power between single filter and MESAs (A) 2 inch depth, (B) 1 inch depth.....	61
Figure III-1 Wet-laid activated carbon fiber (ACF) media manufacturing	69
Figure III-2 SEM images of two nonwoven and two woven ACF filter media	71
Figure III-3 Pictures of nonwoven and woven ACF filter media	71
Figure III-4 Experimental setup for filtration performance testing	73
Figure III-5 Size distribution of salt particles generated	74
Figure III-6 Comparison of particle count upstream and downstream	75
Figure III-7 Effect of filtration velocity on salt particles filtration efficiency.....	76
Figure III-8 Salt particles filtration efficiency with respect to particle diameter for 1 layer nonwoven and woven ACF filter media (Data reported for face velocity of 50 cm/s)	77
Figure III-9 Salt particles filtration efficiency with respect to particle diameter for 1 layer nonwoven ACF filter media and woven ACF filter media in different layers (Data reported for face velocity of 50 cm/s)	79
Figure III-10 Filtration efficiency of activated carbon particles entrapped nonwoven filter media	80
Figure III-11 Pressure drop with respect to face velocity for three nonwoven ACF filter media in different components.....	84
Figure III-12 Pressure drop with respect to face velocity for 1 layer nonwoven ACF filter media and 3 layers woven ACF filter media.....	85

Figure III-13 Quality factor (cal.) with respect to particle diameter for 1 layer nonwoven ACF filter media and 3 layers woven ACF filter media (Data reported for face velocity of 50 cm/s).....	87
Figure III-14 Comparison of nominal increase of pressure drop with respect to deposited mass of salt particles per media area between experimental data and calculation result (Data reported for nonwoven ACF-IV filter media at face velocity of 50 cm/s)...	90
Figure III-15 Nominal increase of pressure drop with respect to deposited mass of salt particles for nonwoven and woven ACF filter media (Data reported for face velocity of 50 cm/s).....	91
Figure III-16 Evolution of salt particles filtration efficiency with respect to particle diameter of (A) Nonwoven ACF-I filter media and (B) 3 layers ACF knit filter media (Data reported for face velocity of 50 cm/s)	92
Figure III-17 Quality factor (cal.) with respect to deposited mass of salt particles for nonwoven and woven ACF filter media (Data reported for face velocity of 50 cm/s).....	93
Figure III-18 Comparison of compressor parasitic power between nonwoven and woven ACF media	96
Figure III-19 Filtration efficiency with respect to particle diameter at various relative humidities (RHs) for: (A) Nonwoven ACF-V filter media, (B) Nonwoven ACF-I filter media (Data reported for face velocity of 50 cm/s)	98
Figure III-20 Filtration efficiency with respect to particle diameter after pretreatment in humid environment for: (A) Nonwoven ACF-V filter media, (B) Nonwoven ACF-I filter media	100
Figure IV-1 Experimental setup for filtration efficiency, particles loading capacity and pressure drop test.....	110
Figure IV-2 Modified PMP model fitting results at low face velocity	113
Figure IV-3 Modified PMP model fitting results at high face velocity	115
Figure IV-4 Filtration efficiency model fitting results of different composite media	118
Figure IV-5 Particles loading estimation process	120
Figure IV-6 Comparison of nominal increase of pressure drop with respect to deposited mass of salt particles per media area between experimental data and calculation result (Data reported at face velocity of 50 cm/s).....	121

Figure V-1 Experimental setup for filtration efficiency, particles loading capacity and pressure drop test	130
Figure V-2 (A) Filtration efficiency curves of VGCF nonwoven media at different compositions, (B) Filtration efficiency of 400 nm particle using different VGCF composition media	132
Figure V-3 Pressure drop curves of VGCF nonwoven media in different composition	133
Figure V-4 SEM images of VGCF entrapped polymer media in different VGCF fractions	134
Figure V-5 Comparison of quality factor of different VGCF nonwoven media	135
Figure V-6 Filtration efficiency curves of CNT filters at different face velocities: A) 10 cm/s and B) 50 cm/s	138
Figure V-7 Comparison results of filtration efficiency and quality factors for different coverage CNT filter media	139
Figure V-8 Comparison results of filtration efficiency and quality factors for different layers of NT-I filter media	140
Figure V-9 Nominal increase of pressure drop with respect to deposited mass of salt particles for five various nonwoven filter media (Data reported for face velocity of 50 cm/s) ..	144
Figure V-10 Quality factor (cal.) with respect to deposited mass of salt particles for five various nonwoven filter media (Data reported for face velocity of 50 cm/s).....	145
Figure V-11 Comparison of compressor parasitic power among various nonwoven filter media (nano and micro scale).....	149
Figure V-12 Filtration efficiency curves of Ni-Media 1 (A), Ni-Media 2 (B) at different relative humidities (RHs).....	151
Figure V-13 Filtration efficiency of 200 nm particle of two tested nickle media at various RHs	152
Figure V-14 (A) Filtration efficiency curves of polymer media at various RHs, (B) Filtration efficiency curves of polymer media after RH pretreatment	153
Figure V-15 Filtration efficiency degradation under different RHs and pretreatments.....	154

List of Tables

Table I-1 Common contaminants and their appropriate rated filter	3
Table II-1 Comparison of average quality factor (cal.) between single filter and MESAs (V-shaped and W-shaped) at different filtration velocities.....	51
Table II-2 Comparisons of particles loading capacity and filter life time between single filter and MESAs (V-shaped and W-shaped): (A) 2 inch deep pleated filter, (B) 1 inch deep pleated filter.....	57
Table II-3 Compressor parasitic power estimation conditions	59
Table III-1 Thickness, SVF of different fibers and total voidage of nonwoven ACF filter media	69
Table III-2 MPPS and minimum efficiency at different face velocities.....	77
Table III-3 Details of three activated carbon particles entrapped nonwoven filter media.....	80
Table III-4 Pressure drop of activated carbon particles entrapped nonwoven filter media	81
Table III-5 Calculated shape factor for ACF and polyester fiber	83
Table III-6 Thickness and pressure drop per media thickness of 1 layer nonwoven ACF filter media and woven ACF filter media in different layers (Data reported for face velocity of 50 cm/s).....	86
Table III-7 Comparison of average quality factor between different nonwoven and woven ACF filter media (Data reported for face velocity of 50 cm/s).....	88
Table III-8 Comparisons of particles loading capacity and filter media life time between nonwoven and woven ACF filter media	93
Table III-9 Compressor parasitic power estimation conditions	95
Table IV-1 Details of different fiber materials	106
Table IV-2 Shape factors of different fibers	111
Table IV-3 Constant A for low face velocity PMP model of various composite media	112

Table IV-4 Composition and thickness of five different composite media tested.....	112
Table IV-5 RMS error of five PMP model fitting curves	113
Table IV-6 Constant B for high face velocity PMP model of different composite media tested	114
Table IV-7 Composition and thickness of four different composite media tested	115
Table IV-8 Coefficients A and B of five different composite media	117
Table IV-9 Calculated RMS errors of various filter media	121
Table V-1 Details of different fiber materials.....	127
Table V-2 Thickness, VGCF and polymer volume fraction of fibers of four different media tested.....	132
Table V-3 Pressure drop at 50 cm/s of four different VGCF nonwoven media	133
Table V-4 Permeability of media at different VGCF fractions	134
Table V-5 Average quality factor of four different VGCF nonwoven media	136
Table V-6 Weight and coverage of carbon nanotubes used for different CNT filter media	138
Table V-7 Experimental results of different CNT coverage filter media	138
Table V-8 Experimental results of different layers of NT-I filter media.....	140
Table V-9 Comparison of cost of VGCF and CNT needed for commercial filter	141
Table V-10 Details of five various nonwoven filter media	143
Table V-11 Comparisons of particles loading capacity and filter media life time among various nonwoven filter media	147
Table V-12 Compressor parasitic power estimation conditions.....	148
Table V-13 Characteristics of two sample media tested.....	150
Table V-14 Details of polymer sample media tested.....	152

Chapter I Introduction and background

I.1 Introduction to air filtration for on-board SOFCs

Air purification is very important and essential to provide clean air and to protect equipment and numerous industrial processes. There are mainly two different types of air contaminants existed, one is gas impurities, such as volatile organic compounds (VOCs), NO, NO₂ and SO₂. The other one is particulate and aerosol, like soot, smoke, dust, sea salt and bacteria, etc [I.1]. Poor air quality could cause severe personal discomforts, including nausea, fatigue, irritation of skin and eyes and degradation of equipment performance as well, such as gas turbines and fuel cells [I.2]. Recently, solid oxide fuel cells (SOFCs) have been considering to be applied as power source on the ships due to the high energy efficiency and low harmful emissions and wastes. However, during the ocean environment, air is not 100% pure. Several contaminants exist in the air, during which sea salt particle is the most deleterious that could lead to severe damage to SOFCs systems and shorten fuel cell life time. These sea salt particles are mainly from two sources. One is naturally from wind stresses over whitecaps and the other one is from wake or the bow spray by ship itself. They could clog the finely divided and highly tortuous flow channels in the fuel cells and also cause corrosion to the fuel cell systems, which is able to significantly degrade the performances of SOFCs [I.3]. Figure I-1 shows an example of SOFC system and a ship in the ocean with large wake and bow spray [I.3].



Figure 0-1 Example of SOFC system and a ship in the ocean with large wake and bow spray

I.2 Background

The operation of fuel cell and gas turbine, by its basic design, need to ingest a large amount of air, which results in large quantities of air particulates. For example, 1 ppm of particles in the ambient air equals to around 12.7 lbs of those particles entering a fuel cell without filtration process per day. Besides, the more advanced of the equipment design, the more sensitive it is to the quality of the air ingested. Filtration could be applied to the inlet air to protect against the adverse effects of air particulates [I.2]. Different types of air impurities from the world-wide environments could cause several types of problems that negatively affect the availability, reliability and operation time of the equipment [I.4]. There are two main purposes of inlet air filtration: one is to clean the air to meet the operational goals of the equipment; the other one is to maintain higher filtration efficiency. If the inlet air filtration doesn't reach the goal, several damages will occur to the machine, such as corrosion and clogging of the system. Figure I-2 illustrates typical particle size distribution for erosion and fouling range [I.2].

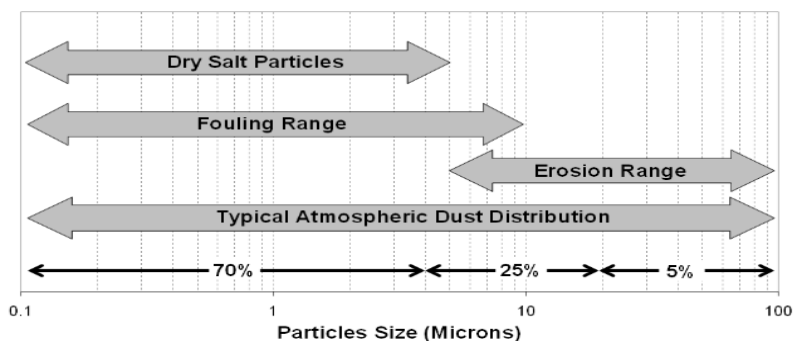


Figure 0-2 Typical particle size distribution of corrosion and fouling range

I.3 Use of filtration

Inlet air filtration has both advantage and disadvantage simultaneously. The negative effect is that a pressure loss could be generated no matter what is placed in the air flow path into the equipment, which could reduce the performance of the equipment and cause more energy cost (parasitic power loss). However, inlet air filtration will protect against the air contaminants to sustain the equipment’s performance above an acceptable level. Therefore, inlet air filtration becomes a trade-off [I.5]. However, filtration is still very necessary. The challenge is to keep pressure loss to a minimum while removing a satisfactory amount of particulates. Inlet air filtration system is designed to filter most of the contaminants existed in the air with less pressure drop. Table I-1 lists some common contaminants and their typical size and the rated filters (based on standard ASHRAE 52.2 1992) [I.6], which can remove these impurities.

Table 0-1 Common contaminants and their appropriate rated filter

Grade	ASHRAE Filter Class	EN Filter Class	Particles Separated
	MERV		
Coarse > 10 micron	1	G1	Leaves, insects, textile fibers, sand, flying ash, mist, rain
	2	G2	
	3	G2	
	4	G2	
	5	G3	Pollen, fog, spray
	6	G3	
	7	G4	
	8	G4	
	9	G4	
Fine > 1 micron	10	F5	Spore, cement dust, dust sedimentation
	11	F6	Clouds, fog
	12	F6	Accumulated carbon black
	13	F7	Metal oxide smoke, oil smoke
	14	F8	Metal oxide smoke, carbon black, smog, mist, fumes
	15	F9	
EPA and HEPA > 0.01 micron	16	E10	Oil smoke in the initial stages, aerosol micro particles, radioactive aerosol
	16	E11	
	16	E12	
	17	H13	Aerosol micro particles
	18	H13	
	19	H14	
ULPA Micro particles		U15	Aerosol micro particles
		U16	
		U17	

Note: Correlations between ASHRAE and EN standards classifications and particle size are approximate.

I.4 History of particulate filtration

History of dust and aerosol filtration is already over 2000 years old. The earliest records of air filtration could date from Roman times, mentioned by Pliny the Elder (ca a.d. 50) and Julius Pollux (ca a.d. 150). Leonardo da Vinci (1452-1519) has mentioned wet cloths as a protection from fumes used in warfare. Agricola also described the problem of dust in mines in his book. And Stockhausen published his *Libellus de Lythargyrill Fumio Noxto Morbifico* (1656) dealing with protection from rock dust one hundred years later. In 1814, Brise Faden invented a respirator, which was a box filled with cotton which had a breathing tube entering in the mouth. During 19th century, medical respirators appeared when Louis Pasteur demonstrated that putrefaction was due to airborne organisms. Early filtration equipment and their further improvement were very well described by Feldhaus (1929) at the beginning of the 20th century [I.7.I.8].

During 20th century, filtration had a huge development, when another field for the application of respirators and gas masks was found. In World War I, gaseous and aerodisperse toxic chemicals were used, which caused a combination of gas and aerosol filter to be discovered. Albrecht, 1931 and Kaufman, 1936 from Germany solved this problem by using fibrous pads. After this, several various types of filters were found, including pore filters and electric filters. Since 1970s, modern period of particle filtration began and the further developments were very positively influenced by the facilities of modern computer techniques. Pich, 1987 and Brown, 1993 described development up until 1986 by two excellent and modern monographs [I.7, I.8].

I.5 Fibrous filter design

In industries, based on different structures, four main types of filters for particulates are existed, including fibrous filter, granular filter, sintered metal filter and pore/membrane filter.

Among all of them, fibrous filter is the most widely used in air filtration due to its low cost and ease of manufacturing on large scale. In addition, this type of filter has very high air permeability which can lower the pressure drop across the filter and consequently implies less loss of energy. Usually, >95% particles removal efficiency is required in industries for particles smaller than 1 μm , fibrous filter is the only choice [I.1].

During fibrous filter design, there are usually three main parameters that need to be considered and optimized, filtration efficiency, pressure drop across the filter and particles loading capacity. According to different air conditions, filters in various parameters are required.

I.5.1 Filtration efficiency

Filtration efficiency is one of the most important parameters, which primarily depends on the type of filter media used. It also varies with the particle size and air conditions, like flow rate and relative humidity (RH) through the media. Usually, clean filter removal efficiency E is closely related to the single fiber collection efficiency E_{Σ} according to an equation obtained by a mass balance on a filter element of thickness dt and integrated on the total filter thickness t [I.7,I.10].

$$E = 1 - \exp\left(\frac{-4\alpha E_{\Sigma} t}{\pi R}\right) \quad (\text{Eq I.1})$$

Filtration process is composed of diffusion, interception, inertial impaction, electrostatic deposition, gravitational settling and sieving. Usually, diffusion, inertial impaction and interception account for the majority of the particles removal, which are shown in Figure I-3 [I.2] and therefore, the total single fiber efficiency E_{Σ} is defined as [I.7, I.11]:

$$E_{\Sigma} = 1 - (1 - E_D)(1 - E_R)(1 - E_I) \quad (\text{Eq I.2})$$

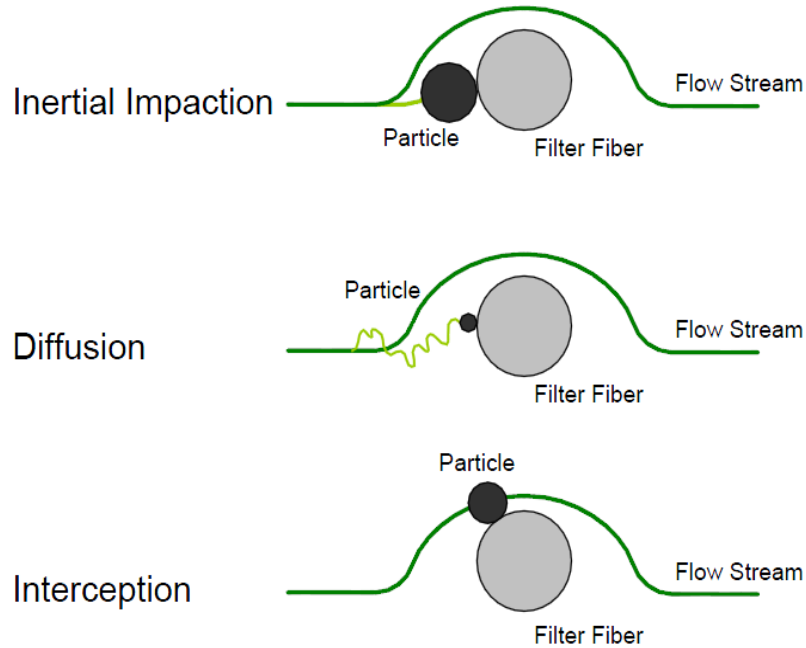


Figure 0-3 Inertial impaction, diffusion and interception mechanisms of particles capture

Inertial impaction is usually applied to particles larger than 0.5 micron and used to describe particulate capture by means of physical contact with the filtration fiber due to deviations from the main streamlines [I.1, I.2]. The streamlines will diverge when the air stream approaches a filter fiber. Since large particles have significant momentum, they may not make this direction change and therefore, the particles' inertia causes them to deviate from the main streamline and trapped to the fiber [I.2]. This type of filtration mechanism is more dominant in high velocity filtration systems, which means the filtration efficiency will increase with larger particle size and higher face velocities [I.7, I.9].

$$E_I = 0.0334Stk^{3/2} \quad (\text{Eq I.3})$$

Interception occurs with medium sized particles (0.4-0.6) that are not large enough to leave the main streamline due to inertia or not small enough to diffuse. The particles will follow the flow path where they will touch a fiber in the filter and be trapped. The efficiency is

primarily dependent on the packing density of the fibers and diameter of fibers and it is the only filtration mechanism that is not relevant with face velocity [I.7, I.9].

$$E_R = 0.6 \frac{1 - \alpha}{Ku} \frac{R^2}{1 + R} \quad (\text{Eq I.4})$$

Diffusion is usually effective only for very small particles less than 0.3 or 0.4 micron within lower flow rates. As the particles randomly move through the filter due to Brownian motion, there is a probability that they will touch a fiber and be trapped. The path the particle takes depends on its interaction with nearby particles and gas molecules, like air. The probability of this kind of capture increases with increasing packing density of fibers, decreased diameter of fiber, and increased resident time within the fiber mesh. Increased resident time can be achieved by lowering the air flow rate [I.2, I.9].

$$E_D = 2.9Ku^{-1/3}Pe^{-2/3} + 0.62Pe^{-1} \quad (\text{Eq I.5})$$

The dimensionless numbers in the above equations are defined as follows:

Peclet number $Pe = Ud_f / D$

Stokes number $Stk = \frac{\rho_p d_p^2 U}{18 \mu d_f}$

Kuwabara number $Ku = -\ln \alpha / 2 - 0.75 + \alpha - 0.25\alpha^2$

Knudsen number $Kn_f = 2\lambda / d_f$

U stands for face velocity of air stream here, D is the coefficient of Brownian diffusion, λ is the gas mean free path, α denotes as the packing fraction, d_p and d_f are the aerosol particle and fiber diameter, respectively.

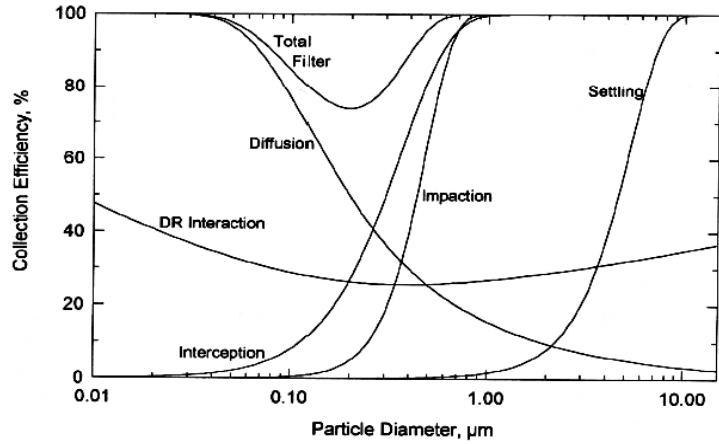


Figure 0-4 Typical filtration curve for varying particle sizes

In addition, as is shown in Figure I-4 above [I.11], which is also the typical filtration curve, we can see that the dominant filtration mechanism is related to the aerosol particle size. From the figure, very small particles are captured by diffusion mechanism because of their Brownian motion and large particles are trapped by inertial impaction because of their high momentum. It also shows the various mechanisms and their impact on filtration efficiency varying with particle size. There exists a range of 0.04 to 0.4 micron, where no mechanism is strong enough to remove the particles. In this range, there is a minimum efficiency of particle capture, which is called most penetrating particle size (MPPS). In particular, MPPS changed with fiber diameter, face velocity and packing fractions. Figure I-5 describes the most penetrating particle size at different face velocities: (1) $U=0.001$ m/s; (2) $U=0.01$ m/s; (3) $U=0.025$ m/s. From the figure, we can see that MPPS decreased when face velocity was improved [I.9].

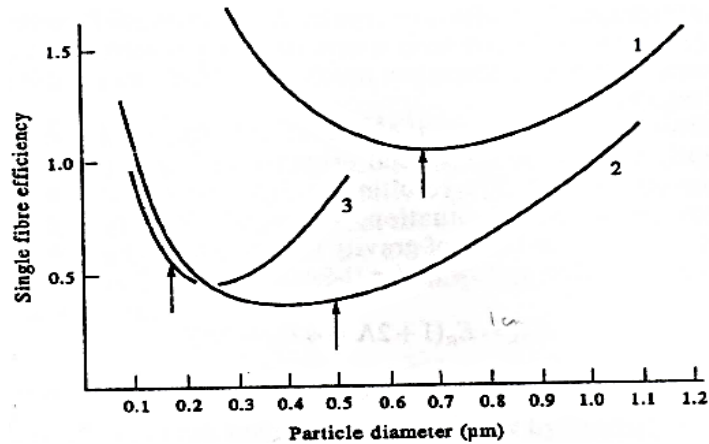


Figure 0-5 Most penetrating particle size (MPPS) at different face velocities

Besides the most important three mechanisms mentioned above, electrostatic settling is another one which is very common in filtration. The electrostatic deposition mechanism is based on the charge of the filter fiber and the particles. A charged fiber can attract both charged and uncharged particles. For an uncharged particle, due to the image effect of charge, an electric field could be induced by the charged fiber and it can charge the particle with an opposite charge, which attracts the particle towards the fiber. Therefore, electrostatic settling mechanism is able to enhance the filtration efficiency without increasing the pressure drop. But it has disadvantages as well. Over a period of time, the efficiency of the filter will decrease due to the loss of charge caused by neutralization and also, large scale manufacturing of filter with consistent charge is a big problem. Due to these reasons, electrostatic filters are not a very popular category of filters. Figure I-6 has shown the effect of electrostatic charge on filtration efficiency, both particle charge and filter fiber charge. In the figure, CTAB (cetrimonium bromide) is a cationic surfactant which has cationic functional group at their head and after CTAB treatment, filter media could have positive charge.

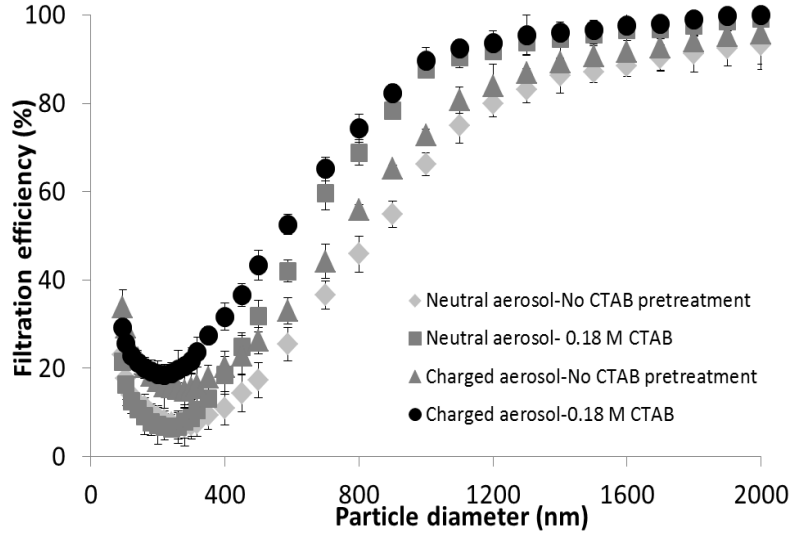


Figure 0-6 Effect of electrostatic charge on filtration efficiency

From Figure I-6, what can be seen is that for same type of filter media, filtration efficiency for charged particles are significantly higher compared to that for neutral particles. Besides, for same type of particle, filter fiber after CTAB treatment is able to increase filtration efficiency due to the image effect of electrostatic charge on the fibers, which can attract much more particles. However, in this dissertation, electrostatic settling mechanism is not concerned as the main filtration mechanism since sea salt particles are usually uncharged. Thus, three “mechanical” filtration mechanisms, diffusion, interception and inertial impaction have been investigated in this work.

I.5.2 Pressure drop across filter

Pressure drop across the filter, is directly to the energy consumption as it is indicative of the work done by the blower to push air through the filter [I.12]. Usually, it is proportional to the filtration efficiency, which means filter with higher filtration efficiency has higher pressure drop as well. Therefore, in order to have best filter performance, an optimization needs to be achieved during filter design. Typically, pressure drop varies with the face velocity of air, which is shown in Figure I-7. At low face velocities, pressure drop is linear with face velocity and when velocity

goes higher, quadratic dependence of pressure drop may be seen due to the compression of filter media, as shown below.

$$\Delta P = AV_M + BV_M^2 \quad (\text{Eq I.6})$$

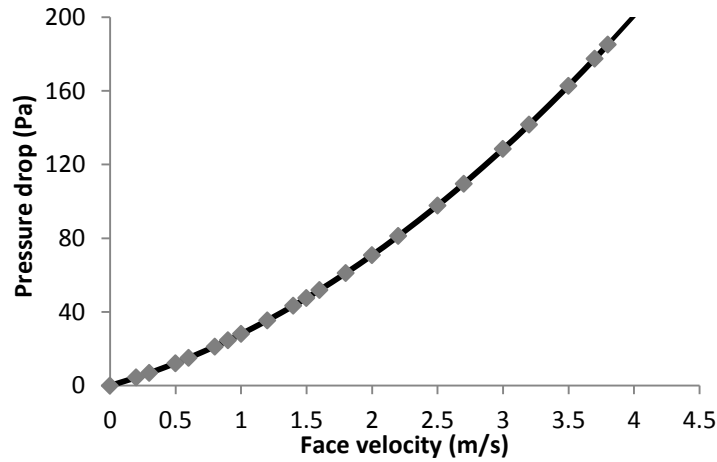


Figure 0-7 Typical profile of pressure drop across filter

I.5.3 Particles loading capacity

As particles deposited into the filter, filter performance will change gradually, including both filtration efficiency and pressure drop across the filter [I.14]. Particles loading capacity is defined as the quantity of contaminant a filter can trap and hold before the maximum allowable back pressure drop is reached, which is shown in Figure I-8. And it is strongly related to filter life time, which is very important in filter design [I.13]. Usually, particles loading could cause an increase in pressure drop across the filter. When the pressure drop gets to a certain limit, the filter needs to be replaced by a clean one in order to lower the energy consumption. Typically, for a commercial 24”by 24” pleated filter, when the pressure drop reaches 1 inch water (249 Pa), it is considered to be useless and needs to be replaced. Therefore, particles loading capacity is calculated as the total amount of particles that are entrapped when filter pressure drop reaches 1 inch water.

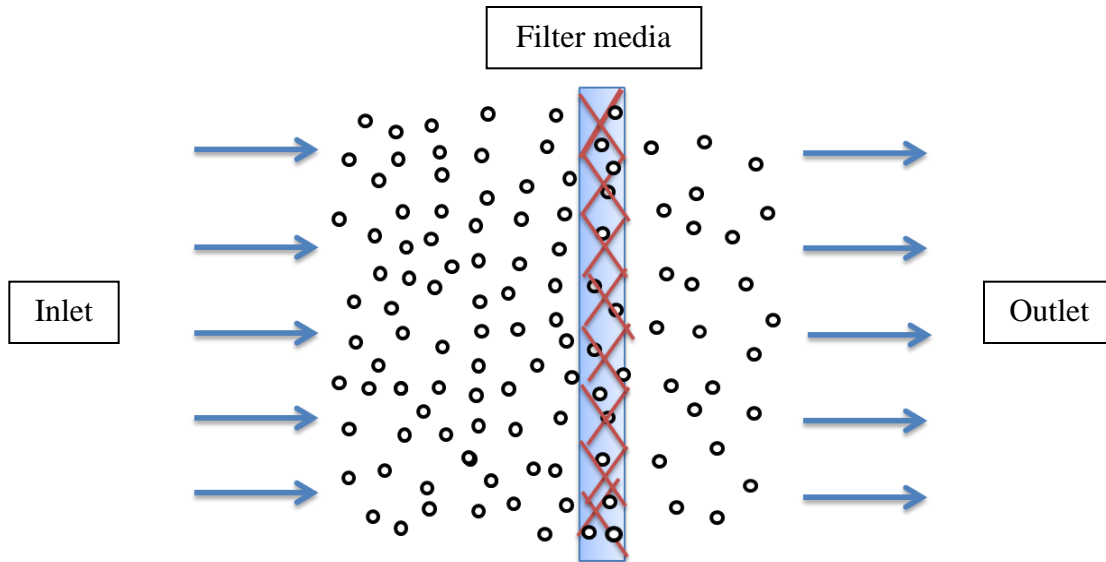


Figure 0-8 Schematic of particles loading by filter media

Usually, particles loading curve is applied to demonstrate this phenomenon, which is nominal increase of pressure drop across the filter vs mass of particles deposited into the filter. The curve is mainly composed of two different parts, one is depth loading and the other one is surface loading. Initially when filter is clean, particles are captured into the depth of media with very small increase of pressure drop. Then with particles deposited into the media gradually, there is no space for particles capture in the depth of media. Thus, particles have to be deposited on the surface of media and a significant increase of pressure drop occurs. The slow initial rise in pressure drop is caused by the depth loading, where the entire filter is not clogged by the particles. The sudden increase in pressure drop is due to clogging and cake formation on the filter which results in higher pressure drop than depth loading. The cake formed on the surface of filter acts as a surface filter, which can also be used as a layer of filter. Typical particles loading curve is shown in Figure I-9.

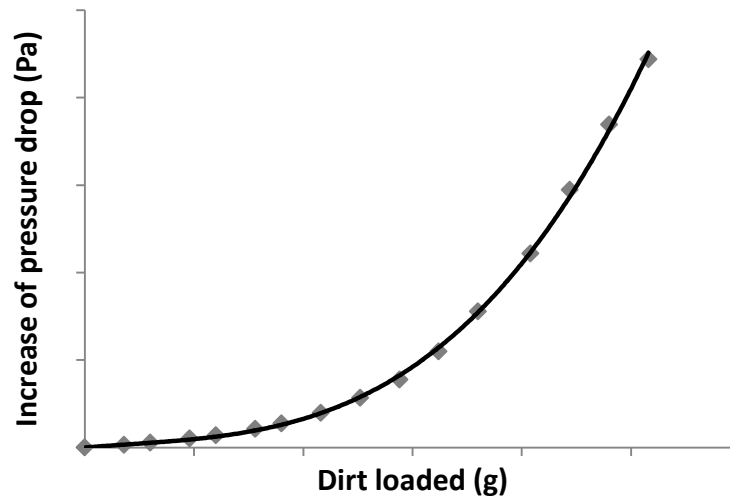


Figure 0-9 Typical particles loading curve of filter

I.5.4 Two main aspects of filter design

Pressure drop, filtration efficiency and particles loading capacity are all dependent on two main filter designing aspects, one is filter media and the other is filter configuration. As for filter pleat and configuration design, filter pleat count, filter packaging configuration and filter depth are the most important factors that could affect filtration performance. Figure I-10 shows the typical single pleated filter and V-shape pleated filter [I.1]. Filter with pleats and in different packaging configurations could increase the filtration media area, which leads to lower filtration velocity through the filter media. Filtration velocity could have effect on both pressure drop across the filter and particles removal efficiency. In terms of pressure drop, lower filtration velocity is able to decrease the filter pressure drop, but correspondingly, friction caused by more pleats and packaging will be increased [I.1]. Due to the exchange of media-influenced flow resistance loss for pleat-influenced flow resistance loss, an optimum pleat number exists that leads to lowest overall pressure drop across the filter, which is shown in Figure I-11[I.5].

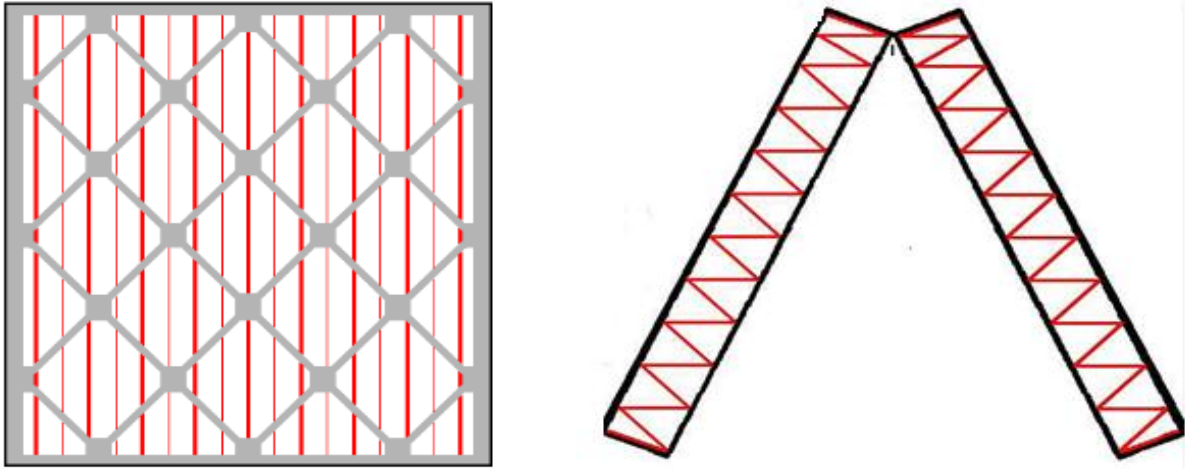


Figure 0-10 Typical single pleated filter and V-shape pleated filter

For particles removal efficiency and loading behavior, they are also dependent on filtration velocity. Particles in different sizes could have various filtration results at different filtration velocities, according to which filtration mechanism regime it's in.

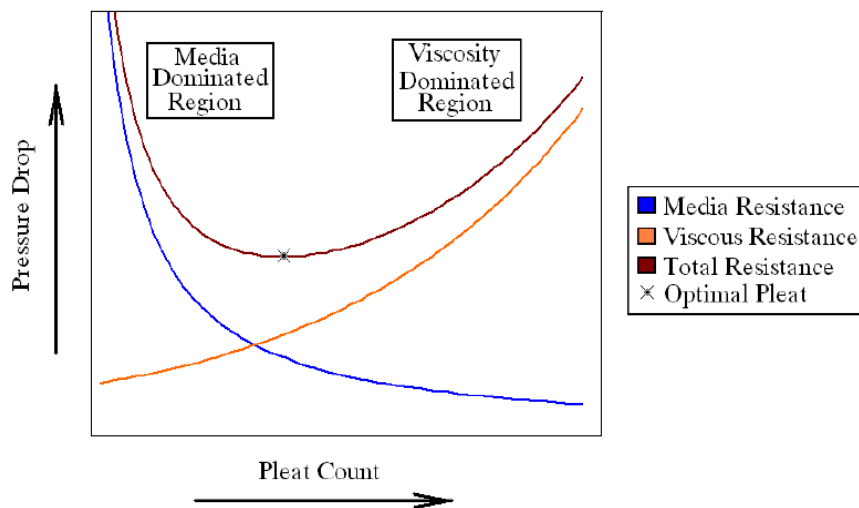


Figure 0-11 Typical “U” pleating curve for optimum pressure drop

As for filter media design, several important parameters need to be considered, including material type, solid volume fraction (SVF), media thickness and fiber diameter. Different parameters could lead to various filtration performances, including pressure drop, filtration efficiency and particles loading capacity. Therefore, in order to achieve best media filtration

performance, different media parameters should be optimized properly. In this work, microfibrinous media (MFM) was applied as the main filter media. Microfibrinous media was developed in 1987 by Department of Chemical Engineering in Auburn University and the Space Power Institute. This kind of media is a sinter-locked network of micron diameter fibers made out of polymer, metal, ceramic or composite with diameters typically ranging between two and twenty microns through a traditional wet-laid paper manufacturing process [I.15-I.18]. Figure I-12 shows a picture of polymer, metal and ceramic media in rolls.



Figure 0-12 Microfibrinous media (polymer, metal and ceramic)

Different type of MFM could be applied in various situations, depending on the air conditions, such as temperature, air flow rate, particles type, relative humidity (RH) and particle size. Therefore, filter media design is to optimize all the parameters with air conditions in order to find a best solution for particles removal.

I.6 Filter media manufacturing

There are mainly two different types of filter media, one is nonwoven and the other one is woven filter media. Woven media consist of two categories - knit and weave, which are both manufactured via knitting or weaving machines. For nonwoven filter media, two major process groups for forming nonwovens exist - dry formed and wet-laid. The simple difference between

the two groups is that they are formed in different mediums. Dry formed media are manufactured in an air medium and wet laid use water as forming medium.

I.6.1 Dry formed processes

Dry formed consist of five major processes: air laid, dry laid, spunbonded, meltblown and electrospun [I.19].

1). Air laid

Air laid structure filter media is mainly formed from cellulose fluff pulp by hammer milled into individualized fibers. Then, the fibers are air conveyed to a moving belt or forming wire to be formed into a fabric. Although air laid media are bulky structures that would like to be likely candidates for filtration media, it has a small filtration market area compared to other types of media.

2). Dry laid

Dry laid forming is the process for forming many of carded webs and felt materials applied in filtration. Dry laid webs are different from air laid media because of raw materials and the way they are handled by process. Longer staple fibers, such as crimped fibers, are the main fiber source for dry laid structures. Similar to air laid forming, aerodynamics action is utilized to form webs, however, a large amount of mechanical processing is applied to individualize, disperse and orient the fibers as well.

3). Spunbonded

This process involves the extrusion of molten polymer to a die block. The die block consists of a polymer flow control assembly and a spinnerette, which is a block of metal having several thousand drilled holes. Then, filament fibers are formed through the spinnerette and cooled by air stream and entangled by a distributing chamber. Finally, the entangled fibers are

deposited onto a moving belt to form a bonded web. Usually, polymer fibers are used in the spunbonded process, such as polyester, nylon, polyethylene and polypropylene.

4). Meltblown

Meltblown filter media are directly formed from a molten resin. They are similar to spunbonded webs forming process. The difference is that high velocity heated air is utilized to attenuate filaments to very fine diameters [I.19]. The attenuated filaments are generally 1-4 μm in diameter and form a very uniform web. The fine fiber structures of meltblown webs make them ideal candidates for high efficiency filter media used in air filtration. Figure I-13 is a diagram of typical meltblown process [I.19].

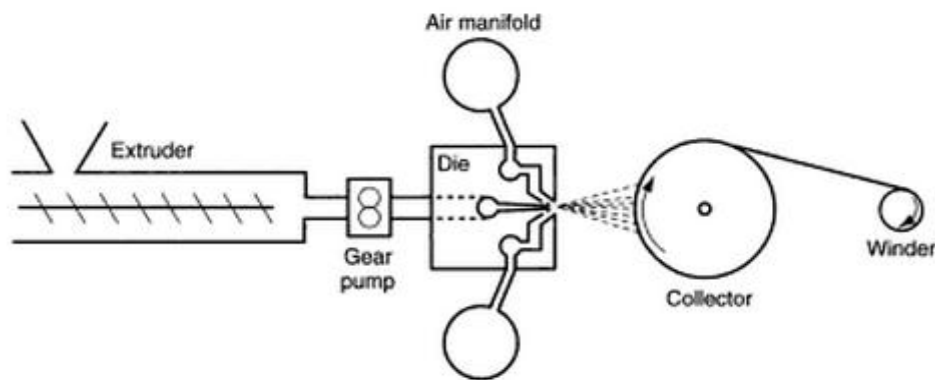


Figure 0-13 Schematic of meltblown process

5). Electrospun process

This process can produce nanofiber webs by applying a high voltage charge to a polymer solution and using the charge to draw the fibers from the tip of a capillary to a grounded collector. The webs are of very fine thickness with limited mechanical properties and the diameter of the fibers is in the range of 0.25 to 1 μm . Currently, these electrospun nanofiber webs are mainly applied in air filtration market.

I.6.2 Wet laid process

This process is essentially a paper machine process, which undergoes the following four basic steps, which is in Figure I-14.

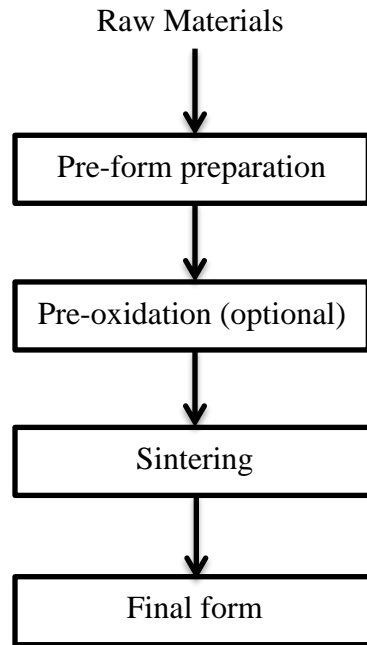


Figure 0-14 Process flow diagram of wet-laid method

A considerable amount of nonwoven media is produced by this method. Usually, wood pulp and natural fibers are applied as fiber source for wet laid. In addition, fibers of polyester, nylon, rayon, glass and any other material that can be reasonable dispersed in water can be used as well. Figure I-15 is a diagram of the wet end of a typical wet laid process system [I.19]. The wet end is a process to disperse fiber into aqueous slurry, which is called stock and feed it into the headbox. The headbox is an equipment to feed the stock to a forming screen where a wet sheet is formed. After the wet sheet is finished, mechanical and thermal devices remove the water and the dry the sheet to the final form. As for the bonding of wet laid media, a bonding agent is usually added to the fiber slurry before the formation process. What agent should be added depends on the fiber material used and mechanical property requested.

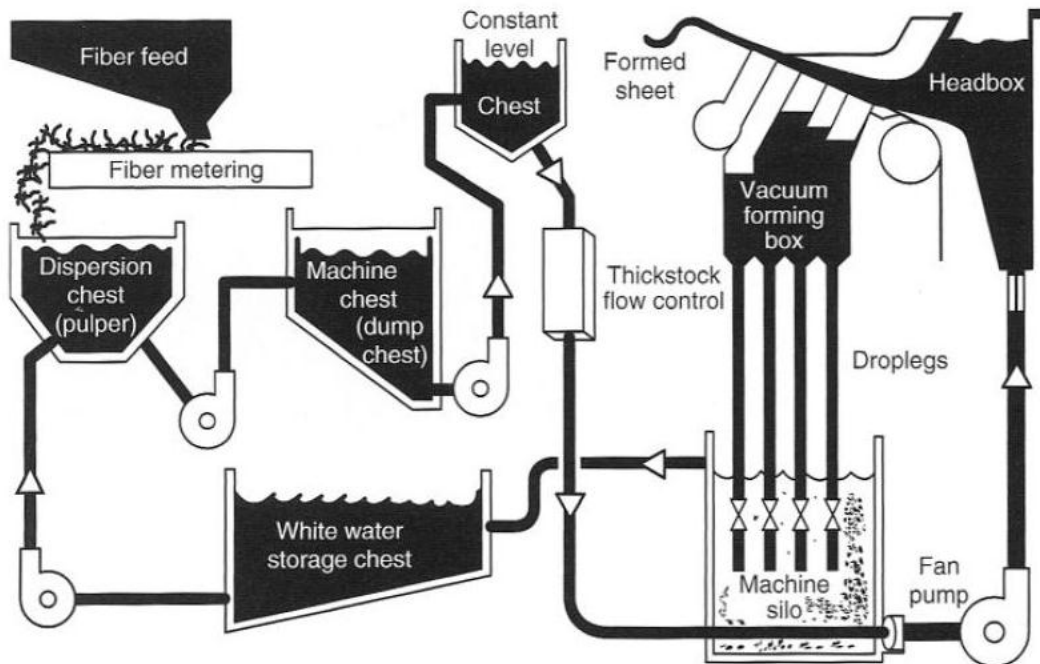


Figure 0-15 Typical diagram of an inclined wire wet lay process

I.7 Laser airborne particle spectrometer (LAS-XII)

I.7.1 Introduction

In this whole work, LAS-X II (shown in Figure I-16) will be applied to measure filtration efficiency for salt particles. It is high sensitivity spectrometer designed for sampling and counting extremely small airborne particles. The spectrometer components have been built into a computer that uses the Windows XP operating system. And Virtual Instrument (VI) software (based on LABVIEW 7.1) is used in the computer to provide control, data display and data logging. There are mainly 6 components in LAS-X II, including 10-inch color LCD flat panel display, USB keyboard with touchpad, 30 GB hard disk, 3.5-inch floppy and CD drives, USB data transfer port and serial port and 10/100 Ethernet interface [I.20].

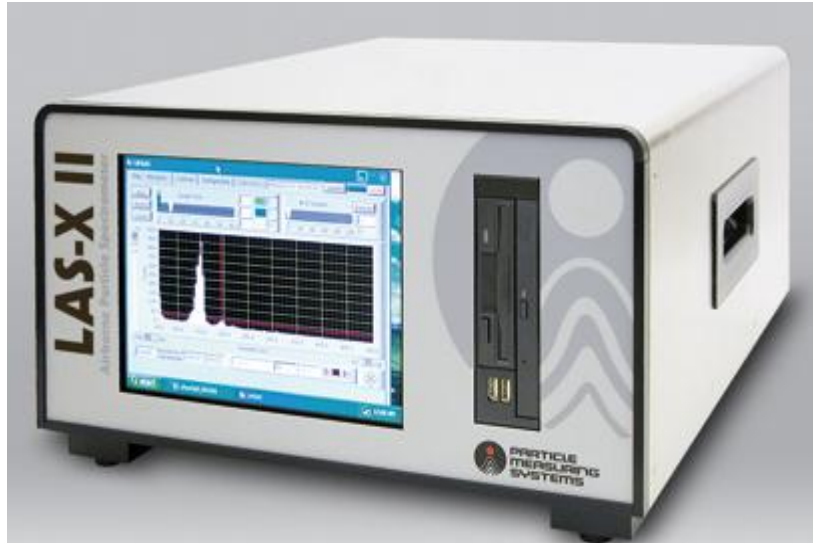


Figure 0-16 LAS-X II Spectrometer

LAS-X II spectrometer uses Helium-Neon (He-Ne) as laser source, which can measure particles from 0.09-7.5 μm up to 100 particle sizing channels. Air flow rate into the spectrometer can be anywhere from 10-100 sccm. One of the advantages is that it is able to sample in extremely dirty environments, such as locations with up to 500,000,000 particles per cubic foot when sampling at 10 sccm. Moreover, it has ability to immediately print high-quality reports from computer and analyze the data while it is still in the computer, using the internal Excel software.

I.7.2 Theory of operations

LAS-X II spectrometer consists of the following general subsystems, flow system, optical system, analog electronics system, digital electronics system and onboard computer, which can be seen in Figure I-17 [I.20].

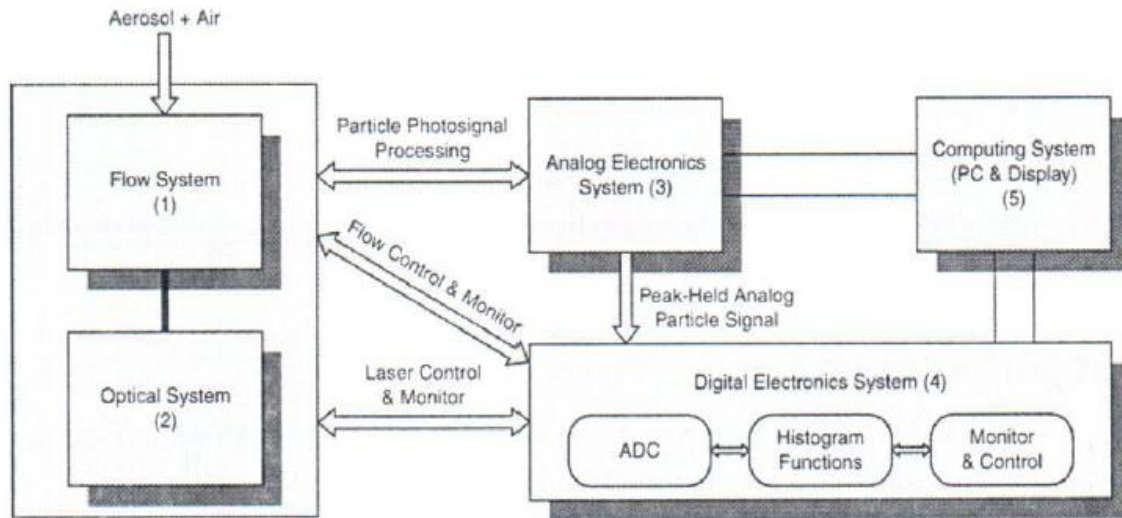


Figure 0-17 Block diagram of optical spectrometer

1). Flow system

Flow system carries the sample through the optical interaction region, including flow control and measurement. Sample flows are between 1 and 100 sccm and the sheath flow is typically 600-800 sccm. Particles are confined to a region of space whose extent is smaller than the laser beam diameter, which gives the instrument exceptional particle-sizing resolution.

2). Main optical system

Optical system generates the laser light, detects the light scattered by the particles, and provides a mechanical enclosure for the optical system and the delivery of the sample aerosol. It also consists of several components, including detection system, laser and optics, and optical block. Among all of those, laser is the most important component, which is shown in Figure I-18. The laser in LAS-X II uses Helium Neon as light source and consists of two separate but integral parts. The first is the laser tube itself. It is a sealed tube to hold in the Helium Neon gas mixture, with a high reflector on one end and a window on the other end. As for the second part, it is an optical block, a sealed mechanical enclosure that holds the second high reflector, which could create a laser cavity through which the sample is flowed. The laser is randomly polarized.

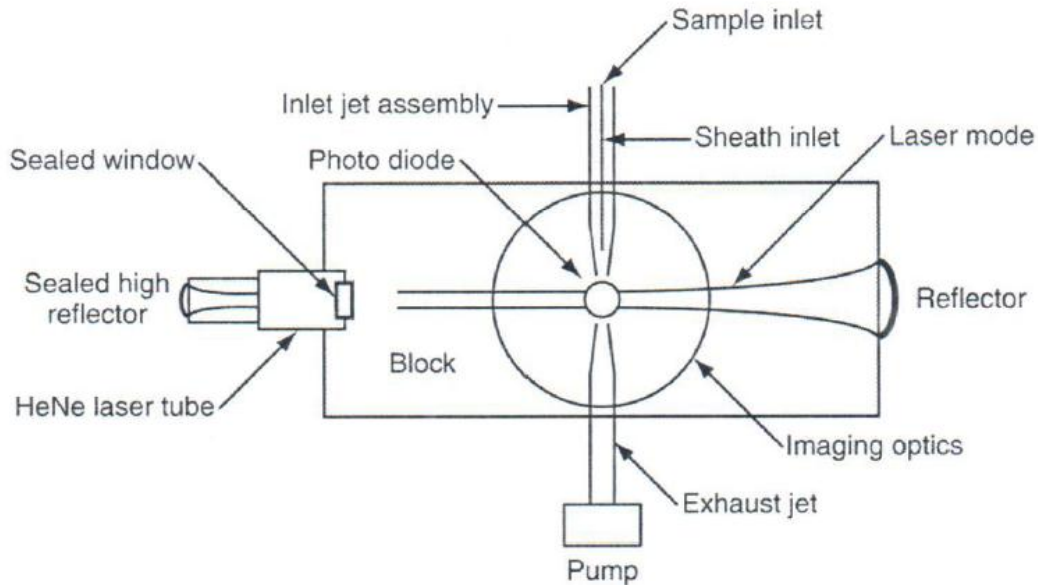


Figure 0-18 LAS-X II spectrometer optical block

3). Analog electronics system

Analog electronics system amplifies and processes the particle signals. The analog chain converts the photocurrent of the detector photodiodes to a voltage and processes that signal, which is called the particle signal. This function is performed for both the primary and secondary detection systems.

4). Digital electronics system

Digital electronics system analyzes particle signals, bin signals according to user-specified bin mappings, generates a histogram of the number of particles in each specified bin, and communicates with the computer and system monitor/control functions.

5). Onboard computer

The onboard computer provides the instrument's user interface. It is a single board computer running the Windows XP operating system. The computer has at least 256 MB of physical memory and a 30 GB hard drive. The monitor is a standard 10.4 inch LCD display built into the instrument's front panel. The user interface is a virtual instrument written in LabView

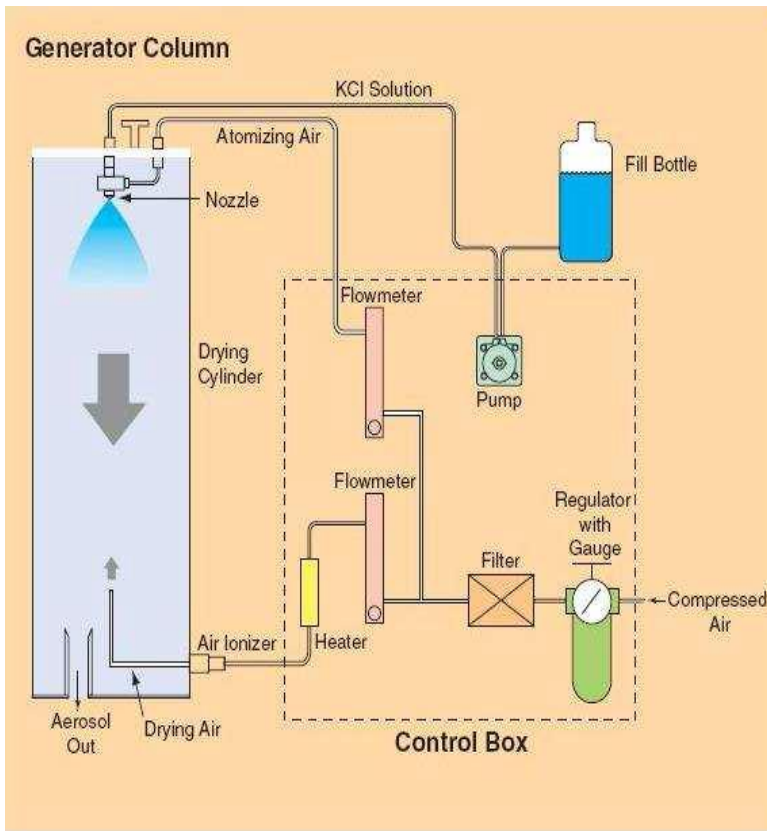
running as a stand-alone executable. Communication with the digital electronics system is via internal serial.

I.8 Large particle generator (TSI 8108)

This large particle generator will be applied in this study for full scale experiments to generate salt particles. It is built to output a polydispersed challenge of salt particles, such NaCl and KCl particles in the range of 0.1 to 10 μm . The particles were generated by pumping salt solution into a spray nozzle where it is mixed with atomizing air. The flow rates of particles and atomizing air stream can be adjusted and controlled. The atomized salt particles are dispersed into a 12 inches diameter by 5 feet high plenum where the wet particles are dried with preheated air stream. In order to neutralize the charges presented on the particles, a Kr-air ionizer is applied in the system. The main reason for charge removal is to prevent the particles from being artificially captured by electrostatic mechanism in the test-rig and filters. The salt particles exist the plenum through a 1.5 inches NPT pipe, which is able to deliver the particles into the center of test-rig facing the direction of air flow. Figure I-19 shows picture and the schematic of this large particle generator (TSI 8108).



(A)



(B)

Figure 0-19 Picture (A) and schematic (B) of TSI 8108 Large Particle Generator

From the figure, what can be seen is that in control box, two flowmeters exist to adjust the flow rates of atomizing air and drying air. This particle generator is able to produce a stable concentration of 600 particles per cubic centimeter of 1 μm and 10 particles per cubic centimeter of 10 μm when nebulizing salt solution, such as NaCl and KCl.

I.9 Characterization techniques

Characterization of a media refers to the measurement of its “characteristics”. Those physical properties of the media are assumed to be responsible for its performance during filtration process. In order to evaluate the mechanism of media filtration, the essential part is media characterization and several different techniques, such as SEM and capillary flow porometry are available.

I.9.1 Scanning Electron Microscopy (SEM)

A scanning electron microscopy (SEM) is a type of electron microscopes that images a sample by scanning it with a beam of electrons in a scan pattern. The SEM generates a beam of incident electrons in an electron column above the sample chamber. The electrons are produced by a thermal emission source, such as a heated tungsten filament, or by a field emission cathode. The energy of the incident electrons can be as low as 100 eV or as high as 100 KeV depending on the objectives that need to be evaluated. The electrons are focused into a small beam via a series of electromagnetic lenses in the SEM column. The energy exchange between the electron beam and the sample results the emission of electrons and electromagnetic radiation, which can be detected to produce images of the objectives. Several different types of signals can be produced in SEM, include secondary electrons, back-scattered electrons and transmitted electrons. The analytical information that can be achieved from SEM contains image of fine surface morphology, image contrast and surface topography, etc.

I.9.2 Capillary flow porometry

It is a characterization based on the displacement of a wetting liquid from the sample pores by applying a gas at increasing pressure. Mainly three analytical informations can be achieved from capillary flow porometry, including bubble point, mean flow pore size and pore size distribution. Membranes, nonwovens, paper, ultrafiltration media and ceramics are usual types of media that can be measured using porometry. In capillary flow porometry an inert gas is used to displace a liquid, which is in the pores. The pressure required to empty the pore corresponds to the pressure necessary to evacuate the liquid from the most constricted part of the pore. This most constricted part is the most challenging one and it offers the highest resistance to remove the wetting liquid. This parameter is very relevant in filtration and similar applications since it is important to know the smallest diameter of the through pores. For the wetting liquid, water, alcohols and silicone oil are common liquids and depending on the sample type, different wetting liquid is applied.

I.9.3 Mercury intrusion porosimetry

Besides capillary flow porometry, mercury porosimetry is another important and useful technique to measure media pore properties. It uses the non-wetting properties of mercury to gain information on the porous characteristics of solid materials: porosity, pore volume, pore size distribution and density. During a typical porosity analysis in a mercury porosimetry analyzer, a higher pressure is needed to force intrusion of mercury in smaller pores, whereas mercury intrusion in larger pores already occurs at low pressure. In this way a wide dynamic range of pore sizes can be measured and a pore size distribution can be obtained starting from 4 nm (pressure = 400 MPa) up to about 800 μm (vacuum). As a consequence, mercury porosimetry is

extremely suitable for materials showing broad distributions of pore sizes or mainly macropores, which is different with capillary flow porometry.

I.9.4 Surface area measurement

Compared to porometry and porosimetry described above, surface area is less significant to filtration performance of media. Surface area is one of the most fundamentally important properties when gaseous contaminant is being considered instead of particulates, like sea salt particles. It can provide the information of available area for dispersion of impregnated species and adsorption area for adsorbate molecules, which can be applied to evaluate the activity and stability of adsorbent. If filter media is used to remove particulates and gaseous contaminants simultaneously, then it is very necessary to measure the surface area of filter media as well, such as activated carbon fiber (ACF) filter media. Measurement of surface area is based on the principles of physical adsorption/desorption of a gas molecule on the high surface area materials. The total surface area is calculated from the area covered by each molecule of the adsorbed materials and the quantity of adsorbed material to form a complete one molecule layer of thickness [I.21]. Isothermal adsorption is one of the most common methods to measure surface area and nitrogen is the most commonly used gas as adsorbate. In this process, gas molecules are condensed onto sample surface. By completely covering the surface and opening the pores of each particle with a condensed gas, surface area analyzer can characterize the surface. The amount of gas adsorbed and the resultant sample pressure are recorded. Several different calculation methods for surface area exist, during which Brunauer, Emmett and Teller (BET) is the most widely used one. In my dissertation, a Quantachrome BET surface area analysis instrument was applied to measure the total surface area and pore volume of high surface area filter media.

I.10 Research goal

Our goal of this research is to experimentally study sea salt particles filtration performance for on board solid oxide fuel cells (SOFCs). Two main aspects are included in the work, which are filter media design and filter configurations design. During these two types of design, four different parameters are mainly investigated and optimized in order to achieve the best filtration performance. Those four parameters are pressure drop across the filter, filtration efficiency, particles loading capacity and compressor parasitic power. After comparing the experiment results of various filter media and different filter configurations, an optimum solution will be obtained for sea salt particles filtration and it will be presented in depth.

I.11 References

- [I.1] Karwa, A. N. (2012). Aerosol Filtration Performance of Novel 3-Dimensional Nonwoven Composites, in Department of Chemical Engineering, Auburn University.
- [I.2] Wilcox, M., Baldwin, R., Hernandez, A. G. and Brun, K. (April 2010). Guideline for Gas Turbine Inlet Air Filtration Systems Gas Machinery Research CouncilSouthwest Research Institute.
- [I.3] Majchrzak, R., Cole, T. and Cervi, M. (1998). U.S. Navy Sea Salt Particle Removal Systems, Carderock DivisionNaval Surface Warfare Center.
- [I.4] National Air Filtration Association (2007). NAFA Guide to Air Filtration. National Air Filtration Association, Virginia Beach, VA 23471.
- [I.5] Sothen, R. A. (2009). Novel Packaging Designs for Improvements in Air Filter Performance, in Department of Chemical Engineering, Auburn University.
- [I.6] ASHRAE 52.2 (1992). Method of Testing General Ventilation Air-cleaning Devices Used for Removal Efficiency by Particle Size, American National Standard, Atlanta, GA, USA.
- [I.7] Spurny, K. R. (1998). Advances in Aerosol Filtration. Lewis.
- [I.8] Davies, C.N. Air filtration, London, New York, Academic Press, 1973.
- [I.9] Brown, R. C. (1993). Air Filtration - An Integrated Approach to the Theory and Application of Fibrous Filters. Pergamon Press.
- [I.10] Karwa, A. N. and Tatarchuk, B. J. (2012a). Pressure drop and aerosol filtration efficiency of microfibrinous entrapped catalyst and sorbent media: Semi-empirical models. Separation and Purification Technology 86:55-63.
- [I.11] Hinds, W. C. (1998). Aerosol Technology: Properties, Behavior, And Measurement of Airborne Particles. John Wiley & Sons, Inc.

- [I.12] Fisk, W. J., Faulkner, D., Palonen, J. and Seppanen, O. (2002). Performance and Costs of Particle Air Filtration Technologies. *Indoor Air* 12:223-234.
- [I.13] Stenhouse, J.I.T. and Trottier, R. (1991). The Loading of Fibrous Filters with Submicron Particles. *Journal of Aerosol Science* 22:777-780.
- [I.14] Brown, R. C. (1993). Effects of loading, in: *Air Filtration - An Integrated Approach to the Theory and Application of Fibrous Filters*. Pergamon Press, 201-236.
- [I.15] Tatarchuk, B. J. (1992). Method of Optimizing Composite Preparation for Electrical Propoeriuets: Maximum Capacitance Electrodes, US Patent # 5,102,745.
- [I.16] Tatarchuk, B. J., Rose, M. R., Krishnagopalan, A., Zabasajja, J. N. and Kohler, D. (1992a). Preparation of Mixed Fiber Composite Structures, US Patent #5,080,963.
- [I.17] Tatarchuk, B. J., Rose, M. R., Krishnagopalan, A., Zabasajja, J. N. and Kohler, D. (1994). Mixed Fiber Composite Structures High Surfaces Area High Conductivity Mixtures, US Patent #5,304,330.
- [I.18] Tatarchuk, B. J., Rose, M. R., Krishnagopalan, A., Zabasajja, J. N. and Kohler, D. (1992b). Mixed Fiber Composite Structures, US Patent #5,096,663.
- [I.19] Hutten, I.M. *Handbook of nonwoven filter media*, first ed., Butterworth-Heinemann, Oxford, 2007.
- [I.20] HSLAS II and LAS-X II spectrometers operations manual, Particle Measuring Systems
- [I.21] Wahid, S. (2014). Noval Catalytic Material with Enhanced Heterogeneous Contacting Efficiency for VOC Removal at Ultra-short Contact Time, in Department of Chemical Engineering, Auburn University.

Chapter II Sea salt particles filtration for SOFCs using pleated filters in novel packaging configurations

II.1 Abstract

Solid Oxide Fuel Cells (SOFCs) are being considered for use as power sources on ships due to their high energy efficiency and low waste emission. However, the exposure of several air contaminants like gaseous impurities and particulates is significantly detrimental to the performance of fuel cells. In the ocean environment, sea salt particles are the most common particulates and their removal from air stream fed into cathode side of fuel cell system is highly essential. Current approach is using coalescers and inertial separators to remove the particles. But these devices are only effective for particles larger than 8 μm in size [II.4]. To remove much smaller particles in a more efficient manner, we focused on the design and optimization of a new type of filter for sea salt particles. Pleated filter design is a common approach in the air filtration industry to increase the available media area and reduce the pressure drop. Multi-Element Structured Arrays (MESAs) that developed by our group represents a new approach that can further increase the filtration area and reduce the pressure drop across the filter by integrating several pleated filters into a single unit. In this study, both single filters and MESAs were tested on a 24" \times 24" full scale test rig (based on ASHRAE 52.2 Standard) for evaluation of filtration performance, including particles removal efficiency, pressure drop across the filter system and particles loading capacity. The different effects of varying filter media type, filter depth, pleat

count and MESAs element count on the filtration performance and particles loading capacity were experimentally investigated. The results and discussion will be presented in depth.

II.2 Introduction

Nowadays, Solid Oxide Fuel Cells (SOFCs) are being considered to be applied to provide electric power for ships with less harmful emissions or wastes. Fuel cells are electrochemical devices that directly convert chemical energy from fuels into electricity via chemical reaction with oxygen in the air or other oxidizing agents [II.1]. However, the air always contains several different kinds of contaminants, both gases and particulates, which can cause severe degradation to the SOFCs [II.2]. In terms of SOFCs during ocean environment, sea salt particle (SSP) is one of the most harmful contaminants to the fuel cells. Therefore, removal of the SSP from air stream fed into cathode side is of significant influence on the operation of the SOFCs. These SSPs are generated naturally from wind stresses over white caps or are ship generated from either the wake or the bow spray (ship generated spray at the bow entrance). Sea salt particles mainly consist of size range from 0.01 to 10 micron [II.3]. Current approach is using coalescers and inertial separators to remove the particles. But these devices are only effective for particles larger than 8 microns in size [II.4]. Microfibrous Materials (MFM), which was manufactured by the Center for Microfibrous Materials Manufacturing at Auburn University has shown great applicability in removing particulate matters in small sizes. However, MFM has substantially higher flow resistance than traditional filtration media due to decreased fiber diameter and tighter packing density [II.5]. Thus, MFM is limited to be applied as media for air filters. To remove much smaller particles in a more efficient manner, we have focused on the design and optimization for a new type of sea salt particles filtration system using pleated filters. A pleated filter is able to extend the media area and reduce the resistance by transforming a flat material into a three dimensional filter,

which can overcome the disadvantages of those highly packed media. MESA, which stands for Multi-Element Structured Array, is a novel design developed by our research group that integrates multiple pleated filter elements into a single filtration unit. The concept of MESA is to further extend the pleated filter design by taking a flat, pleated filter and turns it into a three dimensional array of filters to further extend the filtration media area and reduce the air flow resistance [II.6]. Different configurations of MESA, such as V shape, W shape and VW shape, can be seen in Figure II-1.

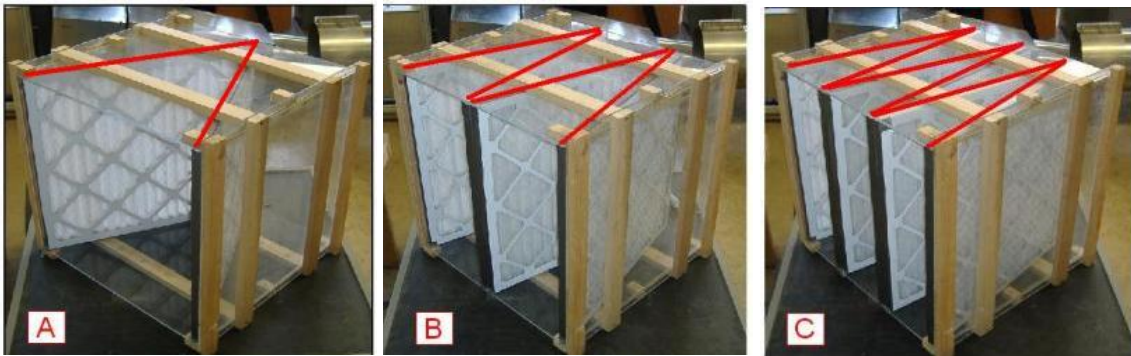


Figure II-1 Different configurations of MESA units: (A) V-shaped MESA, (B) W-shaped MESA, (C) VW-shaped MESA

The aim of this work is to investigate the effects of different filter parameters, such as filter depth and filter pleat count on single filter performance for sea salt particles removal and an optimum solution is determined according to three most important criteria of filter, including filtration efficiency, pressure drop and particles loading capacity. In addition, filtration performance and particles loading capacity of MESAs were tested as well in order to evaluate if MESAs are highly valuable on sea salt particles filtration in comparison with single filters.

II.2 Theoretical study

II.2.1 Filter efficiency

Filter efficiency primarily depends on the type of filter media used within the filters. It also changes with particles size, filtration area and filtration velocity. Usually, clean filter removal efficiency E is closely related to the single fiber collection efficiency E_{Σ} according to an equation obtained by a mass balance on a filter element of thickness dt and integrated on the total filter thickness t [II.7,II.8].

$$E = 1 - \exp\left(\frac{-4\alpha E_{\Sigma} t}{\pi R}\right) \quad (\text{Eq II.1})$$

Where α is the packing density defined as the ratio of the volume of fibers and the total filter volume.

As is known, filters are usually designed to use various mechanisms to remove particles in different sizes. The mechanism employed by the filter depends on several factors, such as filtration velocity, fiber diameter and particle size. A common misunderstanding is that filter media work as a sieve-removing only the particles larger than the pore diameter of the filter media [II.9]. However, various filtration mechanisms exist and sieving is just one of those. In a mechanical filter, different mechanisms work together [II.6] and remove small as well as larger particles at the same time [II.10,II.11]. Filtration process is usually composed of diffusion, interception, inertial impaction, electrostatic deposition, gravitational settling and sieving. For my study, diffusion, inertial impaction and interception account for the majority of the particles removal and therefore, the single fiber efficiency E_{Σ} is defined below as [II.10]:

$$E_{\Sigma} = 1 - (1 - E_D)(1 - E_R)(1 - E_I) \quad (\text{Eq II.2})$$

II.2.2 Pressure drop

Pressure drop across a filter corresponds directly to the energy consumption as it is indicative of the work done by the blower to push air through the filter [II.12,II.13]. The equation of pressure drop across a pleated filter is based on a model built by Ryan Sothen previously. The total pressure drop through a pleated filter is modeled as a summation of individual resistances. The individual resistance is formulated by applying Forchheimer-extended Darcy's Law and Bernoulli's Equation. With the equation of continuity assumed valid, all the individual resistances can be summed and rearranged into the following mode [II.14,II.15]:

$$\Delta P_T = \frac{1}{2} \rho [(2K_G)V_2^2 + (K_C + K_E + K_P)V_3^2] + AV_4 + BV_4^2 \quad (\text{Eq II.3})$$

K_G , K_C , K_E and K_P stand for coefficient of grating, coefficient of contraction, coefficient of expansion and coefficient of pleat, respectively. V_2 , V_3 and V_4 stand for air velocity through grating, pleat inlet and filter media, respectively. A and B are filter media constants, which can be determined empirically.

Since MESA is an extension of single pleated filter, pressure drop of MESA is also developed as an extension of the single pleated filter model by adding two slot resistances. Similar to single pleated filter model, all the individual resistances can be summed and rearranged as below [II.16]:

$$\Delta P_T = \frac{1}{2} \rho [(K_{CB} + K_{EB})V_2^2 + (2K_G + K_S)V_3^2 + (K_{CP} + K_{EP} + K_P)V_5^2] + AV_6 + BV_6^2 \quad (\text{Eq II.4})$$

K_G , K_{CP} , K_{EP} , K_P are previously defined in single filter as coefficients of grating, contraction, expansion and pleat, respectively. K_{CB} and K_{EB} also stand for coefficients of contraction and expansion, but they are referred to the flow into and out of the filter array. K_S is defined as

coefficient of slot of the MESA. V_2 , V_3 , V_5 and V_6 stand for air velocity through MESA slot, grating, pleat inlet and filter media, respectively.

II.2.3 Loading of salt particles

In addition to pressure drop and filtration efficiency, particles loading capacity is another significant parameter that should be considered during filter design [II.17]. With salt particles deposited into the filters, filter performance may change gradually, including both filtration efficiency and filter pressure drop. Therefore, particles loading performance should be investigated as well. Particles loading capacity is defined as the quantity of contaminant a filter element can trap and hold before the maximum allowable back pressure or pressure drop is reached. Particles loading capacity is strongly related to filter life time, which is a significant character during filter design [II.18]. Higher particles loading capacity leads to longer filter life time and increasing filter life time is the most crucial element in reducing filtration costs. However, filter with larger particles loading capacity always has lower particles removal efficiency. Therefore, an optimization can be developed according to both particles loading capacity and filtration efficiency. Usually, particles loading capacity depends on two main aspects, one is filter media and the other one is filter configuration. As for filter media, fiber material and fiber packing density are the two most important parameters that need to be concerned. Different fiber materials and packing densities can lead to various particles loading behaviors. For filter configuration, different filter depths, filter pleat counts and filter elements in MESAs can cause different filtration area and filtration velocity, which leads to various particles loading behaviors. Usually, particles loading behavior is strongly related to filtration mechanisms since particles deposit pattern is different for various mechanisms [II.19].

Particles loading curve is usually applied in this part of study, which is nominal increase of pressure drop across the filter vs mass of particles loaded by the filter. In order to achieve this

curve, filtration efficiency tests and pressure drop measurements were both included. During salt particles loading process, pressure drop across the filter increased gradually and the value was recorded every 20 to 30 mins. According to filtration efficiency and inlet salt particles concentration, the number of salt particles entrapped by the filter during 1 min could be calculated and as well as the total number of particles during that 20 to 30 mins. Since the particle diameter is known, the mass of total particles loaded by the filter was achieved afterwards. However, salt particles in different diameters have various shapes, like sphere, cube or agglomerate. Thus, calculations of mass of salt particles for different particle sizes are different. In this work, salt particles were considered as spheres, cubes and agglomerates for particles smaller than 200nm, between 200 and 800 nm and larger than 800 nm, respectively. As for agglomerates, they could be calculated as spheres with shape factor of 1.4 [II.20]. Equations II.5 to II.8 have shown how to calculate the mass of salt particles in different shapes:

$$Mass_{<200nm} = N_{<200nm} \times \pi / 6 \times (D)^3 \times \rho \quad (\text{Eq II.5})$$

$$Mass_{200-800nm} = N_{200-800nm} \times (D)^3 \times \rho \quad (\text{Eq II.6})$$

$$Mass_{>800nm} = N_{>800nm} \times \pi / 6 \times (1.4D)^3 \times \rho \quad (\text{Eq II.7})$$

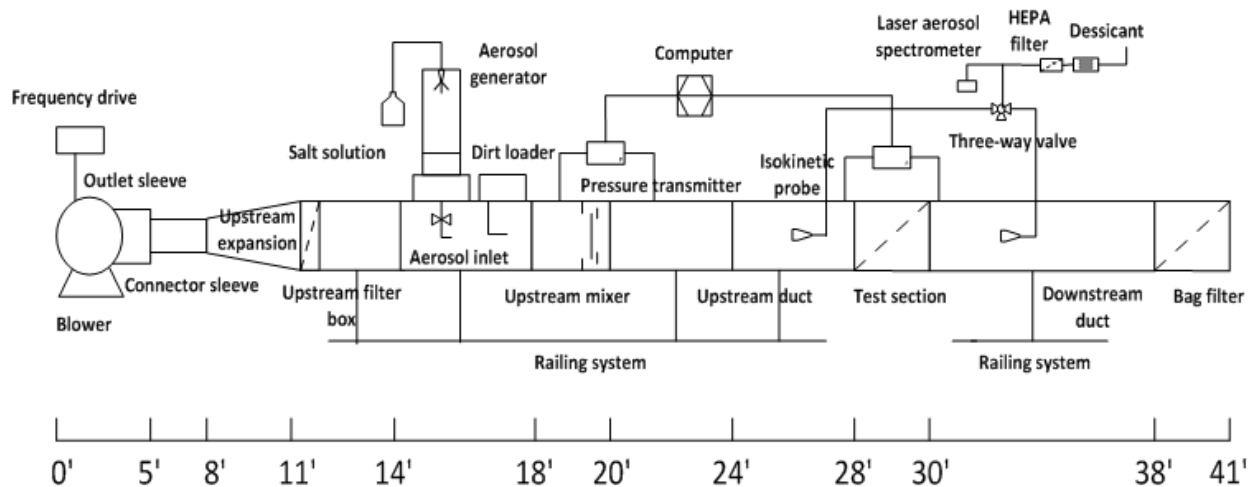
$$Mass_{Total} = Mass_{<200nm} + Mass_{200-800nm} + Mass_{>800nm} \quad (\text{Eq II.8})$$

Since mass of salt particles loaded by the filter and increase of pressure drop across the filter were both known, salt particles loading curve for all tested filters were able to be plotted.

II.3 Experimental

Figure II-2 shows pictures and the schematic of full scale test rig, which was built based on ASHRAE 52.2 Standard [II.21]. The whole system can deliver up to 2000 cfm of air and is able to be applied for pressure drop, particles removal efficiency and particles loading capacity

measurements. The test rig used room air for all the experiments. Room air was introduced into the test rig from a blower driven by a 3 HP motor [II.6]. A filtration box containing a HEPA filter was installed after in order to remove any particles and gas contaminants in the room air. Then, an aerosol generator was followed to nebulize challenge particles that need to be tested. A TSI 8108 Large particle Generator, which can produce salt particles in the range of 0.1 to 10 μm was applied. 15% Sodium chloride solution was pumped at a controlled rate into a spray nozzle where it was mixed with atomizing air. A drying air stream and Kr ionizer were used to dry the salt particles and neutralize any charges in the particles respectively. An upstream mixer was followed to mix and distribute the challenge particles throughout the whole system. After the mixer, two 4' long upstream ducts were installed to self-correct and further distribute the particles along the test rig. Then, it was filter test section, which was held into the place by 8 “quick-grip” clamps. An 8' long downstream duct was followed on a linear motion track, which could be used to adjust the depth of test section [II.6]. At the end of the test rig, a final bag filter was installed to capture any challenge salt particles that passed through the filter test section. The whole test rig was about 41' long and 24' wide.





Upstream duct



Downstream duct

Figure II-2 Experimental setup (Upstream and downstream duct) for filtration performance study of salt particles, including pressure drop, filtration efficiency and particles loading capacity testing

For all the tests, pressure drop transmitter and Laser Aerosol Spectrometer (LAS-XII) were applied to measure the pressure drop across the tested filter and the particles removal efficiency. The efficiency was calculated as per the ASHRAE 52.2 Standard [II.21] with 8-10 samples of 1 min each. Error bars of 95% confidence interval were reported in the filtration efficiency data. In all tests, at least 3 samples were measured to check for the repeatability of data. As for TSI 8108

large particle generator, size distribution of sodium chloride particles is measured as well and is shown in Figure II-3. According to the size distribution, mean diameter of salt particles is 185 nm.

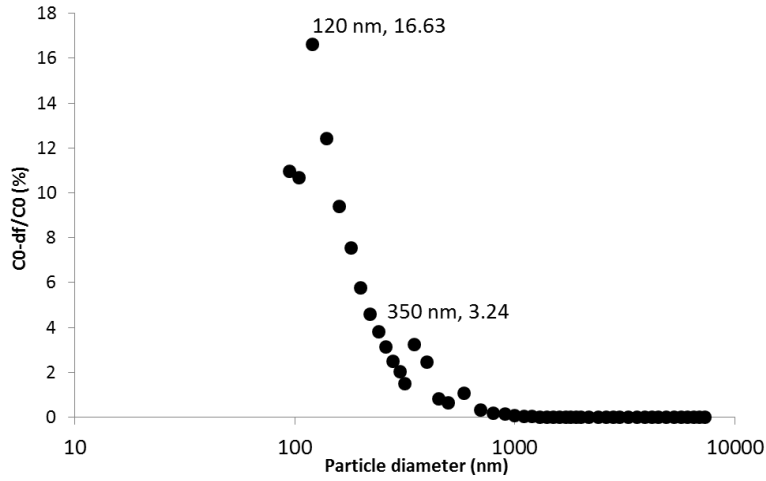


Figure II-3 Size distribution of NaCl particles generated by TSI 8108 (Large generator)

II.4 Results and discussion

II.4.1 Pressure drop of single filters

For single filters with different pleat counts, according to pressure drop model of pleated filter, there is a trade-off between media resistance and geometric resistance, which indicates that a minimum pressure drop exists at a certain pleat count. And the value of the optimal pleat count varies with different filter parameters, including filter depths and filter media types. Figure II-4 shows pressure drop curves of 2 inch and 1 inch filters with different pleat counts. As shown in the figure, pleat count of 20 and pleat count of 44 have the lowest pressure drop for 2 inch filter and 1 inch filter respectively. When pleat count goes up or goes down from that value, pressure drop across the filter increases. Meanwhile, compared to 2 inch filter, pressure drop is higher for 1 inch filter. The reason is that 1 inch filter has smaller filtration area, which causes higher inner filtration velocity through the filter. As the pressure drop model predicted, higher filtration velocity can lead to higher pressure drop. Therefore, 1 inch filter has larger pressure drop than 2 inch filter.

According to this, what can also be predicted is that 4 inch filter has the lowest pressure drop due to its largest filtration area.

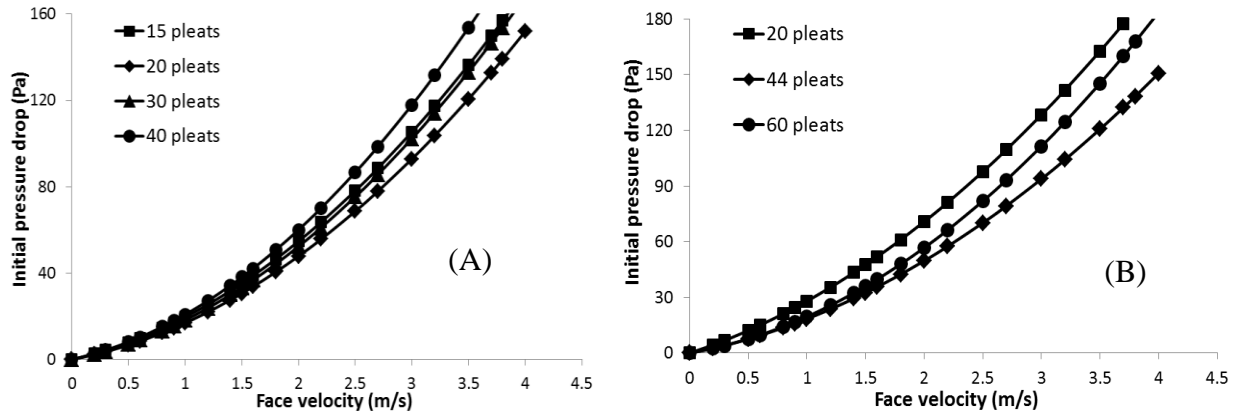


Figure II-4 Pressure drop across different pleat counts filters with respect to face velocity: (A) 2 inch deep pleated filter, (B) 1 inch deep pleated filter

II.4.2 Filtration efficiency of single filters

LAS-X II spectrometer is applied to measure the number of salt particles before and after the filter. In order to make sure that there is no deviation in sample counts using two isokinetic probes between upstream and downstream, a blank test is carried out with no filter installed. Five upstream samples and five downstream samples (total ten samples) are measured for 22 particles size channels (100 nm to 1000 nm) and the results are plotted in Figure II-5.

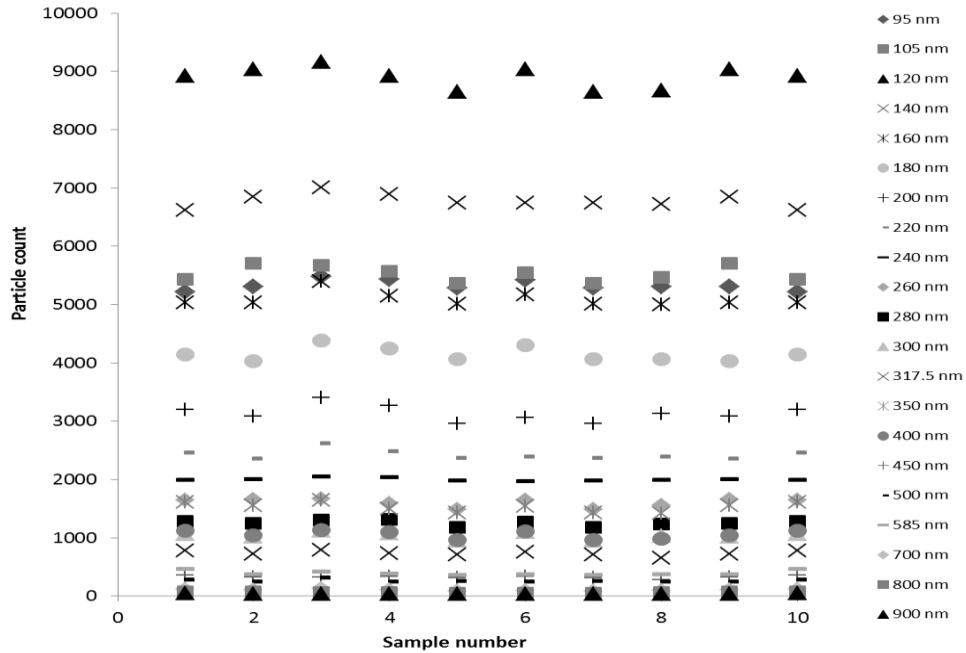


Figure II-5 Comparison of upstream and downstream counting probes

As can be seen in Figure II-5, the two locations (upstream and downstream) have similar particle counts when monitoring a baseline concentration without a filter. Thus, the filtration efficiency data obtained later in this work is accurate and believable.

According to filtration mechanisms, in diffusion dominant regime (particles are less than 500 nm), filtration efficiency increases with smaller particle size due to higher Brownian motion. And in inertial impaction dominant regime (particles are larger than 800 nm), filtration efficiency increases with larger particle size because of high momentum. Thus, there exists a range of 0.04 to 0.4 μm , where no mechanism is strong enough to remove the particles. During this range, there is one point with minimum efficiency of particles capture, which is called most penetrating particle size (MPPS). In this study, filtration velocity is in the range of 1 to 3 m/s, which causes inertial impaction to be more significant compared to diffusion. Besides, increasing filtration velocity leads to the decrease of Most Penetrating Particle Size (MPPS) [II.10]. Both of these two effects result in that for filters tested in my study, MPPS is smaller than 0.1 μm , which is the lower limit of

spectrometer. Therefore, filtration efficiency increases within the whole particle size range (0.1 to 1 μm), which can be seen in Figure II-6.

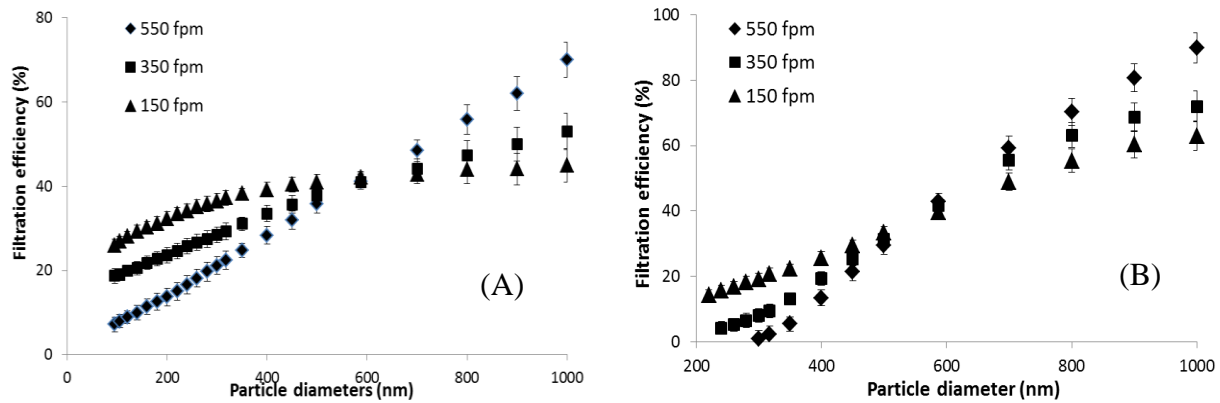


Figure II-6 Salt particles filtration efficiency with respect to particle diameter at different filtration velocities for (A) 2 inch deep pleated filter, (B) 1 inch deep pleated filter

In addition, Figure II-6 shows that filtration efficiency varies for both 2 inch and 1 inch filters at different filtration velocities. In diffusion dominant regime, lower filtration velocity can lead to longer resident time for particles, which causes more particles to be trapped in the filter. In inertial impaction dominant regime, higher filtration velocity is more helpful to the particles capture because of the particles inertia, which leads to higher filtration efficiency for larger particles. There is another mechanism, interception, which is the only mechanism not dependent on filtration velocity [II.22,II.23]. As shown in Figure 4, the intersection of the filtration efficiency curves obtained at various velocities demonstrates the interception efficiency, which is independent of filtration velocity.

The particles removal efficiency of both 2 inch and 1 inch filters for salt particles varies with pleat count as well due to both different filtration media areas and filtration velocities, which can be seen in Figure II-7. When increasing filter pleat count, filtration area is extended and thus much more particles are able to be trapped by the filter. Meanwhile, inner filtration velocity inside

the filter varies because of different filtration media area. Larger filtration media area leads to lower inner filtration velocity at same volume of air flowing through. Therefore, in diffusion dominant regime, filter with higher pleat count shows much higher filtration efficiency due to both larger filtration media area and lower inner filtration velocity. However, for large particles in inertial impaction dominant regime, performance of filter with higher pleat count is decreased at some degree. This suggests that the decrease of inner filtration velocity negates the effect of increase in filtration media area. According to this, filtration velocity plays a more important and dominant role in particles removal efficiency compared to filtration media area.

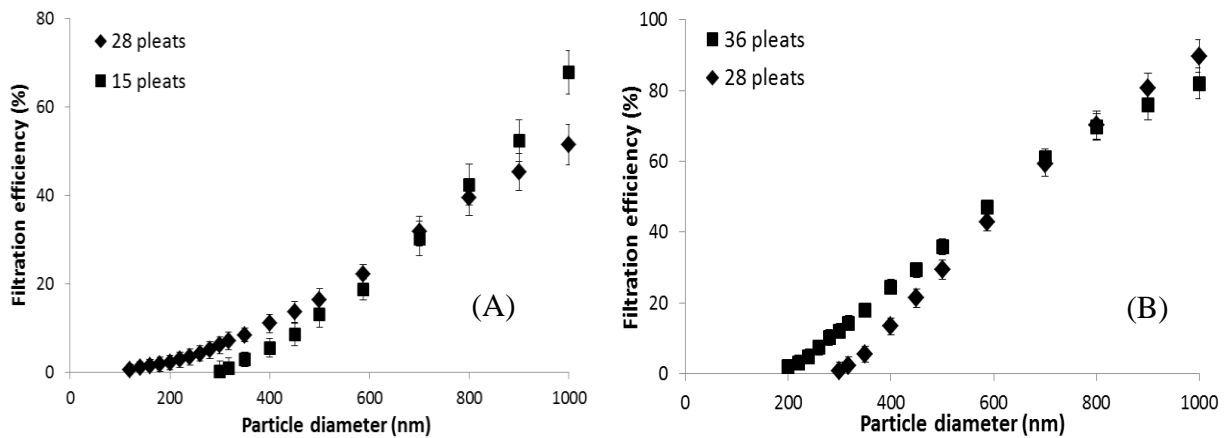


Figure II-7 Salt particles filtration efficiency with respect to particle diameter for different pleat counts filters: (A) 2 inch deep pleated filter, (B) 1 inch deep pleated filter (550 fpm)

II.4.3 Quality factor of single filters

Usually for a filter, higher particles removal efficiency indicates larger pressure drop. In order to judge if the filter is good on its filtration performance and suitable for real applications, a new term, quality factor (QF) [II.11,II.24] is defined to measure whether an increase in pressure drop is warranted by the increase in filtration efficiency. It is calculated as the ratio of fractional capture per unit thickness to the pressure drop per unit thickness [II.25,II.26].

$$QF = \frac{\gamma}{\Delta P / t} = \frac{\gamma t}{\Delta P} = \frac{\ln(1/P)}{\Delta P} = -\frac{\ln(1-E)}{\Delta P} \quad (\text{Eq II.9})$$

According to the equation, what can be seen is that larger filtration efficiency and smaller pressure drop could lead to higher quality factor, which also suggests better filter performance. And from the equation, filtration efficiency plays a more significant role compared to pressure drop because of the logarithm.

As shown in the Figure II-8, for small particles, both 1 inch and 2 inch filters show higher quality factors for more pleats, which is due to higher filtration efficiency resulting from larger filtration area and lower inner filtration velocity. In terms of large particles, quality factors decrease for both 1 inch and 2 inch filters with more pleats because of smaller filtration efficiency resulting from lower inner filtration velocity. In addition, since quality factor is related to pressure drop as well, the trends of the curves are slightly different compared to filtration efficiency curves. For 1 inch filter, crossing point shifts to larger particle size because filter with 28 pleats has higher pressure drop than filter with 36 pleats due to higher inner filtration velocity. As for 2 inch filter, crossing point almost remains the same due to the similar pressure drop of filters with 15 and 30 pleats according to pressure drop model of pleated filter. In a word, quality factor determines the performance of filter and for single filters, larger pleat count is better for small particles removal and vice versa for smaller pleat count.

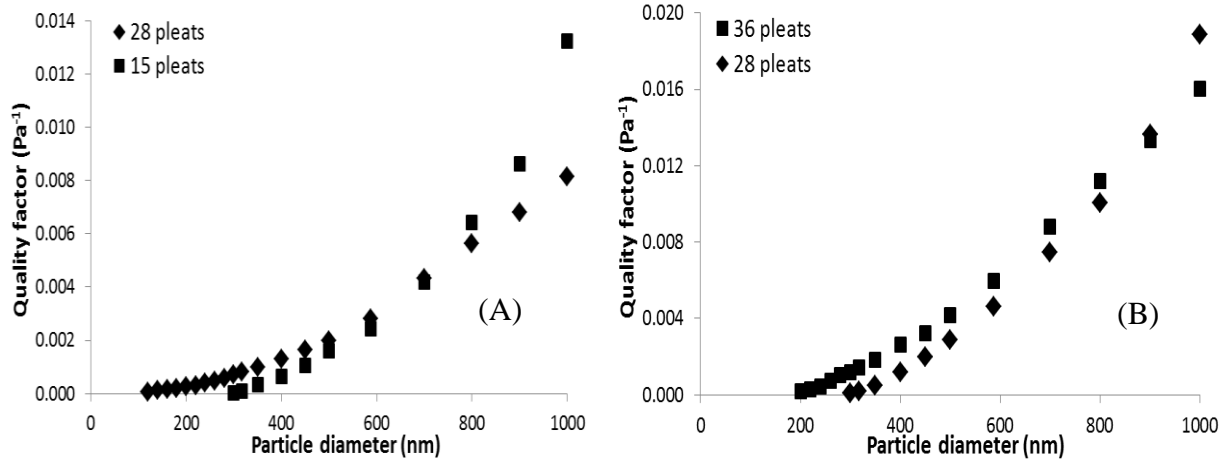


Figure II-8 Quality factor (cal.) with respect to particle diameter for different pleat counts filters:

(A) 2 inch deep pleated filter, (B) 1 inch deep pleated filter (550 fpm)

II.4.4 Comparison of single filters in different depths

Filters in different depths have various filtration media areas and inner filtration velocities, which results in different filtration performance according to various filtration mechanisms (diffusion and inertial impaction). Thus, it is very necessary to evaluate this phenomenon. Pressure drop and filtration efficiency tests were both carried out for filters in different depths but with same pleats and the results are shown in Figure II-9.

As shown in Figure II-9, filter in higher depth has lower pressure drop due to its larger filtration media area and lower inner filtration velocity. As for filtration efficiency, 2 inch filter is higher for small particles and 1 inch filter is higher for large particles. The reason is that since 2 inch filter has larger filtration area and lower inner filtration velocity, for particles in diffusion dominant regime, more particles can be entrapped and captured, which leads to higher particles removal efficiency. However, when particles become larger, inertial impaction is more dominant and due to the lower inner filtration velocity of 2 inch filter, it shows smaller filtration efficiency compared to 1 inch filter. In order to judge the performance of filters in different depths, quality factors were calculated as well and they have shown similar trends as filtration efficiency curves.

But the crossing point shifts to larger particle size due to higher pressure drop of 1 inch filter. Therefore, in terms of filter performance, filter in lower depth is better for large particles and filter of higher depth is better for small particles. According to different real circumstances, filter in different depths can be selected in order to achieve the optimal filtration performance. If small particles (< 400 nm) are the major concern, then higher depth filter is more suitable and if large particles (> 500 nm) need to be removed, then filter of lower depth will perform better.

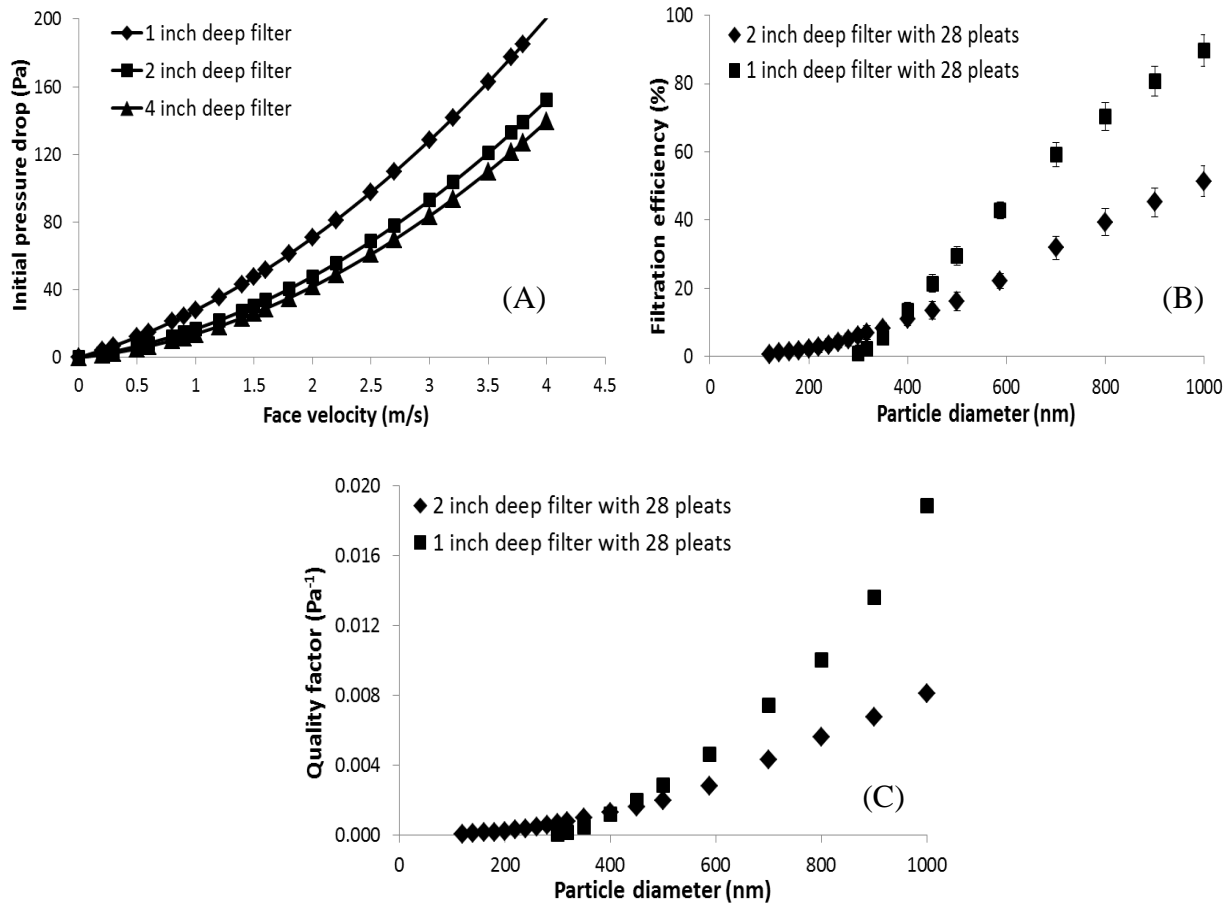


Figure II-9 Comparisons of filtration performance for salt particles between filters of different depths (2 inch deep and 1 inch deep): (A) pressure drop with respect to face velocity, (B) filtration efficiency with respect to particle diameter and (C) quality factor (cal.) with respect to particle diameter

II.4.5 Pressure drop of MESAs

MESAs are able to extremely lower inner filtration velocity due to double or quadruple filtration media area and as a result, it has much smaller pressure drop compared to single filters, which can be seen in Figure II-10.

As for MESAs with different filter pleat counts but same elements, pressure drop curves only show slight differences compared to that of single filters, as shown in Figure II-11. The reason is that for MESA units, there is another type of flow resistance, slot resistance which serves as the dominant resistance compared to media and geometric resistance for single filters. And the slot resistance is same for MESAs with the same elements, such as V shape, W shape or VW shape. Therefore, no matter how many pleats the filter has, MESAs with the same elements have similar pressure drop across the unit.

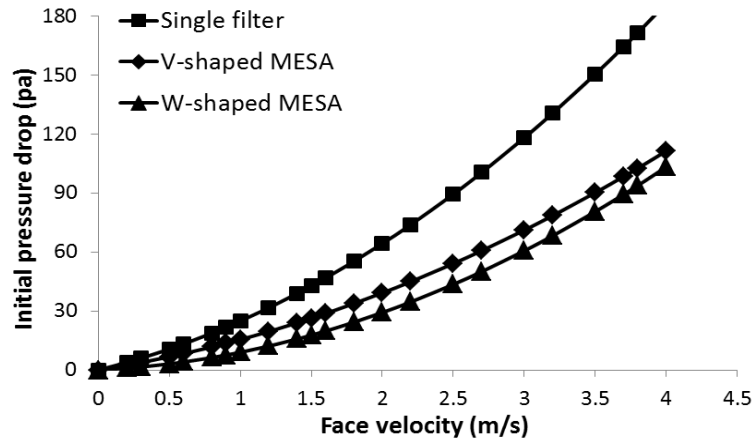


Figure II-10 Pressure drop across single filter and MESAs (V-shaped and W-shaped) with respect to face velocity

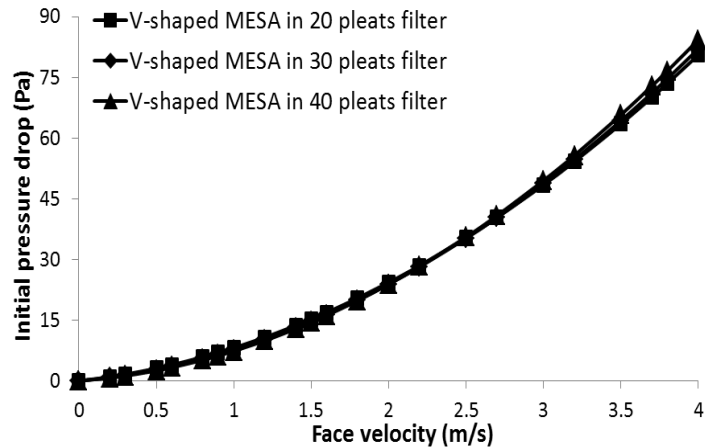


Figure II-11 Pressure drop across V-shape MESA in different pleat counts filters with respect to face velocity

II.4.6 Filtration efficiency of MESAs

MESA units have significantly different particles removal efficiency compared to single filters since filtration efficiency is strongly dependent on both filtration velocity and filtration media area. Figure II-12 shows comparisons of filtration efficiency between MESAs and single filter at different air flow rates (550 fpm and 350 fpm). It indicates that for particles smaller than 800 nm, MESAs have much higher filtration efficiency than single filter at both two air flow rates, which results from MESAs' larger filtration media areas and lower inner filtration velocities.

However, when particles are larger than 800 nm, the trends are different for two air flow rates. At 550 fpm, filtration efficiency of MESA becomes smaller than single filter, which is because that for particles larger than 800 nm where inertial impaction mechanism is more dominant, lower filtration velocity is detrimental to particles capture. Since filtration velocity is more important than filtration media area, the decrease of filtration velocity for MESAs has negated the effect of increase in filtration media area. At 350 fpm, filtration efficiency of MESA is still larger than single filter. The reason is that at low flow rate (350 fpm), inertial impaction

becomes less dominant and the decrease of filtration velocity cannot negate the effect of increase in filtration area for MESAs.

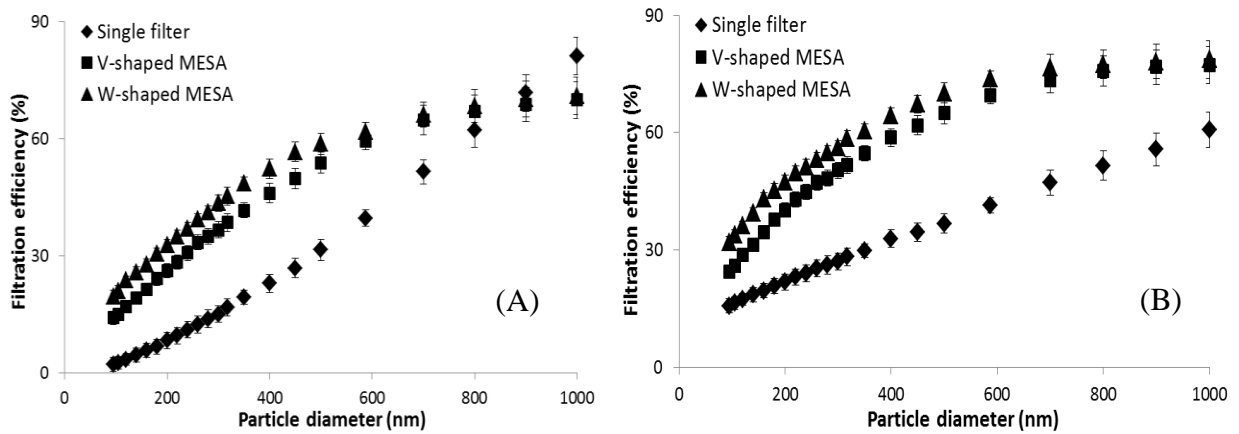


Figure II-12 Salt particles filtration efficiency with respect to particle diameter for single filter and MESAs (V-shaped and W-shaped) at (A) 550 fpm, (B) 350 fpm

II.4.7 Quality factors of MESAs

Quality factor plays a very important role in determining the filtration performance of MESAs as well. As shown in the Figure II-13, MESAs have much higher quality factors compared to single filter for both small and large particles at two different air flow rates, which is due to MESAs' higher filtration efficiency and lower pressure drop. Although at 550 fpm, MESAs have shown smaller filtration efficiency for particles larger than 800 nm, they still demonstrate much higher quality factors. This suggests that the significant decrease of pressure drop for MESAs has compensated the effect of decrease in filtration efficiency. Therefore, MESAs are able to enhance particles filtration performance compared to single filter and they can be potentially applied into real circumstances, such as filtration system for SOFCs during ocean platform. The average quality factors of MESAs (V shape and W shape) at two different air flow rates were calculated and are shown in Table II-1.

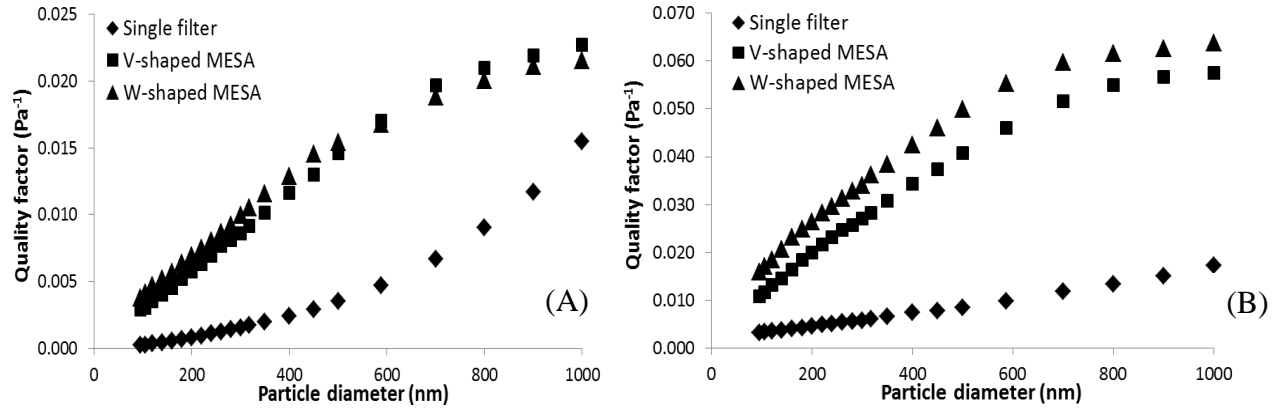


Figure II-13 Quality factor (cal.) with respect to particle diameter for single filter and MESAs (V-shaped and W-shaped) at (A) 550 fpm, (B) 350 fpm

Table II-1 Comparison of average quality factor (cal.) between single filter and MESAs (V-shaped and W-shaped) at different filtration velocities

	Single filter	V-shaped MESA	W-shaped MESA
550 fpm	0.0032	0.0103	0.0111
350 fpm	0.0071	0.0300	0.0372

II.4.8 Results and discussion of loading of salt particles

Single filters with different pleat counts and in different depths were tested at various air flow rates in regards of salt particles loading capacity. Performance of MESAs on salt particles loading were measured as well and the comparison between MESAs and single filters are demonstrated in this part of study.

II.4.8.1 Effect of filtration velocity on particles loading

Three different air flow rates were selected for this study, 150 fpm, 315 fpm and 550 fpm. Same filters (2 inch with 15 pleats) were applied and tested at those selected flow rates. As can be seen in Figure II-14, higher filtration velocity leads to higher increase of pressure drop at the same deposited mass of salt particles per filter media. This also suggests when the filter reaches the maximum pressure drop, it has smaller particles loading capacity at higher filtration velocity.

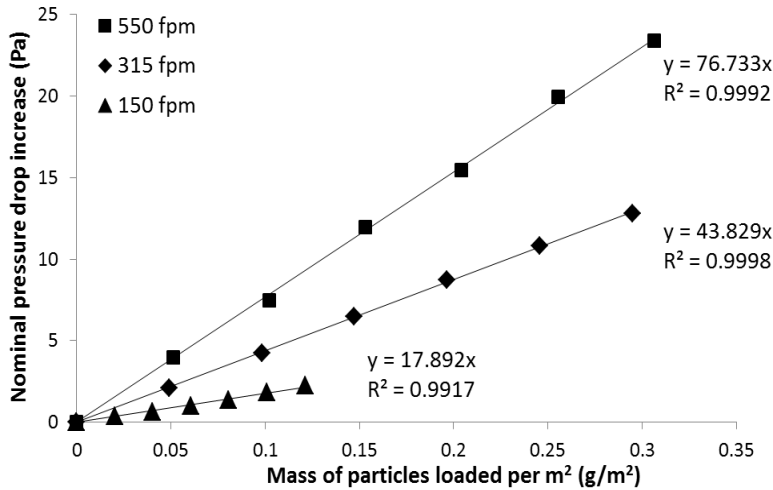


Figure II-14 Nominal pressure drop increase with respect to deposited mass of salt particles for single filter at different filtration velocities

However, in order to test whether this difference between the curves is only due to the difference of filtration velocity, the ratio of $\Delta P/U$ against the deposited mass of salt particles per filter media was plotted and shown in Figure II-15. What we can notice is that the three curves are almost identical and it suggests that the way salt particles deposit into filters is independent on filtration velocity, which has also been observed by other researchers [II.27].

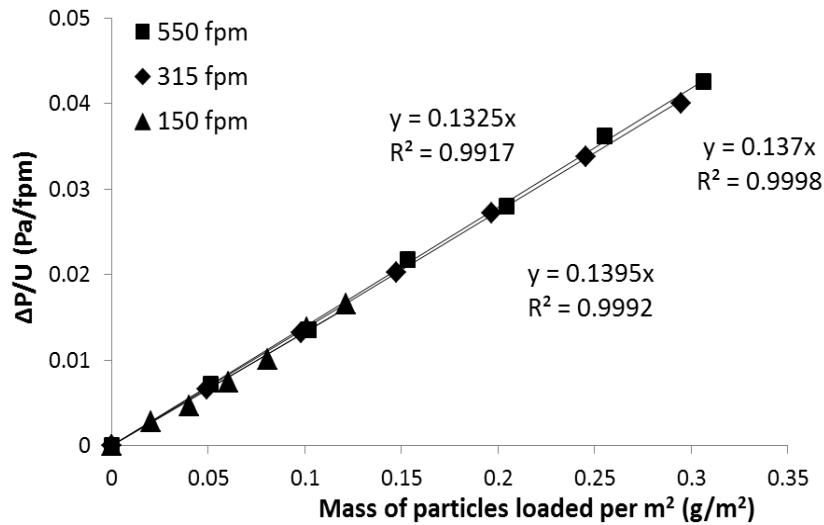


Figure II-15 Evolution of $\Delta P/U$ during loading of salt particles at different filtration velocities

II.4.8.2 Effect of filter pleat count on particles loading

Filter pleat count is an important parameter for particles loading that needs to be considered as well. Three 2 inch single filters with 15, 20 and 30 pleats and three 1 inch single filters with 20, 32 and 44 pleats were tested at same filtration velocities.

As shown in Figure II-16, for both 2 inch and 1 inch filters, particles loading curves for different pleat counts show different slopes due to their various filtration media areas and inner filtration velocities. The results have indicated that for both 2 inch and 1 inch filters, higher pleat count filter has smaller increase of pressure drop compared to lower pleat count filter at same deposited mass of salt particles. It is because that higher pleat count results in larger filtration media area, which suggests that more fibers can be used to capture particles and then, newly captured particles can go to non-occupied fibers instead of being attached by previously entrapped particles. And via this way, pressure drop increases more slowly. Therefore, when the same mass of salt particles deposited into the filter, increase of pressure drop is lower for filters with higher pleat count.

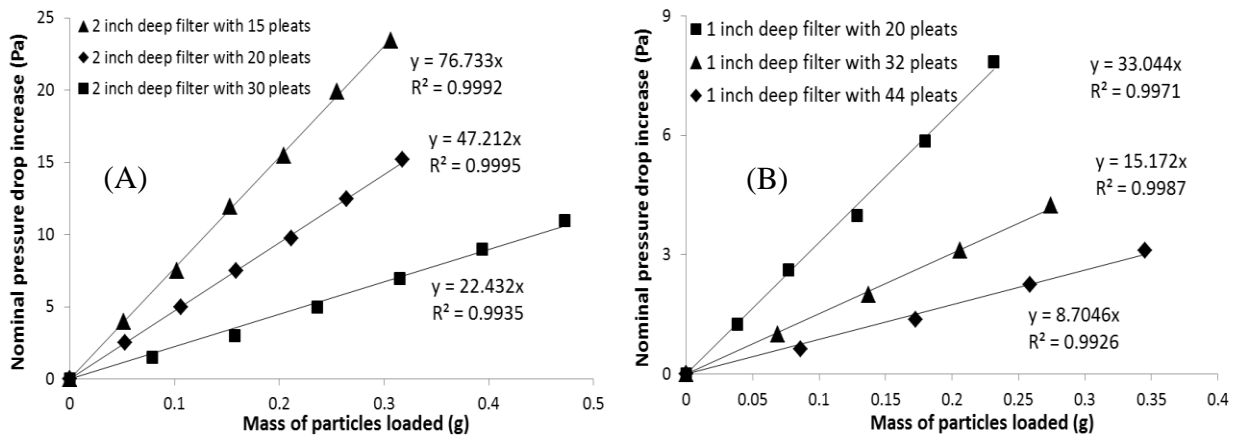


Figure II-16 Nominal pressure drop increase with respect to deposited mass of salt particles for single filters with different pleat counts: (A) 2 inch deep pleated filter, (B) 1 inch deep pleated filter

Meanwhile, since different filtration media areas cause different inner filtration velocities, the effect of filtration velocity is included in the gap between particles loading curves as well. Larger filtration area leads to lower inner filtration velocity and as I talked previously, it has less increase of pressure drop during deposition of salt particles. Overall, for both 2 inch and 1 inch single filters with different pleat counts, these two parameters (filtration media area and filtration velocity) are able to affect the filter performance on salt particles loading simultaneously. In order to further explain this result, Equations II.10 to II.14 below can be applied.

$$\text{From curves in Figure II-15, we can get } \frac{\Delta P_1}{U_1} = K \frac{M_1}{A_1}, \frac{\Delta P_2}{U_2} = K \frac{M_2}{A_2} \quad (\text{Eq II.10})$$

$$\text{Then, } M_1 = \frac{\Delta P_1 A_1}{U_1 K}, M_2 = \frac{\Delta P_2 A_2}{U_2 K} \quad (\text{Eq II.11})$$

$$\text{When the increase of pressure drop is same, } \frac{M_1}{M_2} = \frac{A_1}{A_2} \frac{U_2}{U_1} \quad (\text{Eq II.12})$$

Since the air flow rate through the filter system is same ($A_1 U_1 = A_2 U_2$),

$$\text{therefore, we can achieve } \frac{M_1}{M_2} = \left(\frac{A_1}{A_2}\right)^2 \text{ finally.} \quad (\text{Eq II.13})$$

It indicates that ratio of mass of salt particles loaded by filter is proportional to the square of ratio of filter media area, which includes the effects of both filtration area and filtration velocity.

II.4.8.3 Effect of filter depth on particles loading

Three single filters in different depths (1 inch, 2 inch and 4 inch) but with same pleat counts were tested at same filtration velocities and the results are shown in Figure II-17.

As can be seen in Figure II-17, 4 inch deep filter shows the smallest increase of pressure drop compared to both 1 inch and 2 inch deep filters at same mass of deposited salt particles. As the same as the effect of filter pleat count, this is resulted from much higher filtration media area

and lower inner filtration velocity. Both of the two effects affect the particles loading process in a positive way, and higher particles loading capacity and longer filter lifetime for filter in higher depth can be concluded.

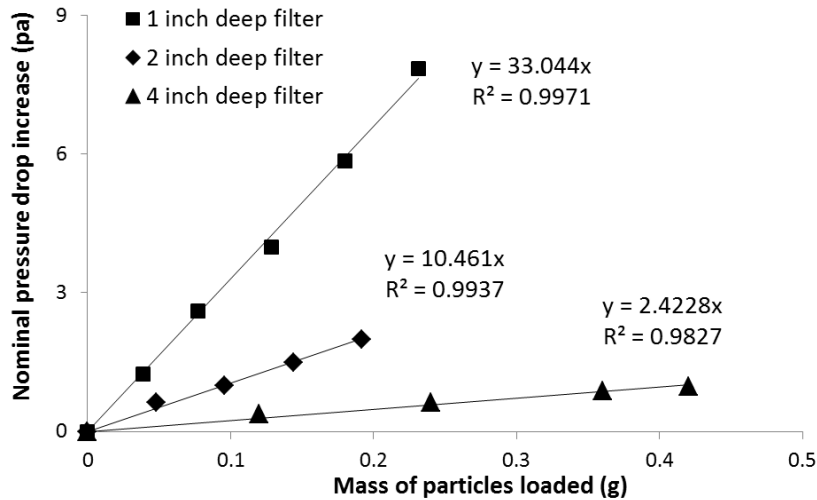


Figure II-17 Nominal pressure drop increase with respect to deposited mass of salt particles for single filters of different depths

II.4.8.4 Comparison of particles loading between MESAs and single filter

Since MESAs can significantly enhance initial filtration performance for salt particles, it is very important for us to investigate if they are still able to behave better during particles loading compared to single filters. Two types of filter (1 inch filter with 20 pleats and 2 inch filter with 15 pleats) were tested using MESAs (V shape and W shape), respectively.

As shown in Figure II-18, for both two types of filters, MESAs have much smaller increase of pressure drop compared to single filters at same deposited mass of salt particles. As I talked previously, MESAs can reduce filtration velocity and increase filtration media area simultaneously. And since these two parameters have positive effects on particles loading process, much more particles can be captured by MESAs without significant increase of pressure drop and therefore,

MESAs show higher salt particles loading capacity, which also suggests much longer filter life time compared to single filters.

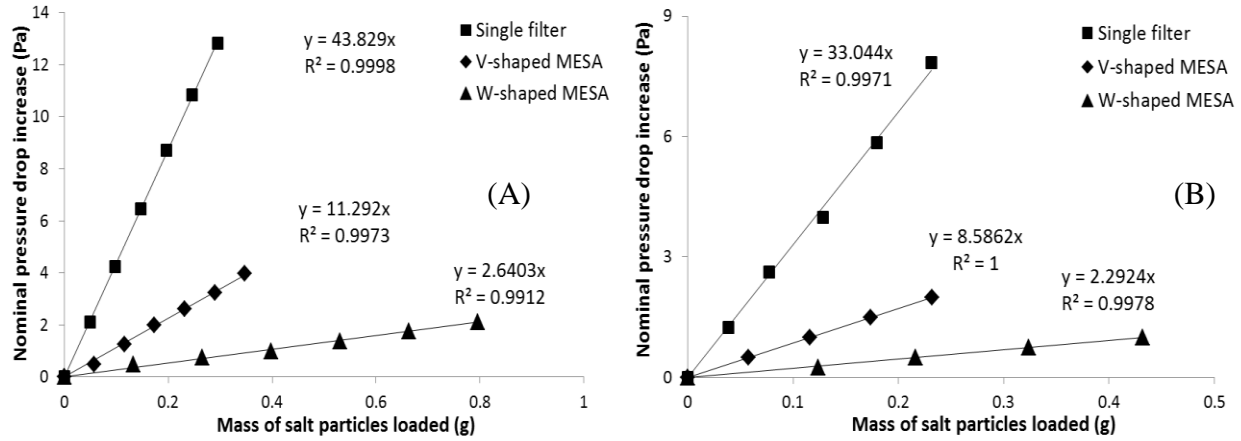


Figure II-18 Nominal pressure drop increase with respect to deposited mass of salt particles for single filter and MESAs (V-shaped and W-shaped): (A) 2 inch deep pleated filter, (B) 1 inch deep pleated filter

From all the results of different single filters and MESAs (V shape and W shape) above, what we can conclude is that mainly two parameters have effects on the particles loading process, one is filtration media area and the other one is filtration velocity. Filters with different pleat counts, depths and in different packaging configurations have different filtration media areas, which leads to different inner filtration velocity through the filter unit. Therefore, both of the two parameters affect the salt particles loading process simultaneously and can double the effect since filtration velocity is inversely proportional to filtration media area. This implies that if one filter is twice larger of filtration media area than the other filter, it can have four times lower increase of pressure drop at same deposited mass of salt particles, which is potentially able to have more or less four times higher particles loading capacity and longer filter life time at same air conditions.

Suggested by filter manufacturer, filter is usually assumed to be useful until pressure drop of 249 Pa (1 inch water) is reached and according to this, the maximum mass of salt particles loaded

could be calculated. Since the experimental concentration of salt particles is 4 times larger than real concentration within ocean environment [II.3], the time for the filters to reach the maximum pressure drop when they are applied to real ocean environment should be 4 times longer. Besides, with an average run time of 8 hours per day, the lifetime of both single filters and MESAs are able to be achieved and the summary is shown in Table II-2.

Table II-2 Comparisons of particles loading capacity and filter life time between single filter and MESAs (V-shaped and W-shaped): (A) 2 inch deep pleated filter, (B) 1 inch deep pleated filter

	Initial pressure drop (Pa)	Final pressure drop (Pa)	Particles loading capacity (g)	Filter life time (Days)
Single filter	81.3	249	3.9	6
V-shaped MESA	39.3	249	18.5	25
W-shaped MESA	29.6	249	83.1	110

	Initial pressure drop (Pa)	Final pressure drop (Pa)	Particles loading capacity (g)	Filter life time (Days)
Single filter	51.4	249	6.0	17
V-shaped MESA	25.4	249	26.0	75
W-shaped MESA	14.9	249	101.8	312

II.4.9 Comparison of compressor parasitic power of different filters

What is compressor parasitic power? Pressure drop across the filter causes a decrease in inlet pressure to the compressor creating a vacuum. The outlet pressure from the compressor is set by the operating pressure of SOFC. This increase in pressure drop ratio across the compressor leads to a decrease in compressor efficiency and an increase in compressor power. Both of these effects are able to cause an overall decrease in SOFC operating efficiency and performance. Therefore, the lower filter pressure drop is, the less compressor parasitic power will be. Figure II-19 shows the flow of air and power through SOFC system [II.28].

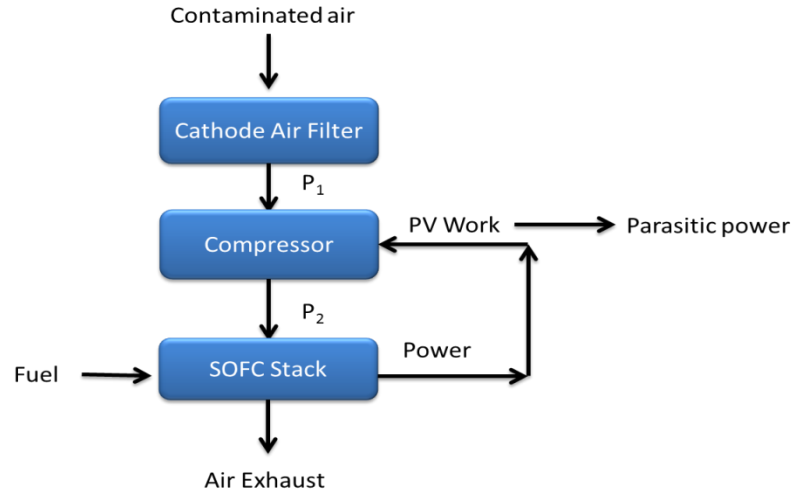


Figure II-19 SOFC energy balance showing the flow of air and power through the system

Usually, compressor parasitic power is calculated using Equation II.14.

$$P_B = \frac{\gamma}{\gamma - 1} \frac{0.371 T_a}{\eta} q_o \left[\left(\frac{p_b}{p_a} \right)^{\frac{\gamma - 1}{\gamma}} - 1 \right] \quad (\text{Eq II.14})$$

Where,

P_B is the power output (kW)

γ is the heat capacity ratio (1.4 for air)

T_a is the temperature of the gas entering the compressor (293 K)

p_a is the compressor inlet pressure, which depends on the pressure drop across the filter before the compressor

p_b is the compressor exit pressure, which is also inlet pressure of SOFC

η is the compressor efficiency (0.8)

q_o is the volume of gas compressed evaluated at 293 K and 1 atm pressure (m³/s)

SOFC's performance needs to be assessed for the full pressure drop range of cathode air filter over its life, not just when the filter is new. Filter pressure drop will increase over the

lifetime of the filter. If a filter is selected only based on the initial pressure drop, then the filter engineer can be expect a lower SOFC performance over the life of the filter or to be frequently changing filters in order to maintain the lower pressure drop required for normal SOFC performance. Therefore, it is very important to investigate compressor parasitic power when particles are loaded gradually.

In order to study this compressor parasitic power VS particles loading phenomenon, several parameters need to be assumed and determined, which is shown in Table II-3.

Table II-3 Compressor parasitic power estimation conditions

Temperature (K)	293 (Room temperature)
Air flow rate (ft ³ /min)	~1260
Inlet salt particle concentration (ppmw)	0.16
Stoichiometric ratio (λ)	2
Average voltage (V_c)	0.6
SOFC power output (KW)	~600
SOFC inlet pressure (inch water)	814 (2 atm)

In the table, air flow rate stands for the required oxygen flow rate to operate a fuel cell, which could be found by the number of faradays provided by a mole of oxygen. Through substitution and simplification, the flowing Equation II.15 is derived [II.28].

$$AirFlowRate = 1.82 \times 10^{-2} \times \lambda \times \frac{P_e}{V_c} \quad (Eq II.15)$$

Where λ is the stoichiometric ratio defined as the total amount of oxygen flow divided by the oxygen used. This equation can be used for all SOFCs regardless of size as an estimate for air flow rate requirements.

Since the pressure drop across the cathode air filter VS particles loading has already been obtained previously and equation for estimating compressor parasitic power is determined, compressor parasitic power during salt particles loading is able to be achieved and the results are demonstrated in Figure II-20 and 21.

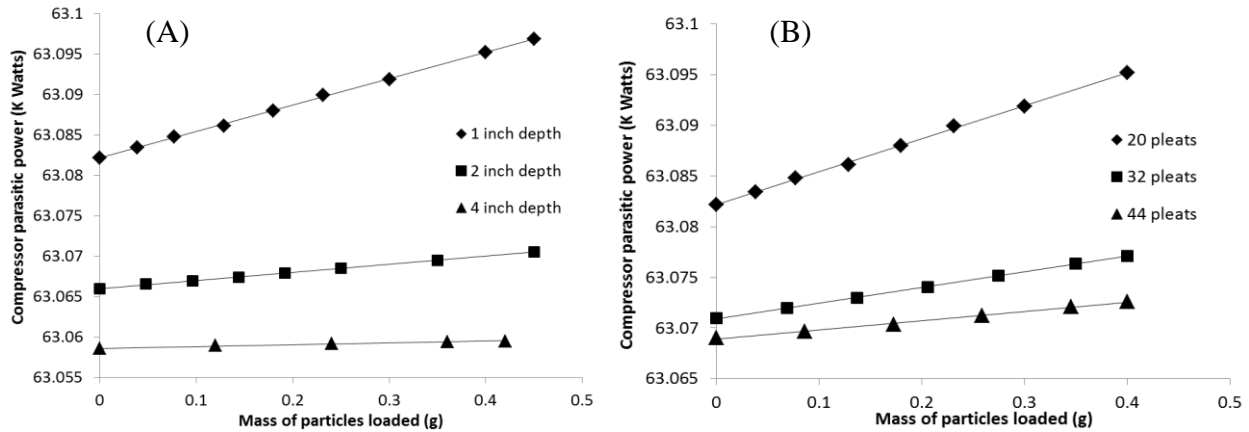


Figure II-20 Compressor parasitic power of single filters in different depths (A) and in different pleats (B)

As shown in Figure II-20, single filters in different depths and pleats have different compressor parasitic power during particles loading due to the filter configurations. Both two figures indicate that filter in higher depth and pleat causes lower compressor parasitic power. The reason can be explained by the larger filtration media area and lower inner filtration velocity through the filter, which is same to particles loading performance.

In Figure II-21, comparison of compressor parasitic power between single filter and MESAs (V shape and W shape) is demonstrated and from the results, what can be seen is that for both 1 inch and 2 inch depth filter, MESAs have much lower compressor parasitic power compared to single filter because of twice or four times bigger filtration area and significantly lower filtration velocity.

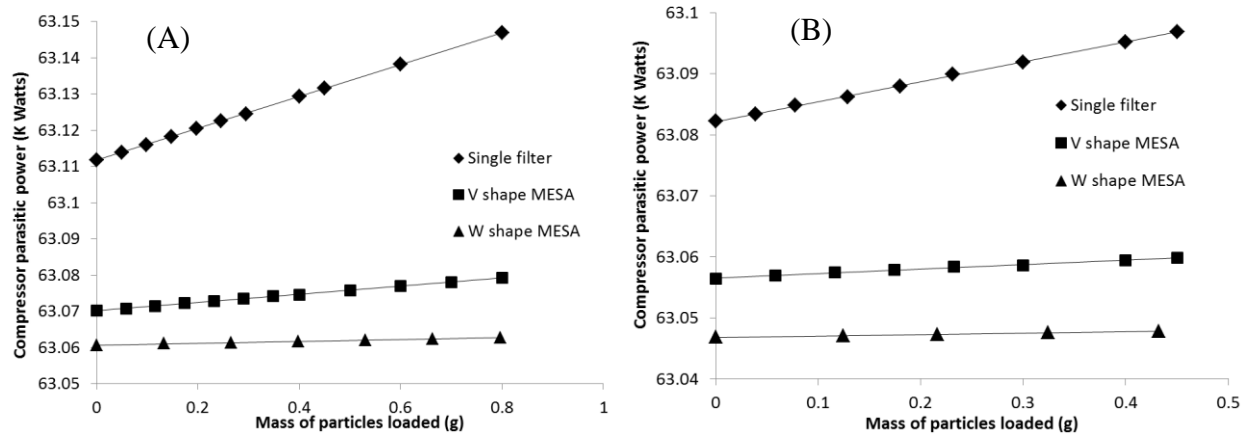


Figure II-21 Comparison of compressor parasitic power between single filter and MESAs (A) 2 inch depth, (B) 1 inch depth

Therefore, from the results above, what can be concluded is that single filters in higher depth and pleats could lead to less compressor parasitic power. And MESAs can decrease compressor parasitic power as well, which means they are able to enhance the SOFC power output and SOFC system performance. So MESAs could be a much better option when they are considered to be applied in real circumstances, like sea salt particles filtration.

According to the data in Table II-3, SOFC power output is calculated as around 600 KW using 315 fpm as air flow rate. And the compressor parasitic power is about 63 KW, which is about 10% of total SOFC power output. Thus, almost 89% of the power that SOFC generates could be used as power source for the ship and it is a legitimate number.

II.5 Conclusion

This work mainly focuses on sea salt particles filtration for SOFCs during ocean environment. Effects of different single filter parameters, such as filter depth and filter pleat count, are studied for evaluation of filter performance, including particles removal efficiency and pressure drop and particles loading capacity. Since both filter depth and filter pleat count affect filtration media area and inner filtration velocity, particles removal efficiency and pressure drop are different

according to the filtration mechanisms for particles in various sizes and pressure drop model of pleated filter respectively. The experimental results have demonstrated that for single filters with different pleats but in same depth, filter with more pleats shows better initial performance for small particles and vice versa for filter with less pleats. For single filters with same pleats but of different depths, initial performance of 1 inch deep filter is better for large particles and 2 inch deep filter is better for small particles. During salt particles loading and compressor parasitic power, filter in higher depth and with larger pleat count can entrap more salt particles and lower the increase of pressure drop due to the double effects of filtration media area and inner filtration velocity, which results in higher particles loading capacity and longer filter lifetime and less compressor parasitic power. According to various circumstances, filter with different parameters can be selected to achieve the optimal filtration performance and particles loading performance as well.

Meanwhile, Multi-Element Structured Arrays (MESAs) designed by our research group were tested as well and the results have shown significantly higher initial filtration performance and much longer filter lifetime compared to single filters due to their larger filtration media area and lower inner filtration velocity through the filter units. Also, MESAs have shown that they could lead to less compressor parasitic power, which can enhance SOFC system performance. Therefore, it can be concluded that MESAs are potentially able to be applied as a new removal system of sea salt particles for SOFCs during ocean platforms.

II.6 References

- [II.1] Yan, W. M., Chu, H. S., Liu, Y. L., Chen, F. L. and Jang, J. H. (2011). Effects of chlorides on the performance of proton exchange membrane fuel cells. *International Journal of Hydrogen Energy* 36:5435-5441.
- [II.2] Jing, F. N., Hou, M., Shi, W. Y., Fu, J., Yu, H. M., Ming, P. W. and Yi, B. L. (2007). The effect of ambient contamination on PEMFC performance. *Journal of Power Sources* 166:172-176.
- [II.3] Majchrzak, R., Cole, T. and Cervi, M. (1998). U.S. Navy Sea Salt Particle Removal Systems, Carderock Division Naval Surface Warfare Center.
- [II.4] Kellar, J. J. (2006). *Functional Filters and Nanoscale Minerals: New Markets/New Horizons*. Society for Mining Metallurgy, Littelton, Colo.
- [II.5] Harris, D., Cahela, D. and Tatarchuk, B.J. (2001). Wet layup and sintering of metal-containing microfibrinous composites for chemical processing opportunities. *Composites part A: Applied Science and Manufacturing* 32:1117-1126.
- [II.6] Sothen, R. A. (2009). *Novel Packaging Designs for Improvements in Air Filter Performance*, in Department of Chemical Engineering, Auburn University.
- [II.7] Benesse, M., Le Coq, L. and Sollicc, C. (2006). Collection efficiency of a woven filter made of multifiber yarn: Experimental characterization during loading and clean filter modeling based on a two-tier single fiber approach. *Journal of Aerosol Science* 37:974-989.
- [II.8] Steffens, J. and Coury, J. R. (2007). Collection efficiency of fiber filters operating on the removal of nano-sized aerosol particles: I-Homogeneous fibers. *Separation and Purification Technology* 58:99-105.
- [II.9] Matteson, M. J. and Orr, C. (1987). *Filtration: Principles and Practices*. Marcel Dekker, Inc.

- [II.10] Brown, R. C. (1993). Particle capture by mechanical means, in: *Air Filtration - An Integrated Approach to the Theory and Application of Fibrous Filters*. Pergamon Press, 73-116.
- [II.11] Hinds, W. C. (1998). *Aerosol technology: Properties, Behavior, And Measurement of Airborne Particles*. John Wiley & Sons, Inc.
- [II.12] Fisk, W. J., Faulkner, D., Palonen, J. and Seppanen, O. (2002). Performance and Costs of Particle Air Filtration Technologies. *Indoor Air* 12:223-234.
- [II.13] Arnold, B.D., Matela, D. and Veeck, A. (2005). Life-cycle costing of air filtration. *ASHRAE Journal* 47:30-32.
- [II.14] Sothen, R. A. and Tatarchuk, B. J. (2008). A Semi-Empirical Pressure Drop Model: Part I- Pleated Filters. *Hvac&R Research* 14:841-860.
- [II.15] Bird, R. B., Stewart, W. E. and Lightfoot, E. N. (2007). *Transport Phenomena*. J. Wiley.
- [II.16] Sothen, R. A. and Tatarchuk, B. J. (2009). A Semi-Empirical Pressure Drop Model: Part II- Multi-Element Pleated Filter Banks. *Hvac&R Research* 15:269-286.
- [II.17] National Air Filtration Association (2007). *NAFA Guide to Air Filtration*. National Air Filtration Association, Virginia Beach, VA 23471.
- [II.18] Stenhouse, J.I.T. and Trottier, R. (1991). The Loading of Fibrous Filters with Submicron Particles. *Journal of Aerosol Science* 22:777-780.
- [II.19] Brown, R. C. (1993). Effects of loading, in: *Air Filtration - An Integrated Approach to the Theory and Application of Fibrous Filters*. Pergamon Press, 201-236.
- [II.20] Zelenyuk, A., Cai, Y. and Imre, D. (2006). From Agglomerates of Spheres to Irregularly Shaped Particles: Determination of Dynamic Shape Factors from Measurements of Mobility and Vacuum Aerodynamic Diameters. *Aerosol Science and Technology* 40: 197-217
- [II.21] ASHRAE 52.2 (1992). *Method of Testing General Ventilation Air-cleaning Devices Used for Removal Efficiency by Particle Size*, American National Standard, Atlanta, GA, USA.

- [II.22] Karwa, A. N. and Tatarchuk, B. J. (2012b). Aerosol filtration enhancement using carbon nanostructures synthesized within a sintered nickel microfibrinous matrix. *Separation and Purification Technology* 87:84-94.
- [II.23] Boulard, D. and Renoux, A. (1998). Stationary and Nonstationary Filtration of Liquid Aerosols by Fibrous Filters, in: Spurny, K.R.(Ed.). *Advances in Aerosol Filtration*, Lewis, 53-83.
- [II.24] Moelter, W. and Fissan, H. (1998). Quality assurance of glass fiber filter media, in: Spurny, K. R. (Ed.). *Advances in Aerosol Filtration*. Lewis, 259-282.
- [II.25] Moelter, W. and Fissan, H. (1997). Structure of a high efficiency glass fiber filter medium. *Aerosol Science and Technology* 27:447-461.
- [II.26] Brown, R. C. (1993). Macroscopic behavior of filters, in: *Air Filtration - An Integrated Approach to the Theory and Application of Fibrous Filters*. Pergamon Press, 1-11.
- [II.27] Thomas, D., Penicot, P., Contal, P., Leclerc, D. and Vendel, J. (2001). Clogging of fibrous filters by solid aerosol particles –Experimental and modeling study. *Chemical Engineering Science* 56:3549-3561.
- [II.28] Kennedy, M. D., Cahela, R. D. and Tatarchuk, J. B. (2007). Fuel cell cathode air filters: Methodologies for design and optimization. *Journal of Power Sources* 168: 391-399.

Chapter III Comparison of filtration performance for sea salt particles between nonwoven and woven activated carbon fiber media

III.1 Abstract

Presence of sea salt particles (SSP) and other gaseous contaminants in the ocean environment could cause severe degradation to performance of Solid Oxide Fuel Cells (SOFCs), which are being considered for use as power sources on ships. Therefore, removal of these particles and gas impurities from the air stream fed into fuel cells has become an issue of major concern. In this study, different activated carbon fiber media were tested for evaluation of performance for salt particles filtration, including pressure drop across the media and filtration efficiency and salt particles loading capacity. Sodium chloride (NaCl) solution (15% w/w) was applied to generate salt particles by being nebulized using an aerosol generator which can produce particles in the range of 100 to 2000 nm. Nonwoven activated carbon fiber media combined with polymer fibers and woven media made entirely of activated carbon fibers, such as knit and single weave, were both investigated in order to understand their different filtration performance for salt particles due to various media structures. Meanwhile, since relative humidity (RH) is significantly higher compared to land during the ocean environment, it could affect the filtration performance, including both pressure drop and particles removal efficiency. Therefore, effect of various RHs on filtration performance was experimentally investigated as well. The results and discussion will be presented in depth.

III.2 Introduction

Currently, Solid Oxide Fuel Cells (SOFCs) are being considered to be applied as power source for ships due to the high energy efficiency and less waste emission. However, during the ocean environment, air always contains several contaminants, including both particulates and gaseous impurities, like SO₂ and VOC. For particulates, they are mainly composed of salt particles, which are generated mainly from wind stresses over whitecaps or from either the wake or the bow spray by the ship itself. These sea salt particles could cause severe degradation to the performance of SOFCs, such as clogging of the finely divided and highly tortuous flow channels or corrosion of the fuel cells [III.1,III.2]. Therefore, removal of salt particles before flowing into fuel cell systems is an essential concern. In the past decades, there have been a lot of achievements in particles filtration studies, including different flow patterns of particles through filter media and different models for particles filtration mechanisms [III.3]. But they mainly focused on the study of particles themselves, like how they move and how they are captured inside the media. In this work, filter media structure is the major concern. Woven and nonwoven media are currently two most widely applied types of filter media. Due to their different structures, they can show different filtration performances for salt particles. And to evaluate the advantages and disadvantages of each type of media is of high significance when the media are applied in real circumstances.

The aim of this study is to investigate the differences of filtration performance for salt particles between nonwoven and woven filter media. Activated carbon fibers are used in this work as the main material since they have shown great capability to remove particles and gaseous contaminants simultaneously [III.4-7]. Activated carbon fibers are usually made from synthetic fibers, like rayon or PAN, via a high-temperature carbonization and activation process. They are microporous (pore sizes of about 10Å) with large specific surface area ranging from 700 to 3000

m²/g and have much smaller density compared to other materials, such as polymer and metal fibers. Due to these features, activated carbon fibers have been used for air filtration since the end of 1970s [III.4].

During this study, filtration experiments were carried out for both nonwoven and woven activated carbon fiber (ACF) media, including pressure drop tests across the filter media, particles removal efficiency measurements and particles loading capacity estimations. Comparisons of performance between nonwoven and woven ACF filter media were made according to the experimental data and estimation results. Moreover, due to much higher relative humidity (RH) in the ocean environment, the effect of RH on the filtration performance for salt particles is highly important and necessary to be studied [III.1]. Different RHs were selected and filtration efficiency tests were conducted in order to evaluate the filtration performance of ACF filter media under different relative humidities.

III.3 Experimental

III.3.1 Materials

Activated carbon fibers with diameter 7 to 8 μm and length of 3 mm were obtained from TOYOBO, Japan. Bi-component polyester fibers with diameter 13 μm and length of 3-6 mm from KOSA, and cellulose fibers from Intramicron Inc., (Auburn, AL) were applied as media binders. Woven activated carbon fiber media, including Zorflex ® knit and Zorflex ® single weave, and nonwoven activated carbon fiber felt from TOYOBO, Japan, were used in experiments without further treatment.

III.3.2 Nonwoven activated carbon fiber media preparation (Wet-laid method)

Activated carbon fibers were dispersed in water using a blender. Since ACFs are lack of hydrogen and oxygen, it is impossible for them to form a strong media by hydrogen bonding [III.8]. Thus, bi-component polyester fiber and cellulose fiber were used as binders in order to

provide strong bonding for ACF media via melting process. To improve the dispersion of polyester fibers in water, 1-2 ml Cruwik-SYN was added as well. The dispersion of activated carbon fibers and binders was transferred to a 16 cm diameter TAPPI hand-sheet former to create preform of nonwoven ACF media [III.9]. The preform was removed and dried at 140-150 °C in air for 15-20 min in order to get rid of water and melt the polyester fiber to form a strong nonwoven activated carbon fiber (ACF) filter media. Figure III-1 demonstrates some pictures of this wet-laid method for nonwoven media preparation. The samples that need to be tested were punched out from the final form of media using a steel circular punch. Each circular sample was about 5.3 cm in diameter. Table III-1 below shows the details of five nonwoven ACF filter media that are manufactured using wet-laid method.

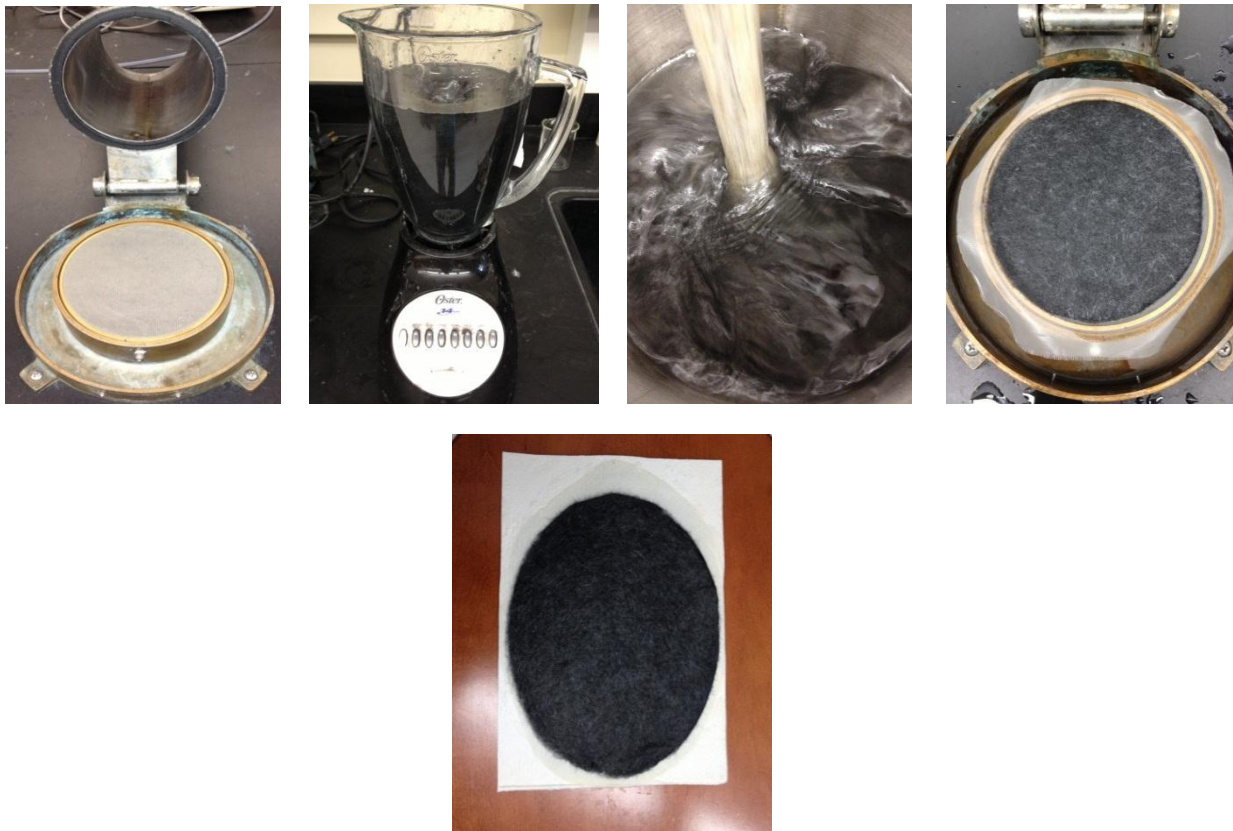


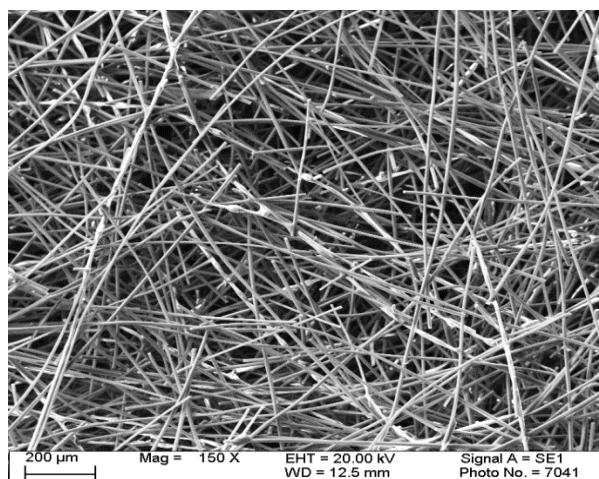
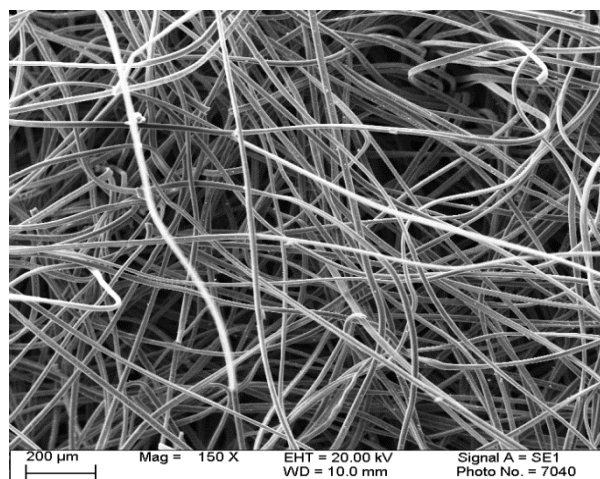
Figure III-1 Wet-laid activated carbon fiber (ACF) media manufacturing

Table III-1 Thickness, SVF of different fibers and total voidage of nonwoven ACF filter media

	Thickness (mm)	SVF of activated carbon fiber (% , cal.)	SVF of polyester fiber (% , cal.)	SVF of cellulose (% , cal.)	Voidage (% , cal.)
Nonwoven ACF-I	3.8	16.50	2.57	N/A	80.93
Nonwoven ACF-II	2.2	14.25	2.21	N/A	83.54
Nonwoven ACF-III	3.7	8.47	5.27	N/A	86.26
Nonwoven ACF-IV	3.4	18.44	2.87	1.09	77.60
Nonwoven ACF-V	1.3	24.11	1.88	2.37	71.64

III.3.3 Structures of ACF filter media

Nonwoven and woven ACF filter media have different media structures due to their various manufacturing processes. In order to investigate this difference, pictures and SEM images of both nonwoven and woven ACF media are shown in Figure III-2 and III-3. As shown in the figure, two nonwoven media, ACF felt and Nonwoven ACF-I, have shown similar media structure, which gives homogeneous pore structure and is called inter-fiber pore. Nonwoven ACF-I media is made of activated carbon fiber and polyester fiber using wet-laid method described earlier. However, from Figure III-1, two woven ACF media, ACF knit and ACF single weave, have demonstrated extremely different media structure compared to nonwoven ACF media. What can be seen is that woven filter media have two various pore structures, which are inter-fiber pore and inter-yarn pore.



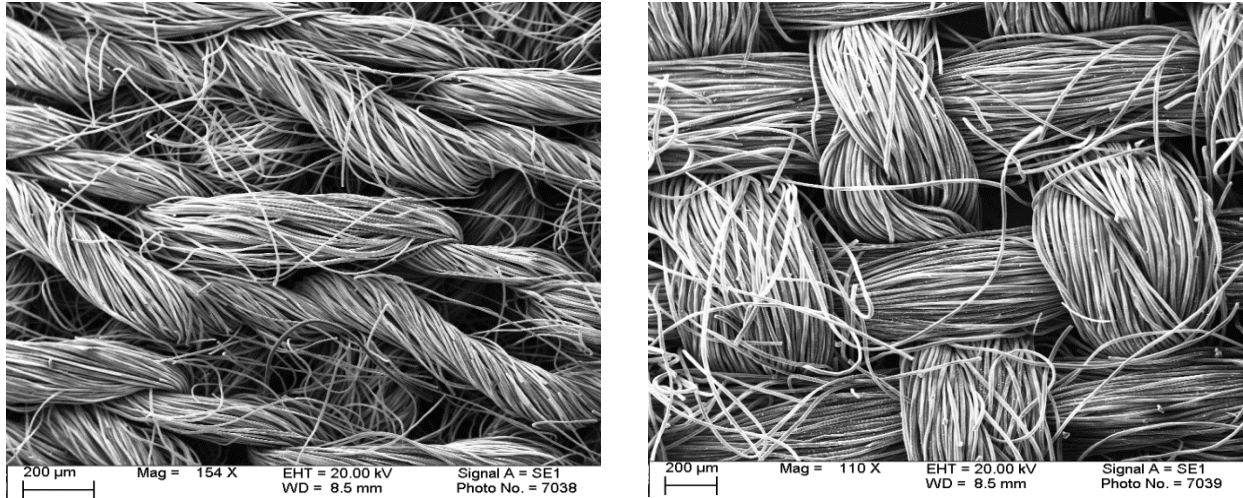


Figure III-2 SEM images of two nonwoven and two woven ACF filter media

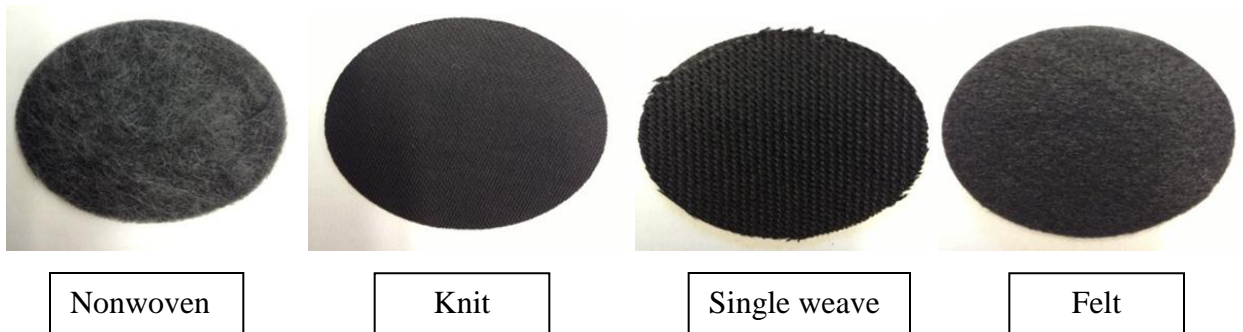


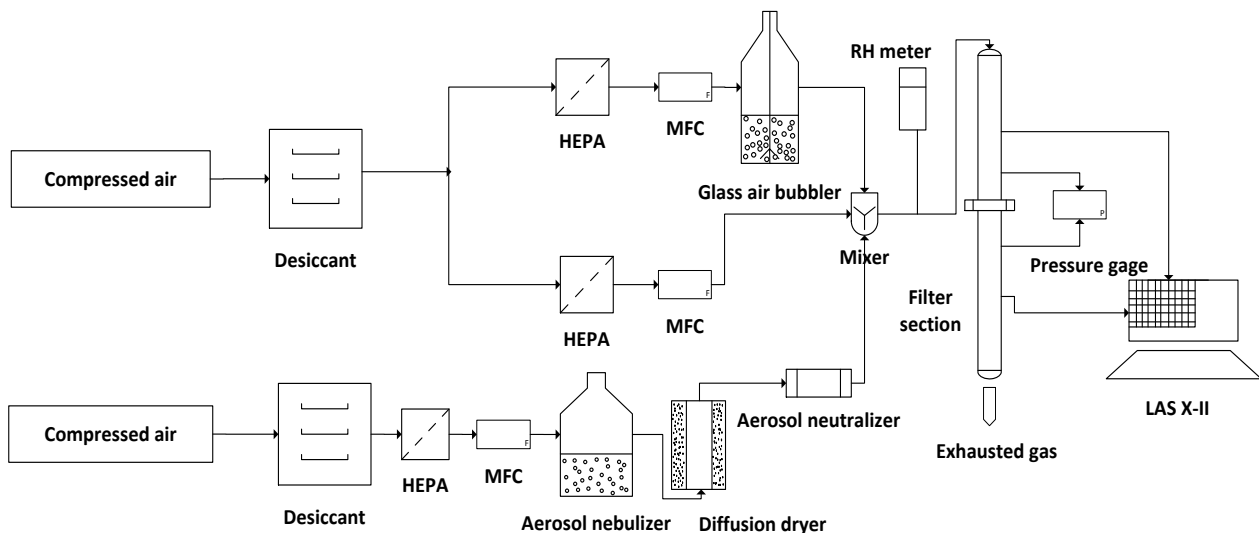
Figure III-3 Pictures of nonwoven and woven ACF filter media

Moreover, inter-yarn pore in woven media is much larger than inter-fiber pore, which makes woven ACF filter media more complicated when used in particulates filtration compared to nonwoven ACF media. The details and comparisons will be presented in later results and discussions.

III.3.4 Filtration efficiency and pressure drop testing setup

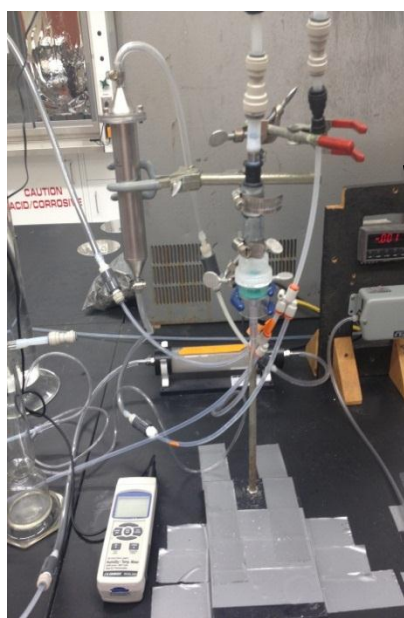
Filtration performance of both nonwoven and woven activated carbon fiber filter media, including pressure drop across the filter media, particles removal efficiency and particles loading capacity, were tested using the setup shown in Figure III-4. Compressed air was passed through silica gel desiccant to get rid of moisture and HEPA filter to eliminate any contaminants in the air stream. There were three main streams flowing in the whole setup. First one was nebulizing air

stream that was applied to generate particles from salt solution. Sodium chloride (NaCl) solution (15% (w/w)) was used in all the experiments. The flow rate of nebulizing air stream was controlled at 1.2-1.5 LPM by mass flow controller (MFC). A polydispersed aerosol nebulizer from Devilbiss was selected after trying several different ones in order to get constant performance all the time. After the nebulizer, the wet sodium chloride particles were passed through a diffusion dryer to remove the water from the wet particles. Diffusion dryer (DD 250) from Air Techniques International (ATI) was used due to its large flow rate and simple operation. Since the particles have some static charges from nebulizing, an aerosol neutralizer body (Model-9000) from Brechtel manufacturing, Inc and two Polonium-210 strips from NRD, LLC were followed to neutralize the particle charges into Boltzman equilibrium. The second air stream was passed through a large glass bubbler with deionized water to obtain saturated air (100% RH) and meanwhile, the third air stream was used to control the relative humidity of the mixed air stream by varying the flow rates ratio of these two air streams. Afterwards, the mixture of all three streams flew into the main filter section, which was composed of a stainless steel pipe (1 inch ID) and flanges since particles don't attach to the walls of stainless steel pipe. The media sample was placed between two flanges with foam gaskets for sealing purpose.

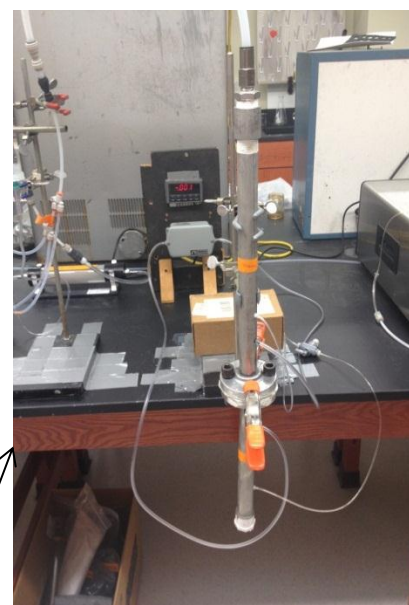




Experimental setup



Salt Particles generator



Filter media section

Figure III-4 Experimental setup for filtration performance testing

The pressure drop across the filter media was tested using a pressure transducer from Omega at different air flow rates. As for the filtration efficiency, a particle counter named Laser Aerosol Spectrometer (LAS-XII) from TSI was applied for all the filtration efficiency measurements. This spectrometer is able to detect particles ranging from 90 to 7500 nm in diameter within 99 channels. The sample flow rate can be varied from 10 sccm to 100 sccm, during

which 50 sccm was selected for all the tests. In this work, filtration velocity was set as 50 cm/s unless notified otherwise. The concentration of salt particles was around 73,000 per 50 cm³ of air with 1460 particles per cm³ of air. For each test, 8 to 10 samples for both upstream and downstream were carried out with 1 min each. Then, average efficiency was calculated using formula below according to ASHRAE 52.2 Standard [III.10]:

$$E = \frac{n_{up} - n_{down}}{n_{up}} \times 100\% \quad (\text{Eq III.1})$$

Error bars with 95% confidence interval was also calculated using Excel 2010 and reported in the filtration efficiency data. In all tests, at least 3 media samples were measured to check for the repeatability of data. As for salt particle nebulizer applied in this work, size distribution of particles generated is measured and the result is given in Figure III-5. According to the distribution, mean diameter of NaCl particles generated is 285 nm.

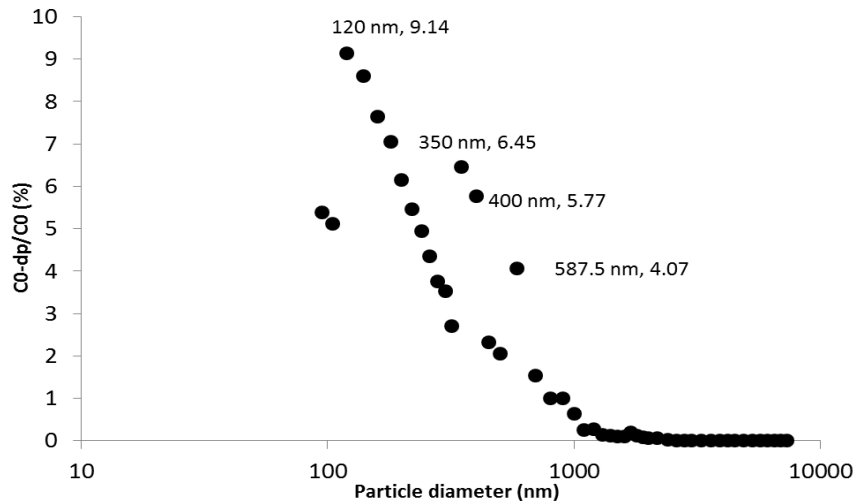


Figure III-5 Size distribution of salt particles generated

III.4 Results and discussion

III.4.1 Filtration efficiency of ACF filter media

LAS-X II spectrometer is used in this work to measure the number of salt particles before and after the filter media. In order to determine if there is deviation in sample counts between the two locations, a blank test is carried out with no filter media. Four samples before and four samples (total eight samples) after are measured and the results are plotted in Figure III-6. As shown in the figure, the two locations show similar counts when monitoring a baseline concentration without the presence of filter media. Therefore, we can conclude that the filtration efficiency data obtained later in this work is accurate and believable.

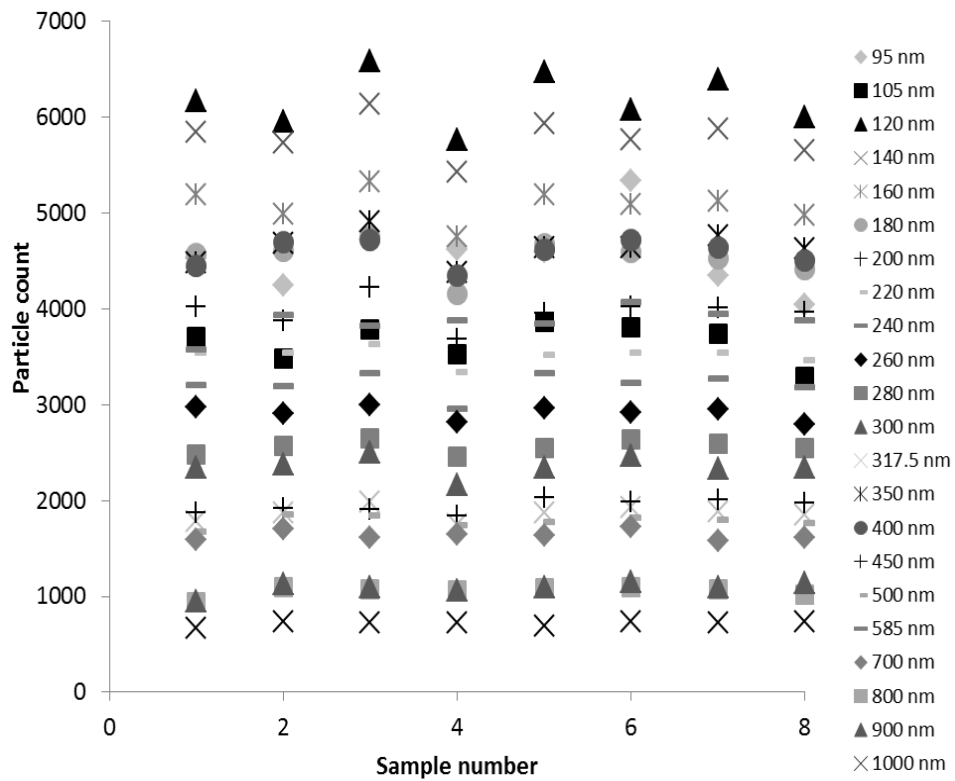


Figure III-6 Comparison of particle count upstream and downstream

III.4.1.1 Effect of filtration velocity on filtration efficiency

Several different kinds of parameters could affect filter media performance, including not only media properties, such as thickness and solid fraction but also air properties, like filtration velocity passing through the media. Figure III-7 shows the change in filtration efficiency at different filtration velocities for nonwoven ACF-I media. As shown in the figure, the filtration efficiency increased with increase in face velocity for large particles (larger than ~300 nm). This is the same trend which is seen for inertial impaction dominant regime under varying filtration velocities. From the model of inertial impaction, we can see that higher face velocity leads to larger Stokes number and greater filtration efficiency. For particles smaller than 300 nm, the filtration efficiency decreased with increase in face velocity which is the same trend for diffusion dominant regime, which can also be seen from the Brownian diffusion model.

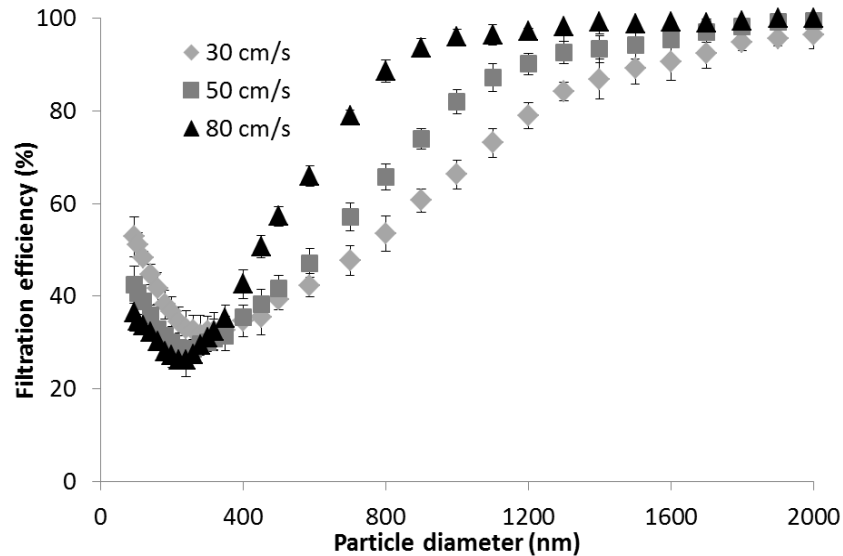


Figure III-7 Effect of filtration velocity on salt particles filtration efficiency

In addition, from Figure III-7, we can find that there is an intersection point, which stands for the interception filtration efficiency. Interception is the only mechanism which is not dependent on face velocity [III.4]. So the crossover of the efficiency curves at different velocities gives the efficiency independent of filtration velocity. And for this media sample, the

interception filtration efficiency is about 30 %. Moreover, the most penetrating particle size (MPPS) lightly shifted toward small particle size with the increase of face velocity, from 280 nm at 30 cm/s to 220 nm at 80 cm/s, which is consistent with the results that R.C. Brown achieved (can be seen in Figure I-5). The details of the result are shown in Table III-2.

Table III-2 MPPS and minimum efficiency at different face velocities

Face velocity (cm/s)	Pressure drop (Pa)	MPPS (nm)	Minimum efficiency (%)
30	198.5	280	31.70
50	329.9	240	28.44
80	547.8	220	26.16

III.4.1.2 Comparison of filtration efficiency between nonwoven and woven ACF filter media

Nonwoven and woven ACF media are manufactured in different procedures, which could lead to various media structures and different particles removal efficiencies. Two different types of woven ACF media (single weave and knit) and three different nonwoven ACF media (nonwoven ACF-I, nonwoven ACF-II and ACF felt) were tested at same conditions and results from experiments are shown in Figure III-8.

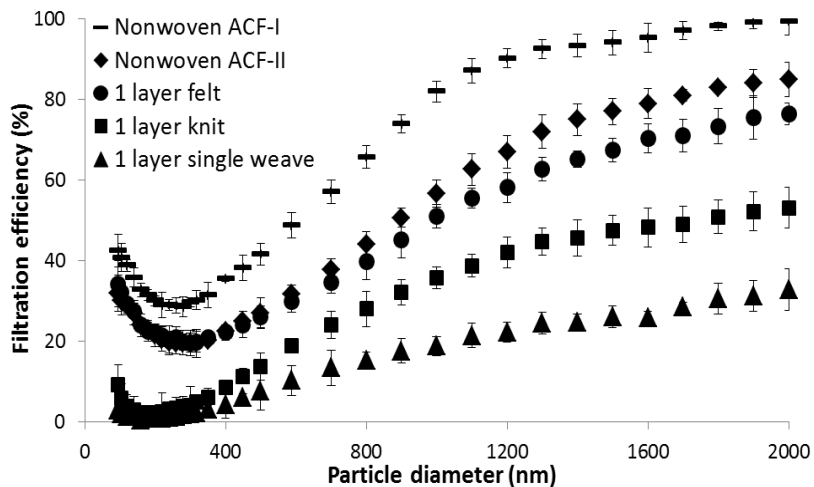


Figure III-8 Salt particles filtration efficiency with respect to particle diameter for 1 layer nonwoven and woven ACF filter media (Data reported for face velocity of 50 cm/s)

As can be observed, filtration efficiency curves for all ACF media tested are in accordance with theoretical filtration study. In diffusion dominant regime, efficiency increases with smaller particles and in inertial impaction dominant regime, efficiency increases with larger particles [III.11,III.12]. MPPS, which stands for most penetration particle size, exists in each curve and it suggests that no filtration mechanism is strong enough to remove particles around that size [III.11]. Moreover, three nonwoven ACF media have shown significantly higher filtration efficiencies compared to other two woven ACF media, which is due to the homogenous pore structure (inter-fiber pore) of nonwoven media and the smaller pore diameter. Woven media have two different pore structures, inter-fiber pore and inter-yarn pore, during which inter-yarn pore is much larger. Due to this, air prefers to flow through these larger inter-yarn pores, which leads to more salt particles penetrating the woven filter media. Meanwhile, since the interstitial filtration velocity inside the inter-yarn pores is higher than other parts of the filter media, Brownian motion of small particles is decreased according to diffusion mechanism which results in lower filtration efficiency [III.13]. It can be further verified from Figure III-8 as well that MPPS decreases for woven ACF media compared to nonwoven ACF media, from 280 nm to 180 nm. This suggests that diffusion of small particles is indeed weakened for woven media due to the higher interstitial velocity through inter-yarn pores.

However, nonwoven ACF media is much thicker than knit and single weave ACF media, which is another reason that nonwoven media have higher filtration efficiency. In order to further understand the effect of media thickness, knit and single weave ACF media in different layers were tested as well. As shown in Figure III-9, filtration efficiencies of both knit and single weave ACF media are becoming higher with the increase of media layers. For knit ACF media, 3 layers of media shows higher filtration efficiency for large particles compared to 1 layer of nonwoven ACF

felt, which suggests the decrease of media pore volume after stacking three layers together and increase of particles inertia due to higher interstitial filtration velocity compensated the effect of larger inter-yarn pore structure. For small particles, 1 layer ACF felt has higher filtration efficiency due to lower filtration velocity inside inter-fiber pores, which results from stronger Brownian motion. However, for single weave ACF media, 3 layers of media still shows lower filtration efficiency than 1 layer ACF felt for both small and large particles, which can be explained by the fact that significantly larger inter-yarn pores negated the effect of increase of media thickness and higher interstitial filtration velocity. Meanwhile, we can see that MPPS of nonwoven ACF media is still larger compared to all other woven ACF media. This indicates even if stacking several layers of woven ACF media together, they still have higher interstitial filtration velocity inside the pores compared to nonwoven media, which leads to lower Brownian motion of small particles.

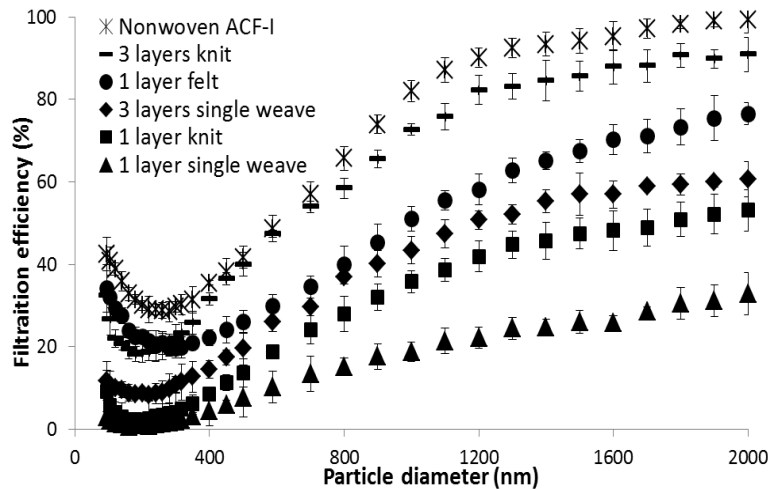


Figure III-9 Salt particles filtration efficiency with respect to particle diameter for 1 layer nonwoven ACF filter media and woven ACF filter media in different layers (Data reported for face velocity of 50 cm/s)

III.4.1.3 Filtration efficiency of activated carbon particles (ACP) entrapped nonwoven media

The main reason that activated carbon is applied in this study is due to the porous structure which can be used to adsorb gaseous contaminants in the air as well. Besides activated carbon fiber (ACF), activated carbon particles (ACP) can also be entrapped into nonwoven filter media. In order to evaluate if activated carbon particles could increase the filtration performance of nonwoven media for salt particles like activated carbon fiber (ACF), activated carbon particles (ACP) entrapped nonwoven filter media were manufactured using wet-laid method as described previously. Three different amounts of activated carbon particles (Mesh size 80×140) were selected, 2g, 4g and 6g, and experiments on filtration efficiency were carried out at 50 cm/s and dry air condition. The details of three tested filter media are listed in Table III-3 and the experiment results are shown in Figure III-10.

Table III-3 Details of three activated carbon particles entrapped nonwoven filter media

	Mass of AC (g)	Mass of polymer fiber (g)	Thickness (mm)	Volume fraction of AC (%)	Volume fraction of polymer (%)	Voidage (%)
Media 1	2	5	1.9	5.98	12.83	81.19
Media 2	4	5	2.2	10.33	11.08	78.59
Media 3	6	5	2.5	13.63	9.75	76.62

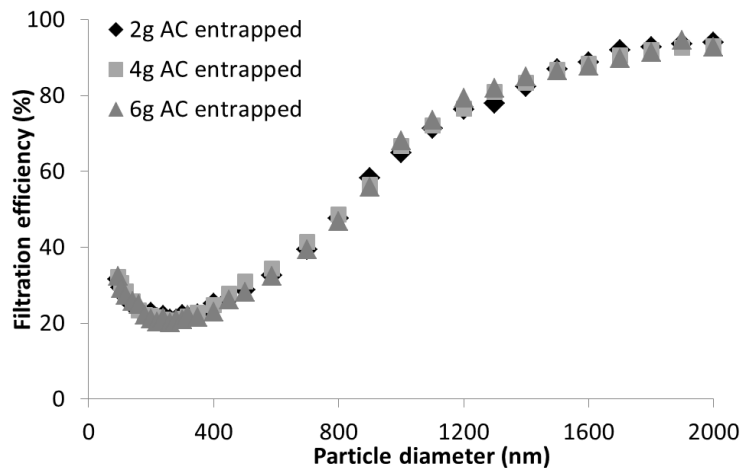


Figure III-10 Filtration efficiency of activated carbon particles entrapped nonwoven filter media

As shown in Figure III-10, three filtration efficiency curves are almost identical with each other, which indicates that activated carbon particles have nothing to do with salt particles filtration. And compared to same mass of activated carbon fiber (ACF) entrapped nonwoven media, activated carbon particles (ACP) entrapped nonwoven media have shown smaller filtration efficiency, which is because that ACP could not be used to entrap particles like ACF. Besides, after entrapping activated carbon particles, pressure drop of media is increased and is shown in Table III-4. Therefore, what we can find is that activated carbon particles (ACP) could not improve filtration performance of nonwoven filter media for salt particles, which is different with activated carbon fibers.

Table III-4 Pressure drop of activated carbon particles entrapped nonwoven filter media

	Pressure drop (Pa)
2g AC	189.2
4g AC	214.9
6g AC	256.5

III.4.2 Pressure drop across ACF filter media

III.4.2.1 Pressure drop across nonwoven ACF media

Pressure drop corresponds directly to the energy consumption as it is indicative of the work done by pushing air through the filter media [III.14,III.15]. Higher pressure drop will cost more energy. Thus, pressure drop across filter media is another important parameter that needs to be considered. Several popular models have already been used for estimating pressure drop across void structures, like Ergun equation, which is quite useful and accurate when used to describe pressure drop over a packed column full of particles [III.16]. However, it has some limits for porous media pressure drop estimation since it did not include the form drag losses. A porous media permeability (PMP) model derived previously by Donald R. Cahela from our research group has shown good estimation of pressure drop for nonwoven porous media. PMP equation combined

viscous loss, inertial loss, friction loss and form drag loss terms together, and is shown in Equation III.2 [III.17, III.18].

$$\frac{\Delta P}{L} = 72 \frac{\mu v}{(\phi D)^2} \frac{c^2}{(1-c)^3} \frac{\tau^2}{\cos^2 \theta} (1 + X_{fd}) + 6 \frac{\tau^3}{\cos^3 \theta} \frac{\rho v^2}{2(\phi D)} \frac{c}{(1-c)^3} (C_f + \frac{C_{FD}}{4} (1-c))$$

(Eq III.2)

Where $\tau = (\frac{2+c}{c})$, $X_{fd} = \frac{(1-c)^2}{12c}$ and $C_{FD} = C_D - C_f$

In the equation, μ is air viscosity, v is filtration velocity, c is fiber solid fraction, Φ is shape factor of fiber, θ is flow path angle, C_f is coefficient of friction, C_D is coefficient of drag and C_{FD} is coefficient of form drag.

However, there is a lack of a reliable experimental method to measure the flow path angle θ for different materials and thus, some modification needs to be done for PMP equation to make it applicable for various materials, including activated carbon fiber and polyester fiber and their combination. The modified PMP equations for both single material and combination are shown in Equation III.3 and Equation III.4.

$$\frac{\Delta P}{L} = A \frac{\mu v}{(\phi D)^2} \frac{c^2}{(1-c)^3} \tau^2 (1 + X_{fd}) + B \tau^3 \frac{\rho v^2}{(\phi D)} \frac{c}{(1-c)^3} (C_f + \frac{C_{FD}}{4} (1-c)) \quad (\text{Eq III.3})$$

$$\frac{\Delta P}{L} = A \mu v \frac{c^2}{(1-c)^3} \tau^2 ((\sum \frac{x_i}{\phi_i D_i})^2 + x_{fd} \sum \frac{x_i}{(\phi_i D_i)^2}) + B \tau^3 \rho v^2 \frac{c}{(1-c)^3} (C_f + \frac{C_{FD}}{4} (1-c)) \sum \frac{x_i}{\phi_i D_i}$$

(Eq III.4)

The drag coefficient for a sphere in turbulent flow is approximately 0.6 and coefficient of friction is around 0.42~0.47 [III.19].

In Equation III-4, there are four variables, constant A, constant B, shape factor of ACF and shape factor of polyester fiber, that need to be determined. As for shape factor Φ

[III.20,III.21], it mainly accounts for the deviation of fiber shape from an ideal sphere ($\Phi=1$) [III.19] and can be calculated empirically by using Blake Kozeny equation [III.16], which is shown in Equation III.5. Shape factor Calculated shape factors for ACF and polyester fiber are shown in Table III-5.

$$\frac{\Delta P}{L} = 150 \frac{\mu v}{(\phi D)^2} \frac{c^2}{(1-c)^3} \quad (\text{Eq III.5})$$

Table III-5 Calculated shape factor for ACF and polyester fiber

Fiber types	Shape factor (Φ)
Activated carbon fiber (7 to 8 μm)	5.02
Polyester fiber	2.35

From the shape factor table, we can see that activated carbon fiber has significantly larger Φ compared to ideal sphere. The reason is that activated carbon fiber belongs to highly porous material which has significantly larger surface area, which causes it to be much different from the shape of ideal sphere.

For constants A and B, they need to be determined experimentally by fitting pressure drop data of one sample media into the modified PMP equation and verifying the accuracy of these two constants by applying them to fit the pressure drop data of other sample media. After trial and error, the determined constants A and B are 96 and 4.61, respectively. Therefore, the modified PMP equation for nonwoven activated carbon fiber media is shown in Equation III.6.

$$\frac{\Delta P}{L} = 96\mu v \frac{c^2}{(1-c)^3} \tau^2 \left(\left(\sum \frac{x_i}{\phi_i D_i} \right)^2 + x_{fd} \sum \frac{x_i}{(\phi_i D_i)^2} \right) + 4.6\tau^3 \rho v^2 \frac{c}{(1-c)^3} \left(C_f + \frac{C_{FD}}{4} (1-c) \right) \sum \frac{x_i}{\phi_i D_i}$$

(Eq III.6)

Pressure drop of three nonwoven ACF filter media (Details shown in Table III-1) were tested and the modified PMP model fitting results with RMS errors are shown in Figure III-8.

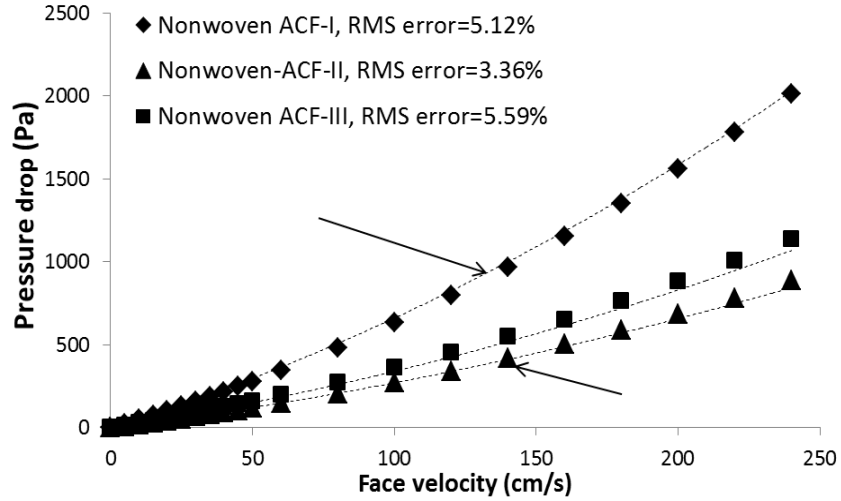


Figure III-11 Pressure drop with respect to face velocity for three nonwoven ACF filter media in different components

RMS error stands for Root Mean Square error [III.17], and is defined by Equation III.7. As can be seen in Figure III-11, modified PMP equation fits the experimental data quite well with three RMS errors less than 6%. So what we can conclude is that modified PMP equation could be applied to estimate pressure drop of nonwoven ACF media.

$$Error_{RMS} (\%) = \sqrt{\frac{\sum (\frac{\Delta P_{model} - \Delta P_{experimental}}{\Delta P_{model}})^2}{n}} \times 100 \quad (\text{Eq III.7})$$

III.4.2.2 Comparison of pressure drop between nonwoven and woven ACF media

Figure III-12 has shown pressure drops of different ACF filter media, including both woven and nonwoven media. As shown in Figure III-12, 1 layer of nonwoven ACF felt and Nonwoven ACF-II have lower pressure drops compared to 3 layers of knit and 3 layers of single weave ACF media due to the homogenous pore structure of nonwoven ACF media. Interstitial filtration velocity is much higher inside the inter-yarn pores and thus, it leads to higher air flow resistance across the woven ACF media. However, it can be seen that nonwoven ACF-I shows higher pressure drop than other woven ACF media, which results from its much larger thickness

compared to other woven media. Therefore, thickness plays an important role in pressure drop of filter media as well.

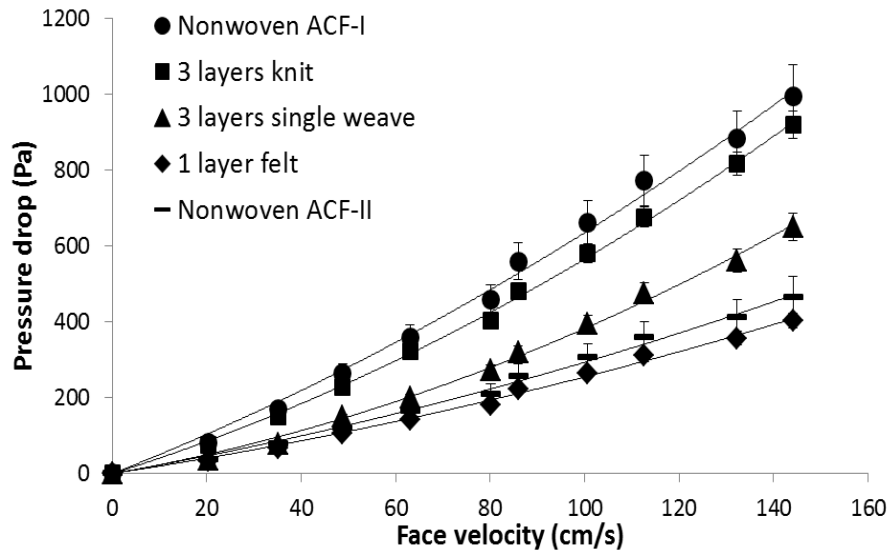


Figure III-12 Pressure drop with respect to face velocity for 1 layer nonwoven ACF filter media and 3 layers woven ACF filter media

In order to eliminate the effect of media thickness, pressure drop per media thickness was calculated. Table III-6 shows the brief summary of thickness and pressure drop per media thickness for different nonwoven and woven ACF media. As can be seen in Table III-6, compared to knit and single weave ACF media, pressure drops per media thickness of nonwoven ACF media are much lower, which indicates that nonwoven ACF media have smaller air flow resistance. This can be explained by the homogeneous pore structure of nonwoven media as well. Higher filtration velocity inside the inter-yarn pore consumes more energy work that needs to be done by pushing air through. Meanwhile, for woven ACF media, including both knit and single weave, increasing number of media layers results in higher pressure drop per thickness. This indicates that stacking several layers of woven media together could increase air flow resistance through the filter media, which is due to the extra resistance generated at the interface between different media layers.

Table III-6 Thickness and pressure drop per media thickness of 1 layer nonwoven ACF filter media and woven ACF filter media in different layers (Data reported for face velocity of 50 cm/s)

	ACF portion (%)	Number of layers	Thickness (mm)	Pressure drop (Pa)	Pressure drop per thickness (Pa/mm)
Nonwoven ACF-I	66.7	1	3.8	274.02	72.11
Nonwoven ACF-II	66.7	1	2.2	130.50	59.32
Knit	100	1	0.50	78.12	156.24
		2	1.0	163.84	163.84
		3	1.45	247.20	170.48
Single weave	100	1	0.5	42.80	85.60
		3	1.45	140.40	96.83
Felt	100	1	2.0	114.00	57.00

III.4.3 Quality factor of nonwoven and woven ACF filter media

Usually for filter media, higher particles removal efficiency indicates larger pressure drop. In order to judge if the filter is good on its filtration performance and suitable for real applications, a new term, quality factor (QF) [III.22,III.23] is defined to measure whether an increase in pressure drop is warranted by the increase in filtration efficiency. It is calculated as the ratio of fractional capture per unit thickness to the pressure drop per unit thickness [III.24,III.25].

$$QF = \frac{\gamma}{\Delta P / t} = \frac{\gamma t}{\Delta P} = \frac{\ln(1/P)}{\Delta P} = -\frac{\ln(1-E)}{\Delta P} \quad (\text{Eq III.8})$$

According to Equation III.8, what can be seen is that larger filtration efficiency and smaller pressure drop leads to higher quality factor, which also suggests better filter performance. And because of the logarithm from the equation, filtration efficiency plays a more significant role compared to pressure drop.

Quality factor changes gradually when particles are loaded by filter media. In this part of study, all quality factors calculated are based on initial performance of a clean filter media with no salt particles loaded. Figure III-13 presents quality factors of both nonwoven and woven ACF

media. As can be observed, all three nonwoven ACF media show higher quality factors compared to knit and single weave ACF media, which suggests that nonwoven ACF media are superior on filtration performance for salt particles. This can be explained by the higher filtration efficiency and lower pressure drop of nonwoven filter media resulting from the homogeneous pore structure. During previous discussions, the number of layers of woven media is an important parameter that needs to be considered as well. Filter media with more layers have both higher pressure drop and particles removal efficiency. Therefore, in order to understand the filtration performance of woven media in different layers, average quality factors of different ACF media in various layers were calculated and are shown in Table III-7.

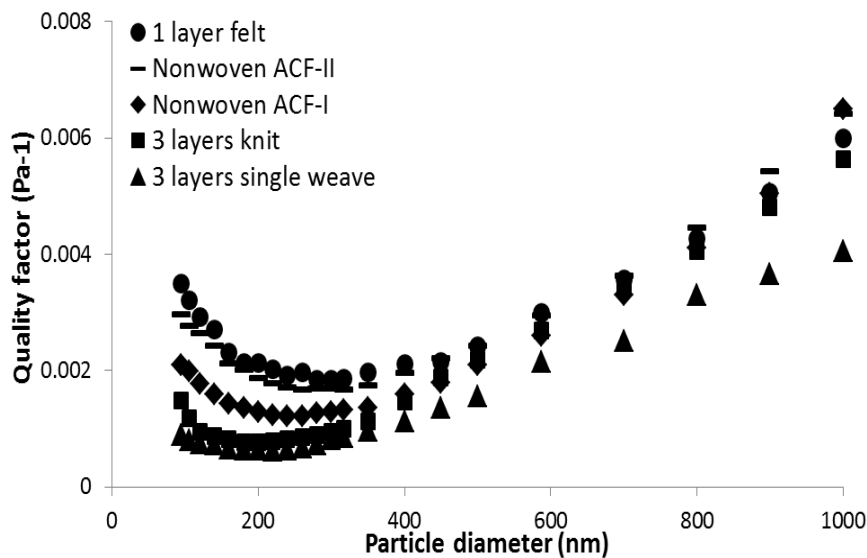


Figure III-13 Quality factor (cal.) with respect to particle diameter for 1 layer nonwoven ACF filter media and 3 layers woven ACF filter media (Data reported for face velocity of 50 cm/s)

As can be observed in Table III-7, for both knit and single weave ACF media, more layers results in higher quality factor and therefore, better media filtration performance for salt particles. This suggests that when stacking several layers of woven media together, the increase of filtration efficiency is able to compensate the effect of increase in pressure drop, which can be explained by

the transformation of media structure from inhomogeneous (double pore structure) to homogeneous (single pore structure). And what can be concluded from this is that the filtration performance of woven media in several layers is comparable to that of nonwoven media in one layer.

Table III-7 Comparison of average quality factor between different nonwoven and woven ACF filter media (Data reported for face velocity of 50 cm/s)

	Average quality factor (Pa⁻¹)
Nonwoven ACF-I	0.00216
Nonwoven ACF-II	0.00264
Felt	0.00277
3 layers knit	0.00179
2 layers knit	0.00156
1 layer knit	0.00150
3 layers single weave	0.00137
1 layer single weave	0.00132

III.4.4 Loading of salt particles using nonwoven and woven ACF media

In addition to pressure drop and initial filtration efficiency, particles loading capacity is another significant parameter that needs to be considered for evaluation of filtration performance [III.26]. With salt particles deposited into the filter media, filtration performance may change gradually, including both filtration efficiency and pressure drop across the media. Therefore, loading of particles should be investigated as well. Particles loading capacity is defined as the quantity of contaminant filter media can trap and hold before the maximum allowable back pressure or pressure drop is reached. Particles loading capacity is strongly related to life time of filter media, which is a significant character during filter media design [III.27]. Higher particles loading capacity results in longer useful life time and increasing the life time of filter media is the most crucial element in reducing filtration costs. However, filter media with larger particles

loading capacity always have lower particles removal efficiency. Therefore, an optimization can be developed according to both particles loading capacity and filtration efficiency.

Particles loading curve is used in this part of study as well and it is the nominal increase of pressure drop across the media vs total mass of deposited particles into the media. In order to achieve this curve, filtration efficiency tests and pressure drop measurements were both conducted. During salt particles loading process, pressure drop of media increased gradually with time and the value was recorded every 5 mins. According to filtration efficiency and inlet salt particle concentration, the number of salt particles entrapped by the filter media during 1 min can be calculated and as well as the total number of particles during 5 mins. The estimation method of mass of salt particles loaded is same to the one used in Chapter II [III.28,III.29].

In order to verify if this estimation method is correct, one sample ACF media was tested and estimation result was compared with experimental data obtained from analytical balance. In Figure III-14, lines stand for estimation result and dots stand for experimental data. As can be observed, for this sample ACF media, estimation result is able to fit with experimental data quite well. To demonstrate how well the two results match each other, Root Mean Square (RMS) error [III.17] was calculated and is shown in Figure III-8 as well. It shows that RMS error is less than 5%, which suggests that this estimation method for mass of particles deposited into the filter media is correct.

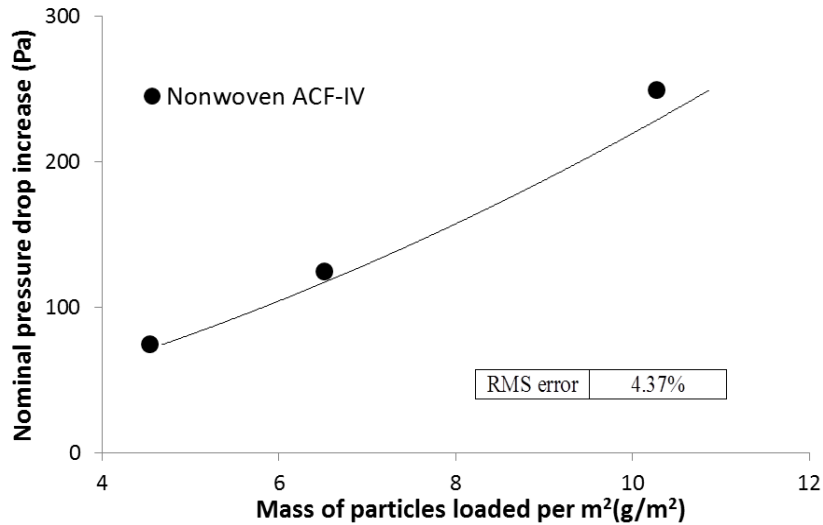


Figure III-14 Comparison of nominal increase of pressure drop with respect to deposited mass of salt particles per media area between experimental data and calculation result (Data reported for nonwoven ACF-IV filter media at face velocity of 50 cm/s)

Two nonwoven ACF filter media (Nonwoven ACF-I and nonwoven ACF-IV) and two woven ACF filter media (3 layers knit and 5 layers single weave) were tested for estimation of filter media loading performance for salt particles. As shown in Figure III-115, compared to nonwoven ACF media, knit and single weave ACF media have significantly higher increase of pressure drops at same deposited mass of salt particles, which is due to their inhomogeneous pore structures. Since inter-yarn pore in the woven filter media is able to cause higher interstitial filtration velocity than inter-fiber pore in the nonwoven media, clogging of salt particles is intensified and thus, resulting in higher air flow resistance across the filter media. This phenomenon was also observed by other researchers [III.5,III.13]. In addition, thickness of ACF filter media plays an important role on salt particles loading as well. Usually, depth media loading usually has significantly lower increase of pressure drop compared to surface media loading, which suggests that thicker filter media are able to entrap and load more particles at same increase of pressure drop than thinner filter media. Since nonwoven ACF media have higher thickness

compared to woven ACF media, they can load a significant amount of salt particles without much increase of pressure drop across the filter media.

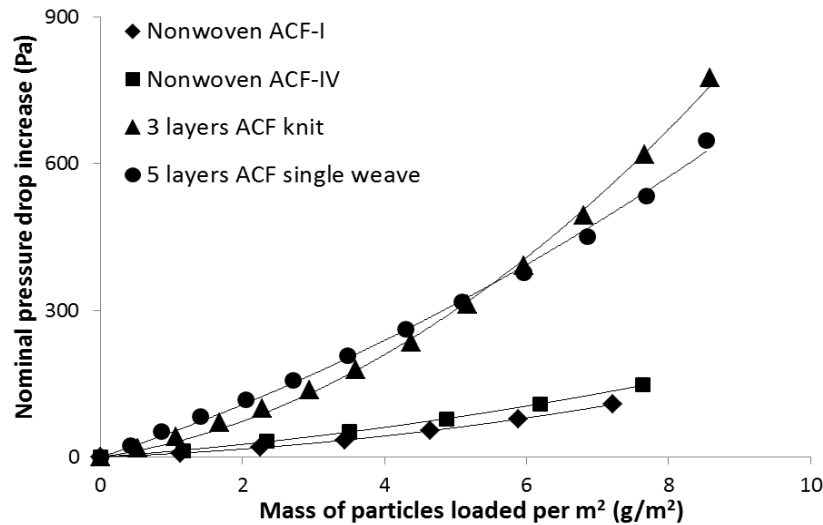


Figure III-15 Nominal increase of pressure drop with respect to deposited mass of salt particles for nonwoven and woven ACF filter media (Data reported for face velocity of 50 cm/s)

Previous discussion of filter media performance mainly focused on initial filtration performance. However, in terms of real filtration applications, filtration performance changes with loading of particles. Therefore, it is highly essential to study the variation of filter media performance with clogging. Figure III-16 shows evolution of filtration efficiency with salt particles loading of both nonwoven and woven ACF filter media. As can be observed, filtration efficiency increases with particles loading for both nonwoven and woven media. This can be explained by the fact that voidage of filter media decreases gradually when salt particles are captured and loaded by filter media. Those entrapped salt particles occupy finite spaces and can subsequently act as collection sites for future particles, thus contributing to the filtration efficiency. Meanwhile, transition from depth filtration to surface (cake) filtration after salt particles start to accumulate on the filter media surface can significantly enhance particles collection efficiency due to the role of salt particles cake. However, it can also be seen that increase of filtration efficiency of nonwoven

ACF media with particles loading is much higher compared to that of woven (knit) ACF media at same increase of pressure drop, which results from the fact that nonwoven media can entrap and load more salt particles due to its homogeneous pore structure compared to woven media.

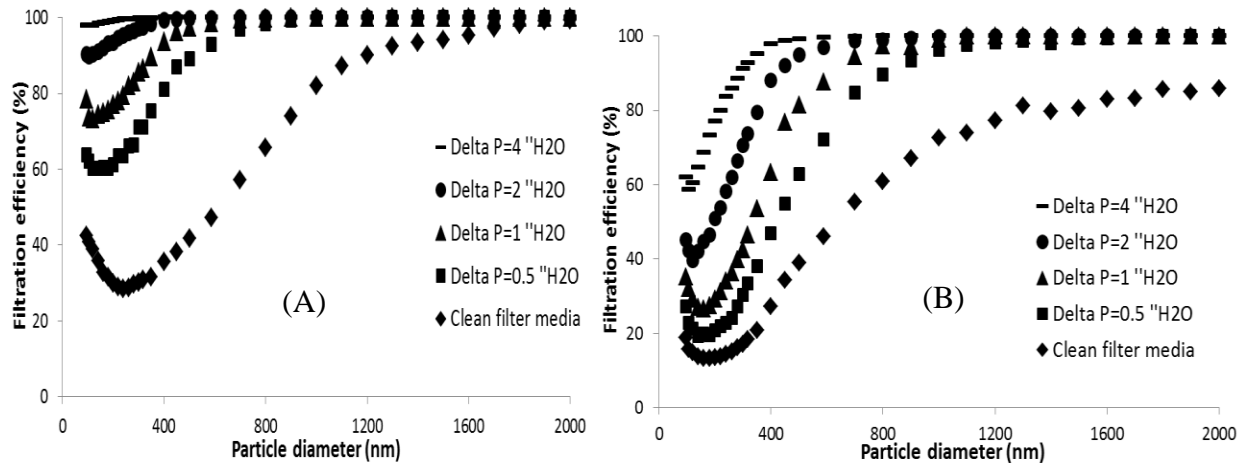


Figure III-16 Evolution of salt particles filtration efficiency with respect to particle diameter of (A) Nonwoven ACF-I filter media and (B) 3 layers ACF knit filter media (Data reported for face velocity of 50 cm/s)

In order to have a further investigation, quality factors of both nonwoven and woven ACF media vs mass of salt particles deposited per media area were plotted in Figure III-17 as well. As shown in Figure III-17, woven ACF media, including both knit and single weave, show much smaller quality factors compared to nonwoven ACF media with loading of salt particles. This suggests that nonwoven filter media have better filtration performance with clogging than woven filter media, which can be explained by the higher increase of filtration efficiency and lower increase of pressure drop resulting from the homogeneous pore structure. Meanwhile, for both nonwoven and woven ACF media, there is a maximum quality factor existed during particles loading. After that, quality factor decreases with particles clogging and it is because that the increase of pressure drop has negated the effect of increase in filtration efficiency.

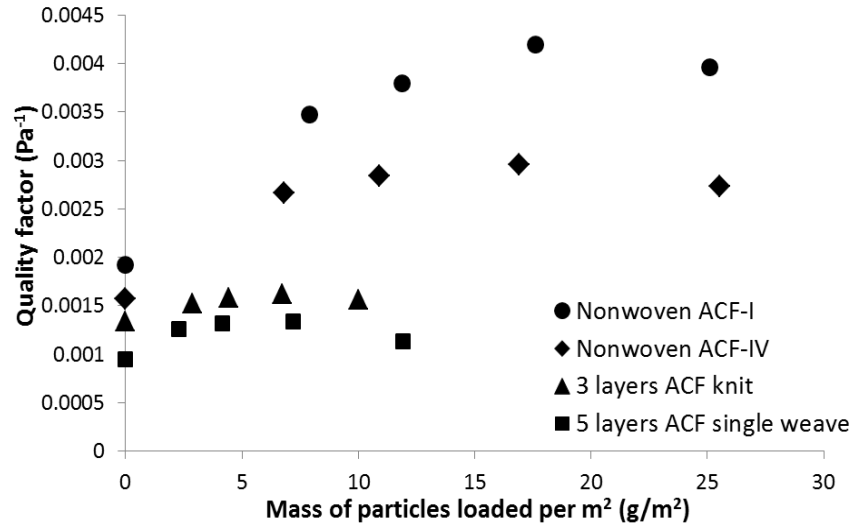


Figure III-17 Quality factor (cal.) with respect to deposited mass of salt particles for nonwoven and woven ACF filter media (Data reported for face velocity of 50 cm/s)

In order to further compare the filter media performance, particles loading capacity and filter media lifetime were achieved as well. Assuming 4 inch water (996 Pa) is the maximum pressure drop that filter media can reach, the maximum mass of salt particles loaded could be calculated. Since the experimental salt particles concentration is 105 times larger than real concentration within ocean environment [III.1], the time for the filter media to reach the maximum pressure drop when they are applied to real ocean environment should be 105 times longer. Besides, with an average run time of 8 hours per day, the lifetime of both nonwoven ACF media and woven ACF media are able to be estimated. As shown in Table III-8, nonwoven ACF filter media are potentially able to have much longer useful lifetime and higher particles loading capacity than woven ACF filter media, which is very important during filtration industry. Therefore, what can be concluded is that nonwoven filter media is more suitable for filtration for salt particles than woven filter media and could be applied in real filtration circumstances.

Table III-8 Comparisons of particles loading capacity and filter media life time between nonwoven and woven ACF filter media

	Initial pressure drop (Pa)	Final pressure drop (Pa)	Particles loading capacity (g/m ²)	Filter media life time (Days)
Nonwoven ACF-I	280.0	996	21.52	40
Nonwoven ACF-IV	471.7	996	17.47	31
ACF knit	247	996	8.52	14
ACF single weave	293	996	9.30	15

III.4.5 Comparison of compressor parasitic power between nonwoven and woven ACF media

Similar to analysis in Chapter II, compressor parasitic power was calculated as well for both nonwoven and woven ACF filter media because it is highly related to the power output of SOFC system. Higher compressor parasitic power could lead to lower SOFC power output, which is harmful to SOFC performance. As mentioned in Chapter II, compressor parasitic power is usually calculated using the equation below.

$$P_B = \frac{\gamma}{\gamma - 1} \frac{0.371T_a}{\eta} q_o \left[\left(\frac{p_b}{p_a} \right)^{\frac{\gamma-1}{\gamma}} - 1 \right] \quad (\text{Eq III.9})$$

Where,

P_B is the power output (kW)

γ is the heat capacity ratio (1.4 for air)

T_a is the temperature of the gas entering the compressor (293 K)

p_a is the compressor inlet pressure, which depends on the pressure drop across the filter before the compressor

p_b is the compressor exit pressure, which is also inlet pressure of SOFC

η is the compressor efficiency (0.8)

q_o is the volume of gas compressed evaluated at 293 K and 1 atm pressure (m³/s)

SOFC's performance needs to be assessed for the full pressure drop range of cathode air filter over its life, not just when the filter is new. Filter pressure drop will increase over the lifetime of the filter. If a filter is selected only based on the initial pressure drop, then the filter engineer can expect a lower SOFC performance over the life of the filter or to be frequently changing filters in order to maintain the lower pressure drop required for normal SOFC performance. Therefore, it is very important to investigate compressor parasitic power when particles are loaded gradually.

In order to study this compressor parasitic power VS particles loading phenomenon, several parameters need to be assumed and determined, which is shown in Table III-9.

Table III-9 Compressor parasitic power estimation conditions

Temperature (K)	293 (Room temperature)
Air flow rate (ft ³ /min)	~395
Inlet salt particle concentration (ppmw)	4.0
Stoichiometric ratio (λ)	2
Average voltage (V_c)	0.6
SOFC power output (KW)	~190
SOFC inlet pressure (inch water)	814 (2 atm)

In the table, air flow rate stands for the required oxygen flow rate to operate a fuel cell, which could be found by the number of faradays provided by a mole of oxygen. Through substitution and simplification, the following Equation III.10 is derived [II.28].

$$AirFlowRate = 1.82 \times 10^{-2} \times \lambda \times \frac{P_e}{V_c} \quad (Eq III.10)$$

Where λ is the stoichiometric ratio defined as the total amount of oxygen flow divided by the oxygen used. This equation can be used for all SOFCs regardless of size as an estimate for air flow rate requirements.

Since the pressure drop across the cathode air filter VS particles loading has already been obtained previously and equation for estimating compressor parasitic power is determined, compressor parasitic power during salt particles loading is able to be achieved and the results are demonstrated in Figure III-18.

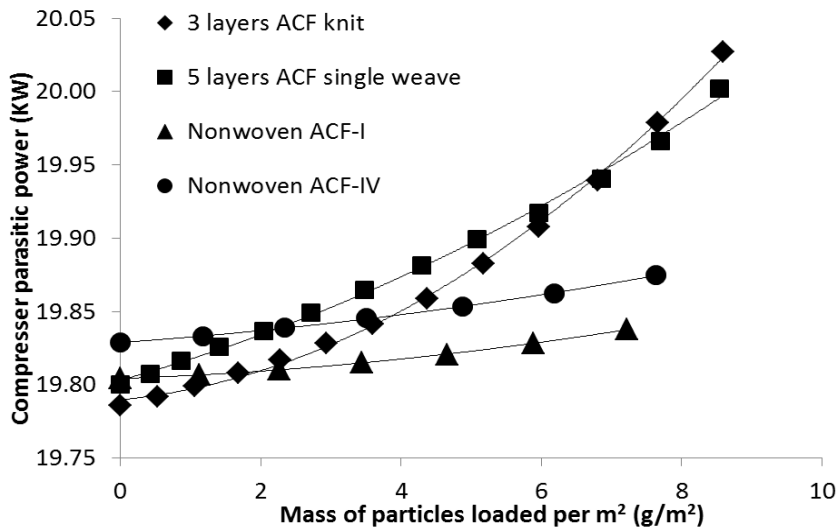


Figure III-18 Comparison of compressor parasitic power between nonwoven and woven ACF media (Data reported for face velocity of 50 cm/s)

As shown in Figure III-18, nonwoven and woven media have two different trends for compressor parasitic power during particles loading process. For two nonwoven ACF media, they indicate very slight increase of compressor parasitic power when salt particles are loaded gradually. However, both ACF knit and ACF single weave media have shown significantly large increase of compressor parasitic power compared to nonwoven media, which means nonwoven media are able to enhance the SOFC power output and SOFC system performance. This is due to the much lower increase of pressure drop of nonwoven media, which can be explained by the

homogeneous inter-fiber pore structure. Therefore, nonwoven filter media could be a much better option when they are considered to be applied in real circumstances, like sea salt particles filtration.

According to the data in Table III-9, SOFC power output is calculated as around 185 KW using 50 cm/s of air flow velocity. And the compressor parasitic power is about 19 KW, which is like 10% of total SOFC power output. Thus, almost 89% of the power that SOFC generates could be used as power source for the ship, which is a legitimate number.

III.4.6 Effect of relative humidity (RH) on ACF media filtration for salt particles

Relative humidity (RH) is an important air property that needs to be investigated for particulates filtration, especially for salt particles during ocean environment. Since relative humidity is extremely higher in the sea, the effect of RH on filtration for salt particles cannot be ignored. RH is the ratio of the partial pressure of water vapor in an air-water mixture to the saturated vapor pressure of water at a prescribed temperature. It is potentially able to affect the filtration performance of filter media, including both pressure drop and filtration efficiency [III.30-32]. Sodium chloride (NaCl) particles belong to hydrophilic particles with deliquescent point of 75% and when RH is above it, particles become saturated as liquid particles (droplets). Therefore, in order to fully understand the RH effect on filtration performance, two RHs (0%, 50%) below the deliquescent point and one RH (80%) above the deliquescent point were selected for this relative humidity study.

Two ACF filter media (Nonwoven ACF-I and nonwoven ACF-V) were tested regarding of filtration efficiency at various relative humidities. As shown in Figure III-19, for both two ACF filter media, increasing relative humidity results in higher filtration efficiency when RH is below the deliquescent point of sodium chloride (75%). This can be explained by the fact that activated carbon fiber is highly porous material with large surface area, which leads to a large amount of

water absorbed into the fiber pores when passing humid air through. Due to this, capillary tension [III.33,III.34] between salt particles and ACF pore surface becomes the most dominant adhering force for particle collection and therefore, much more particles are able to be entrapped and captured by the filter media. Moreover, because of hydrophilicity of sodium chloride, particle sizes are increased by absorbing water from the air stream and results in the further decrease of penetration. It can also be observed that increases of average filtration efficiency at 50% RH for two different ACF media are different, 7.57% for nonwoven ACF-I and 10.89% for nonwoven ACF-V. This is due to the higher solid volume fraction of activated carbon fiber for nonwoven ACF-V, which also suggests it is activated carbon fiber that plays the dominant role in the increase of filtration efficiency at higher relative humidity.

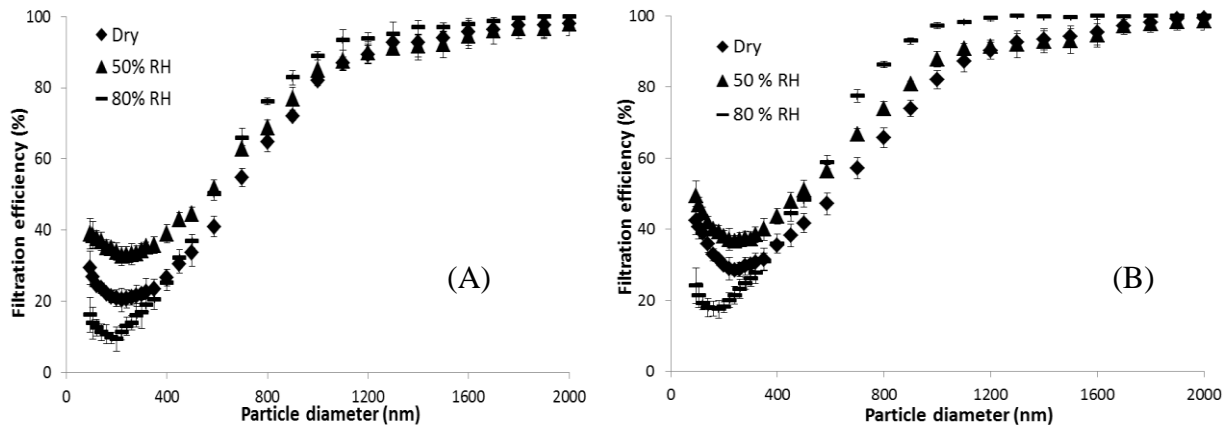


Figure III-19 Filtration efficiency with respect to particle diameter at various relative humidities (RHs) for: (A) Nonwoven ACF-V filter media, (B) Nonwoven ACF-I filter media (Data reported for face velocity of 50 cm/s)

However, when relative humidity goes up to 80%, the trend is different. For particles smaller than 400-500nm, filtration efficiency decreases and vice versa for particles larger than 500 nm. This indicates that there is a decrease in filtration efficiency for small particles by diffusion but an increase for large particles by inertial impaction, which was also observed by other researchers

[III.32]. This phenomenon can be explained by the phase transformation of salt particles when relative humidity is higher than deliquescent point and different filtration mechanisms for particles in various size ranges. Large particles are in form of droplets (liquid phase) at 80% RH and can start filling up the interstitial spaces between the fibers and inter-fiber pores as well, which results in less large salt particles penetrating the filter media. But for small particles, due to the change of phase from solid particles to wet droplets, Brownian motion of particles is highly weakened and even suspended. Also, for collection of those small particles that still remain solid phase, less interstitial spaces between fibers exist due to the filling up by wet salt droplets. Therefore, filtration efficiency of small particles becomes lower when relative humidity increases to 80%.

In addition, humidity pretreatment experiments [III.35] for two ACF filter media were conducted as well in order to further understand the effect of relative humidity on filtration for salt particles. Before experiments, two ACF filter media were pretreated in an environment of 50% RH for a period of time. Afterwards, the filter media were tested against sodium chloride particles in dry air stream. As shown in Figure III-20, filtration efficiencies of both two ACF media are improved after pretreatment in humid environment. However, the increase of efficiency is only about 3-4% for 5h pretreatment and 4-5% for 12h pretreatment. Compared to the increase of directly passing humid air through the filter media which is around 10-15%, this increase is much smaller. This can be explained by the fact that particle size remains the same during dry air stream and only the increase of capillary tension between particles and ACF pore surface due to pretreatment in humid air accounts for the improvement of filtration efficiency. Overall, it can be concluded that relative humidity (RH) indeed affects the filtration performance of ACF filter media for salt particles.

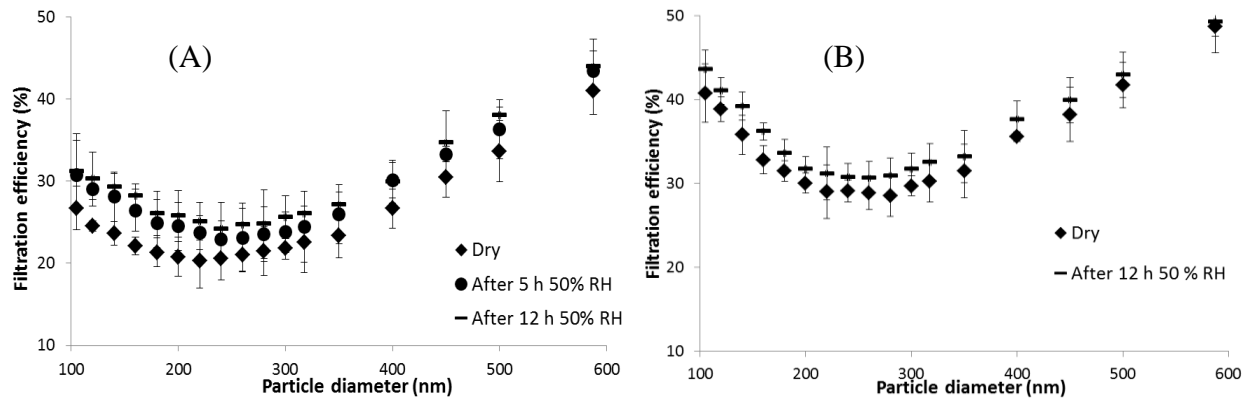


Figure III-20 Filtration efficiency with respect to particle diameter after pretreatment in humid environment for: (A) Nonwoven ACF-V filter media, (B) Nonwoven ACF-I filter media

III.5 Conclusion

This work mainly focused on the potential of nonwoven and woven activated carbon fiber (ACF) filter media, to be applied for sea salt particles filtration for SOFCs during ocean platforms. Comparisons of filtration performance, including pressure drop across the filter media and filtration efficiency and particles loading capacity and compressor parasitic power between nonwoven and woven ACF media were demonstrated. It was observed that nonwoven ACF media had lower pressure drop per thickness and higher initial filtration efficiency compared to woven ACF media, which resulted in higher quality factors and thus, better filtration performance for salt particles. This can be explained by the different pore structures of nonwoven and woven media. Due to the larger size of inter-yarn pores inside the woven media, air selects them as preferential path flowing through, which causes higher interstitial velocity inside inter-yarn pores and much more particles penetrating the media. Moreover, stacking several layers of woven ACF media together was able to show better filtration performance for salt particles. This revealed that the increase of filtration efficiency compensated the effect of increase in pressure drop for multiple layers of woven ACF media, which is due to the transformation from inhomogeneous pore

structure to homogeneous pore structure. Thus, for woven media, multiple layers can be a good solution for filtration for salt particles. Estimations of particles loading capacity and filter media life time suggested that nonwoven ACF media was able to load much more salt particles without significant increase of pressure drop across the filter media. This was attributed to the lower interstitial velocity through inter-fiber pores and higher thickness of nonwoven ACF media. Therefore, it can be concluded that compared to woven ACF media, nonwoven ACF media are potentially able to present better filtration performance for salt particles, including both initial performance and performance with particles loaded.

This study also showed that relative humidity (RH) had significant effect on filtration performance of ACF filter media for salt particles due to the highly porous structures of ACF and hydrophilicity of sodium chloride particles. High relative humidity (80% RH) can cause a decrease in filtration efficiency for small particles by diffusion but an increase in filtration efficiency for large particles by inertial impaction.

III.6 References

- [III.1] Majchrzak, R., Cole, T. and Cervi, M. (1998). U.S. Navy Sea Salt Particle Removal Systems, Carderock Division Naval Surface Warfare Center.
- [III.2] Wilcox, M., Baldwin, R., Hernandez, A. G. and Brun, K. (April 2010). Guideline for Gas Turbine Inlet Air Filtration Systems, Gas Machinery Research Council and Southwest Research Institute.
- [III.3] Payet, S., Boulaud, D., Madelaine, G. and Renoux, A. (1992). Penetration and Pressure-drop of A HEPA Filter During Loading with Submicron Liquid Particles. *Journal of Aerosol Science* 23:723-735.
- [III.4] Spurny, K. R. (1998). Carbon fiber filters with aerosol separation and gas adsorption properties, in: Spurny, K. R. (Ed.). *Advances in Aerosol Filtration*. Lewis, 407-414.
- [III.5] Lorimier, C., Le Coq, L., Subrenat, A. and Le Cloirec, P. (2008). Indoor air particulate filtration onto activated carbon fiber media. *Journal of Environmental Engineering-Asce* 134:126-137.
- [III.6] Rochereau, A., Benesse, M., Le Coq, L. and Subrenat, A. (2008). Combined air treatment: Effect of composition of fibrous filters on toluene adsorption and particle filtration efficiency. *Chemical Engineering Research and Design* 86:577-584.
- [III.7] Rochereau, A., Le Coq, L., Subrenat, A. and Le Cloirec, P. (2007). Influence of complex fibrous media composition on their performances for VOC and particle removal. *Environmental Technology* 28:1365-1375.
- [III.8] Liu, W. (2010). Activated carbon fiber filter media for proton exchange membrane fuel cell, in Department of Polymer and Fiber Engineering, Auburn University.

- [III.9] Karwa, A. N. and Tatarchuk, B. J. (2012b). Aerosol filtration enhancement using carbon nanostructures synthesized within a sintered nickel microfibrinous matrix. *Separation and Purification Technology* 87:84-94.
- [III.10] ASHRAE 52.2 (1992). Method of Testing General Ventilation Air-cleaning Devices Used for Removal Efficiency by Particle Size, American National Standard, Atlanta, GA, USA.
- [III.11] Brown, R. C. (1993). Particle capture by mechanical means, in: *Air Filtration - An Integrated Approach to the Theory and Application of Fibrous Filters*. Pergamon Press, 73-116.
- [III.12] Boulard, D. and Renoux, A. (1998). Stationary and Nonstationary Filtration of Liquid Aerosols by Fibrous Filters, in: Spurny, K.R.(Ed.). *Advances in Aerosol Filtration*. Lewis, 53-83.
- [III.13] Benesse, M., Le Coq, L. and Sollicec, C. (2006). Collection efficiency of a woven filter made of multifiber yarn: Experimental characterization during loading and clean filter modeling based on a two-tier single fiber approach. *Journal of Aerosol Science* 37:974-989.
- [III.14] Fisk, W. J., Faulkner, D., Palonen, J. and Seppanen, O. (2002). Performance and Costs of Particle Air Filtration Technologies. *Indoor Air* 12:223-234.
- [III.15] Arnold, B. D., Matela, D. and Veeck, A. (2005). Life-cycle costing of air filtration. *ASHRAE Journal* 47:30-32.
- [III.16] Bird, R. B., Stewart, W. E. and Lightfoot, E. N. (2007). *Transport phenomena*. J. Wiley, 183-191.
- [III.17] Karwa, A. N. and Tatarchuk, B. J. (2012a). Pressure drop and aerosol filtration efficiency of microfibrinous entrapped catalyst and sorbent media: Semi-empirical models. *Separation and Purification Technology* 86:55-63.

- [III.18] Harris, D., Cahela, D. and Tatarchuk, B.J. (2001). Wet layup and sintering of metal-containing microfibrinous composites for chemical processing opportunities. *Composites part A: Applied Science and Manufacturing* 32:1117-1126.
- [III.19] Cahela, D. and Tatarchuk, B.J. (2001). Permeability of sintered microfibrinous composites for heterogeneous catalysis and other chemical processing opportunities. *Catalysis Today* 69:33-39.
- [III.20] Carman, P.C. (1956). *Flow of gases through porous media*. Butterworths Scientific Publications.
- [III.21] Perry, R.H. and Green, D.W. (2008). *Perry's chemical engineers' handbook*. McGraw-Hill.
- [III.22] Hinds, W.C. (1998). *Aerosol Technology: Properties, Behavior, And Measurement of Airborne Particles*. John Wiley & Sons, Inc.
- [III.23] Moelter, W. and Fissan, H. (1998). Quality assurance of glass fiber filter media, in: Spurny, K. R. (Ed.). *Advances in Aerosol Filtration*. Lewis, 259-282.
- [III.24] Moelter, W. and Fissan, H. (1997). Structure of a high efficiency glass fiber filter medium. *Aerosol Science and Technology* 27:447-461.
- [III.25] Brown, R. C. (1993). Macroscopic behavior of filters, in: *Air Filtration - An Integrated Approach to the Theory and Application of Fibrous Filters*. Pergamon Press, 1-11.
- [III.26] National Air Filtration Association (2007). *NAFA Guide to Air Filtration*. National Air Filtration Association, Virginia Beach, VA 23471.
- [III.27] Stenhouse, J.I.T. and Trottier, R. (1991). The Loading of Fibrous Filters with Submicron Particles. *Journal of Aerosol Science* 22:777-780.

- [III.28] Zelenyuk, A., Cai, Y. and Imre, D. (2006). From Agglomerates of Spheres to Irregularly Shaped Particles: Determination of Dynamic Shape Factors from Measurements of Mobility and Vacuum Aerodynamic Diameters. *Aerosol Science and Technology* 40: 197-217
- [III.29] Thomas, D., Penicot, P., Contal, P., Leclerc, D. and Vendel, J. (2001). Clogging of fibrous filters by solid aerosol particles –Experimental and modeling study. *Chemical Engineering Science* 56:3549-3561.
- [III.30] Miguel, A. F. (2003). Effect of air humidity on the evolution of permeability and performance of a fibrous filter during loading with hygroscopic and non-hygroscopic particles. *Journal of Aerosol Science* 34:783-799.
- [III.31] Gupta, A., Novick, V. J., Biswas, P. and Monson, P. R. (1993). Effect of humidity and particle hygroscopicity on the mass loading capacity of high-efficiency particulate air (HEPA) filters. *Aerosol Science and Technology* 19:94-107.
- [III.32] Newnum, J. D. (December 2010). The Effects of Relative Humidity on Respirator Performance, in *Occupational and Environmental Health*, University of Iowa.
- [III.33] Brown, R. C. (1993). Effects of loading, in: *Air Filtration - An Integrated Approach to the Theory and Application of Fibrous Filters*. Pergamon Press, 201-236.
- [III.34] Ranade, M.B. (1987). Adhesion and removal of fine particles on surfaces. *Aerosol Science and Technology* 7:161-176.
- [III.35] Stevens, G.A. and Moyer, E.S. (1989). “Worst Case” Aerosol Testing Parameters: II. Efficiency Dependence of Commercial respirator Filters on Humidity Pretreatment. *Am. Ind. Hyg. Assoc. J* 50:265-270.

Chapter IV Theoretical study of various nonwoven microfibrinous filter media: Pressure drop, filtration efficiency and particles loading capacity

IV.1 Introduction

In addition to experimental analysis of filtration performance of different filter media for sea salt particles (SSPs) [IV.1], theoretical analysis is another important study that needs to be considered in order to fully understand the media filtration performance. Three parameters are included in this study, pressure drop across the filter media, particles filtration efficiency and particles loading capacity. Both experiment results and model estimation results are demonstrated and compared to see if they match with each other.

IV.2 Experimental

IV.2.1 Materials

Five different types of materials are used in this study, which are bi-component polyester fiber from KOSA, Nickle fiber (alloy Ni-200) with length of 3-6 mm from Intramicron Inc (Auburn, AL), Activated carbon fiber with length of 3 mm from TOYOBO, Japan, Vapor grown carbon nanofiber (VGCF) (PR-19-XT-PS) from Pyrograf Products, Inc and cellulose, respectively. The details are shown in Table IV-1.

Table IV-1 Details of different fiber materials

	Density (g/cm³)	Diameter (micron)
Nickle	8.7	4 and 8
Polymer	1.125	13
ACF-25	0.35	7-8
VGCF	1.6	~150 nm

Cellulose	1.78	~20
-----------	------	-----

IV.2.2 Nonwoven media preparation

Media making process is different for varying fibers due to different properties. Overall, there are mainly three steps, pre-form preparation, pre-oxidation and sintering.

Pre-form preparation

As for polymer, they were dispersed in water using a blender. 1 ml Cruwik-SYN was added to improve the dispersion of the suspension of polymer fibers in water. Nickel fibers were dispersed in water with high viscosity, which was increased by the addition of 0.75% (w/w) hydroxyethyl cellulose (HEC). 2-3 ml 0.1N sodium hydroxide (NaOH) was used to enhance the hydrolysis of HEC in the suspension. 20% (w/w) cellulose was added as pre-binder of the pre-form [IV.2]. For activated carbon fiber, they were dispersed in water with other different materials to create a composite media, like nickel, polymer and cellulose. Then, the liquid suspension was transferred to a 6.25 inch diameter TAPPI hand-sheet former to create preforms of media. The preforms were then removed and dried at 40-70 °C to get rid of water.

Pre-oxidation

This step is optional and mainly to eliminate cellulose from nickel preforms by oxidation in air diluted with nitrogen at ~400 °C. And the structure of the preforms without cellulose is extremely weak and needs further sintering. As for polymer and those activated carbon fiber composites, this step can be skipped because activated carbon fiber could be oxidized by air at such high temperature.

Sintering

The preforms obtained from first step and pre-oxidized from second step were sintered at different temperatures due to different properties of fibers. The purpose of sintering is to further increase the bonding between fibers and make media more strong and robust. For metal fibers,

like nickel, the preforms were sintered at 950 °C using 5-10% hydrogen in nitrogen for 40 min [IV.3]. Polymer fibers were usually sintered at 140-170 °C in air. In terms of activated carbon fiber composite, the sintering temperature varied depending on the other type of material.

After all the steps, samples of media that need to be tested were punched out from the final form of media using a steel circular punch. Each sample was about 2.1 inch in diameter. In order to increase the packing fraction of media, samples could be compressed at some degree.

IV.2.3 Experimental setup

Filtration efficiency and pressure drop were measured using the setup in Figure IV-1. Compressed air was passed through silica gel desiccant to get rid of moisture and HEPA filter to eliminate contaminants in the air stream. There are three main streams in the whole setup. First one is nebulizing air stream to generate aerosols from salt solution. 15% (w/w) sodium chloride (NaCl) solution was used in the nebulizer. A mass flow controller (MFC) was applied to control the flow rate of nebulizing air stream at around 1.2-1.5 LPM. A polydispersed aerosol nebulizer was selected after trying several different ones in order to get constant performance all the time. After the nebulizer, the wet sodium chloride particles were passed through diffusion dryer to remove the moisture of the particles. Diffusion dryer (DD 250) from Air Techniques International (ATI) was used due to its large flow rate and simple operation. Since the particles have some static charges due to aerosolizing, an aerosol neutralizer body (Model-9000) from Brechtel manufacturing, Inc and two Polonium-210 strips (from NRD, LLC) were used to neutralize the particle charges into Boltzman equilibrium. The second air stream was passed through a large glass bubbler with deionized water to obtain saturated air (100% RH) and the third air stream was used to control the RH of the mixed air stream by varying the flow rate ratio of these two air streams. Then, the mixture of all three streams went into the main filter section, which is composed of a stainless steel pipe (1 inch ID) and flanges since particles don't attach to

the walls of stainless steel pipe. The media sample was placed between two flanges with foam gaskets for sealing purpose.

The pressure drop across the filter media was measured using a pressure transducer from Omega at different air flow rates. As for the filtration efficiency, a particle counter named Laser Aerosol Spectrometer (LAS-XII) from TSI was applied for all the filtration tests in this work. This spectrometer can detect particles from 90 to 7500 nm in diameter within 99 channels. The sample flow rate can be varied from 10 sccm to 100 sccm, during which 50 sccm was selected for all the tests. In this work, face velocity for all tests were 0.5 m/s unless notified otherwise. The concentration of the particles was around 73,000 per 50 cc of air with 1460 particles per cc of air. According to the particle size distribution obtained, the median particle diameter is around 284 nm with geometric standard deviation (GSD) of 6.18. For each test, 5 to 10 samples for both upstream and downstream were carried out with 1 min each. Then, average efficiency was calculated using formula below [IV.4]:

$$E = \frac{n_{up} - n_{down}}{n_{up}} \times 100\% \quad (\text{Eq IV.1})$$

Error bars with 95% confidence interval was also calculated using Excel 2010 and shown in the results. The figure below shows the schematic of the experimental setup.

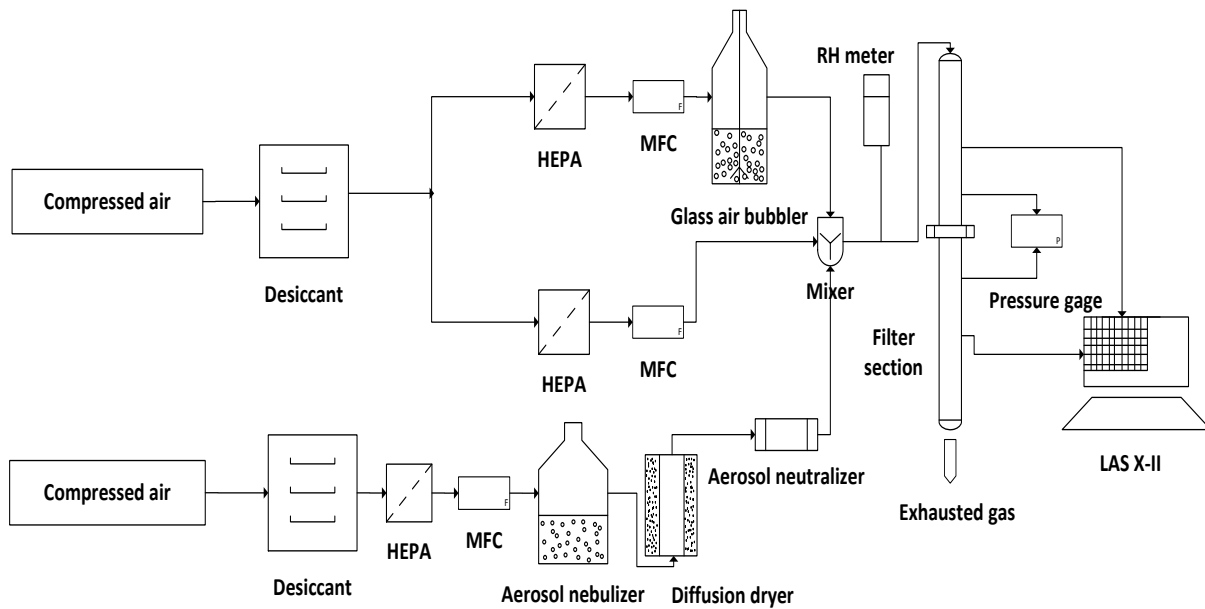


Figure IV-1 Experimental setup for filtration efficiency, particles loading capacity and pressure drop test

IV.3 Results and discussions

IV.3.1 Pressure drop analysis (laminar flow region)

Pressure drop corresponds directly to the energy consumption as it is indicative of the work done by pushing air through the media. High pressure drop will cost more energy [IV.5]. Several popular models have already been used for estimating pressure drop across void structures, including the Blake Kozeny equation and the Davies model [IV.6]. Among them, the Blake Kozeny equation (viscous loss term in the Ergun equation) is the most popular one, shown in Equation IV-2. It is quite useful and accurate when used to describe pressure drop due to viscous losses over a packed column full of particles. But it also has its own limit, like not perfect for large void fractions since it did not include the form drag losses. Porous media permeability (PMP) model derived previously by Donald R. Cahela from Auburn University showed good estimation of pressure drop for nonwoven porous media. PMP equation combined both two viscous loss terms, friction loss and form drag loss, which is shown in Equation IV-3.

For viscous friction loss, it used capillary channel flow model for Blake Kozeny equation and for viscous form drag loss, free particle Stokes' flow model was applied [IV.7, IV.8].

$$\frac{\Delta P}{L} = 150 \frac{\mu v}{(\phi D)^2} \frac{c^2}{(1-c)^3} \quad (\text{Eq IV.2})$$

$$\frac{\Delta P}{L} = 72 \frac{\mu v}{(\phi D)^2} \frac{c^2}{(1-c)^3} \frac{\tau^2}{\cos^2 \theta} (1 + X_{fd}) \quad (\text{Eq IV.3})$$

Where $\tau = \left(\frac{2+c}{c}\right)$ and $X_{fd} = \frac{(1-c)^2}{12c}$

From the PMP equation, we can see the flow path angle (θ) is also an important factor that affects the pressure drop. However, there is a lack of a reliable experimental method to measure it for different materials and thus, some modification needs to be done for PMP equation to make it applicable for various materials and their composites [IV.9].

The modified PMP equations for both single material and composite media are shown below:

$$\frac{\Delta P}{L} = A \frac{\mu v}{(\phi D)^2} \frac{c^2}{(1-c)^3} \tau^2 (1 + X_{fd}) \quad (\text{Eq IV.4})$$

$$\frac{\Delta P}{L} = A \mu v \frac{c^2}{(1-c)^3} \tau^2 \left(\sum \frac{x_i}{(\phi_i D_i)^2} + x_{fd} \sum \frac{x_i}{(\phi_i D_i)^2} \right) \quad (\text{Eq IV.5})$$

Two variables (A and Φ) have to be determined for different materials. As for Φ , which stands for shape factor, can be calculated empirically by using the Blake Kozeny equation. Shape factor mainly accounts for the deviation of particle shape from an ideal sphere ($\Phi=1$). Calculated shape factors for various materials are shown in Table IV-2. For constant A, it has to be determined experimentally by fitting the pressure drop data into the PMP equation using shape factors obtained from Blake Kozeny equation. The determined constants for various composites are also given in Table IV-3.

Table IV-2 Shape factors of different fibers

Fiber types	Shape factor (Φ)	Sample used for calculation
Activated carbon fiber-25	5.02	ACF-25 (16.5%) + polymer (2.57%)
Ni (8 micron)	0.91	Ni (8 micron) with 41% SVF
Ni (4 micron)	1.03	Ni (4 micron) with 36 % SVF
Polymer (13 micron)	2.35	Polymer (13 micron) with 39% SVF
Cellulose	3.48	Ni (40%) + cellulose (19%)

Table IV-3 Constant A for low face velocity PMP model of various composite media

	Constant A
Polymer (13 micron)	112
Ni	79
ACF + Polymer + Cellulose	91
ACF + Ni + Cellulose	89
ACF + Polymer	96

From the shape factor table, we can see that activated carbon fiber has significantly larger Φ compared to other materials. The reason is that activated carbon fiber has porous structure inside the fibers leading to much higher surface area.

In order to prove if the modified PMP equation gives good estimation for different materials and their composites, five media samples in different components were tested (Table IV-4) and the modified PMP model fitting results are shown in Figure IV-2.

Table IV-4 Composition and thickness of five different composite media tested

	ACF-25	Polymer (13 micron)	Ni	Cellulose	Thickness
Media 1	16.5%	2.57%	N/A	N/A	3.8 mm
Media 2	22.4%	1.74%	N/A	1.1%	1.4 mm
Media 3	22.4%	N/A	4 micron 0.45%	2.2%	0.6 mm
Media 4	N/A	20.89%	N/A	N/A	0.7 mm
Media 5	N/A	N/A	8 micron 7.71%	N/A	0.4 mm

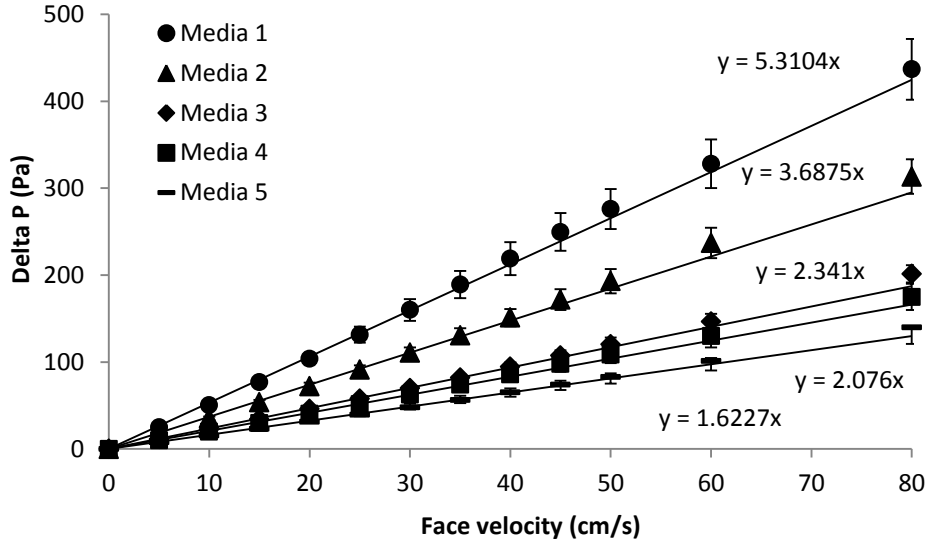


Figure IV-2 Modified PMP model fitting results at low face velocity

As shown in Figure IV-2, modified PMP equation can fit the experimental data quite well with RMS error less than 6%, especially for low face velocity. The Root mean square (RMS) errors, defined by Equation IV-6, for the five samples were calculated and shown in Table IV-5 [IV.9].

$$Error_{RMS}(\%) = \sqrt{\frac{\sum \left(\frac{\Delta P_{model} - \Delta P_{experimental}}{\Delta P_{model}} \right)^2}{n}} \times 100 \quad (\text{Eq IV.6})$$

Table IV-5 RMS error of five PMP model fitting curves

	PMP RMS error (%)
Media 1	3.63
Media 2	5.01
Media 3	3.44
Media 4	4.53
Media 5	4.40

IV.3.2 Pressure drop analysis (turbulent flow region)

Same as laminar flow region, there have already been several models for pressure drop estimation at high face velocity, like the Burke-Plummer equation (inertial loss term in Ergun

equation) shown in Equation IV.7. It is applied for pressure drop over a packed bed of particles at high face velocity. However, it also has some limits for porous media pressure drop estimation.

A PMP model for high face velocity is also derived earlier by using a friction factor correlation for turbulent flow inside a pipe, which is shown in Equation IV.8 [IV.8].

$$\frac{\Delta P}{L} = \frac{7}{4} \frac{(\rho v^2)}{\phi D} \frac{c}{(1-c)^3} \quad (\text{Eq IV.7})$$

$$\frac{\Delta P}{L} = 6 \frac{\tau^3}{\cos^3 \theta} \frac{\rho v^2}{2(\phi D)} \frac{c}{(1-c)^3} (C_f + \frac{C_{FD}}{4}(1-c)) \quad C_{FD} = C_D - C_f \quad (\text{Eq IV-8})$$

Where C_f is the coefficient of friction, C_{FD} is coefficient of form drag and C_D is coefficient of drag

Modified PMP equation for high face velocity is obtained by substituting constants from low face velocity PMP equation and coefficients were determined empirically, which are shown in Table IV-6.

$$\frac{\Delta P}{L} = B \tau^3 \frac{\rho v^2}{(\phi D)} \frac{c}{(1-c)^3} (C_f + \frac{C_{FD}}{4}(1-c)) \quad (\text{Eq IV.9})$$

$$\frac{\Delta P}{L} = B \tau^3 \rho v^2 \frac{c}{(1-c)^3} (C_f + \frac{C_{FD}}{4}(1-c)) \sum \frac{x_i}{\phi_i D_i} \quad (\text{Eq IV.10})$$

$$C_D = 0.6, C_f = 0.42 \sim 0.47$$

Table IV-6 Constant B for high face velocity PMP model of different composite media tested

	Constant B
ACF + Ni + Cellulose	4.12
ACF + Polymer + Cellulose	4.26
Polymer	5.82
ACF + Polymer	4.61

Four media samples in different components were tested (Table IV-7) from low velocity to high face velocity and the modified PMP model fitting results with RMS errors are shown in Figure IV-3.

Table IV-7 Composition and thickness of four different composite media tested

	ACF-25	Polymer (13 micron)	Ni (4 micron)	Cellulose	Thickness
Media 1	16.5 %	2.57 %	N/A	N/A	3.8 mm
Media 2	22.4 %	N/A	0.45 %	1.65 %	1.35 mm
Media 3	22.4 %	1.74 %	N/A	1.1 %	1.4 mm
Media 4	N/A	20.89 %	N/A	N/A	0.7 mm

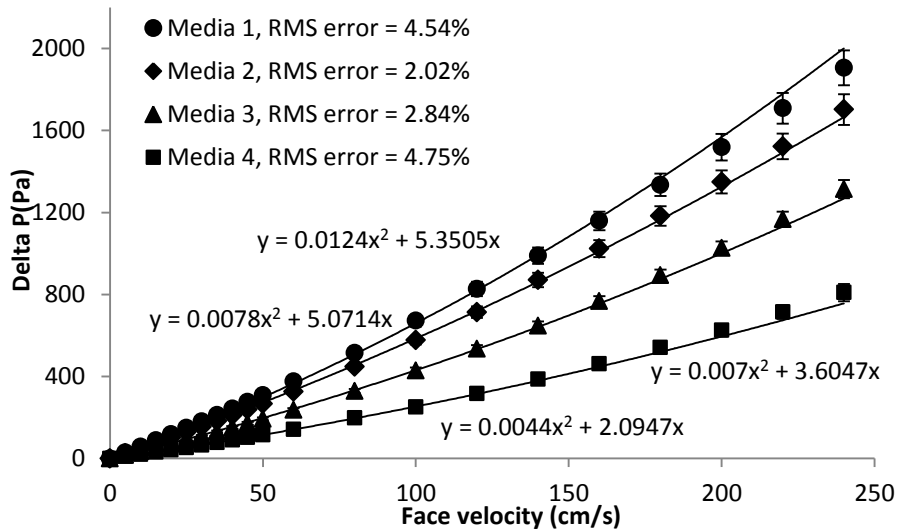


Figure IV-3 Modified PMP model fitting results at high face velocity (with RMS errors)

From Figure IV-3 and RMS errors, we can see that modified PMP equation for high face velocity could also fit the experimental data very well with RMS errors less than 5%. Therefore, what we conclude is that PMP equation modified by different constants and coefficients for various materials and their composites could be used to estimate the pressure drop across the porous media at both low face velocity and high face velocity accurately.

IV.3.3 Filtration efficiency analysis

Filtration usually has several different mechanisms, during which Brownian diffusion, interception, and inertial impaction are three most important ones. Several empirical models have

been established for each mechanism [IV.10-IV.12]. In this work, three popular models were selected for each mechanism based on the structural characteristics of filter media and air properties, like fiber diameter and air flow rate [IV.13]. Because all the existed models are established empirically for a particular type of filter, there is no one model which could be applied to all different types of material. Therefore, modified filtration efficiency models were made to estimate different types of filter media, which are shown below [IV.14]:

$$E_D = A \left(\frac{1-\alpha}{Ku} \right)^{1/3} Pe^{-2/3} C_d C_d'' \quad (\text{Eq IV.11})$$

$$C_d = 1 + 0.388 Kn_f \left(\frac{(1-\alpha)Pe}{Ku} \right)^{1/3} \quad C_d'' = \frac{1}{1 + A \left(\frac{1-\alpha}{Ku} \right)^{1/3} Pe^{-2/3} C_d}$$

$$E_R = B \frac{1-\alpha}{Ku} \frac{R^2}{1+R} \quad (\text{Eq IV.12})$$

$$E_I = 0.0334 Stk^{3/2} \quad (\text{Eq IV.13})$$

The dimensionless numbers in the above equations are defined as follows:

$$\text{Peclet number} \quad Pe = Ud_f / D$$

$$\text{Stokes number} \quad Stk = \frac{\rho_p d_p^2 U}{18\mu d_f}$$

$$\text{Kuwabara number} \quad Ku = -\ln \alpha / 2 - 0.75 + \alpha - 0.25\alpha^2$$

$$\text{Knudsen number} \quad Kn_f = 2\lambda / d_f$$

U denotes here face velocity of air stream, D the coefficient of Brownian diffusion, λ the gas mean free path, α the packing fraction, d_p and d_f the aerosol particle and fiber diameter, respectively [IV.14].

Assuming diffusion, interception and inertial impaction are three independent filtration mechanisms, the total single fiber efficiency due to all the three actions is defined below:

$$E = 1 - (1 - E_D)(1 - E_R)(1 - E_I) \quad (\text{Eq IV.14})$$

Then, the overall filtration efficiency can be calculated using equation below:

$$E_T = 1 - \exp\left(\frac{-4\alpha Et}{\pi(1-\alpha)d_f}\right) \quad (\text{Eq IV.15})$$

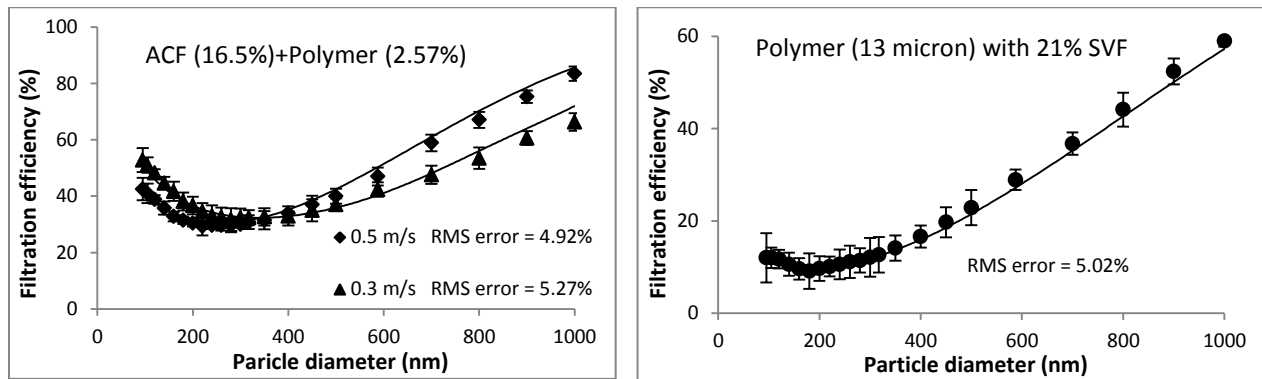
Coefficients A and B in diffusion and interception models were all empirically determined by fitting the experimental data obtained from LAS-XII into the model. The coefficients are both dependent on various types of materials. Table IV-8 shows some empirical values fitted by using sample media for coefficients A and B:

Table IV-8 Coefficients A and B of five different composite media

	Coefficient A	Coefficient B
Ni (4 micron)	3.8	1.45
Polymer (13 micron)	3.0	2.2
ACF + Polymer	1.3	0.1
ACF + Ni + Cellulose	3.6	0.9
ACF + Polymer + Cellulose	1.0	0.11

The data fitting using the modified efficiency models for five samples is shown in Figure

IV-4.



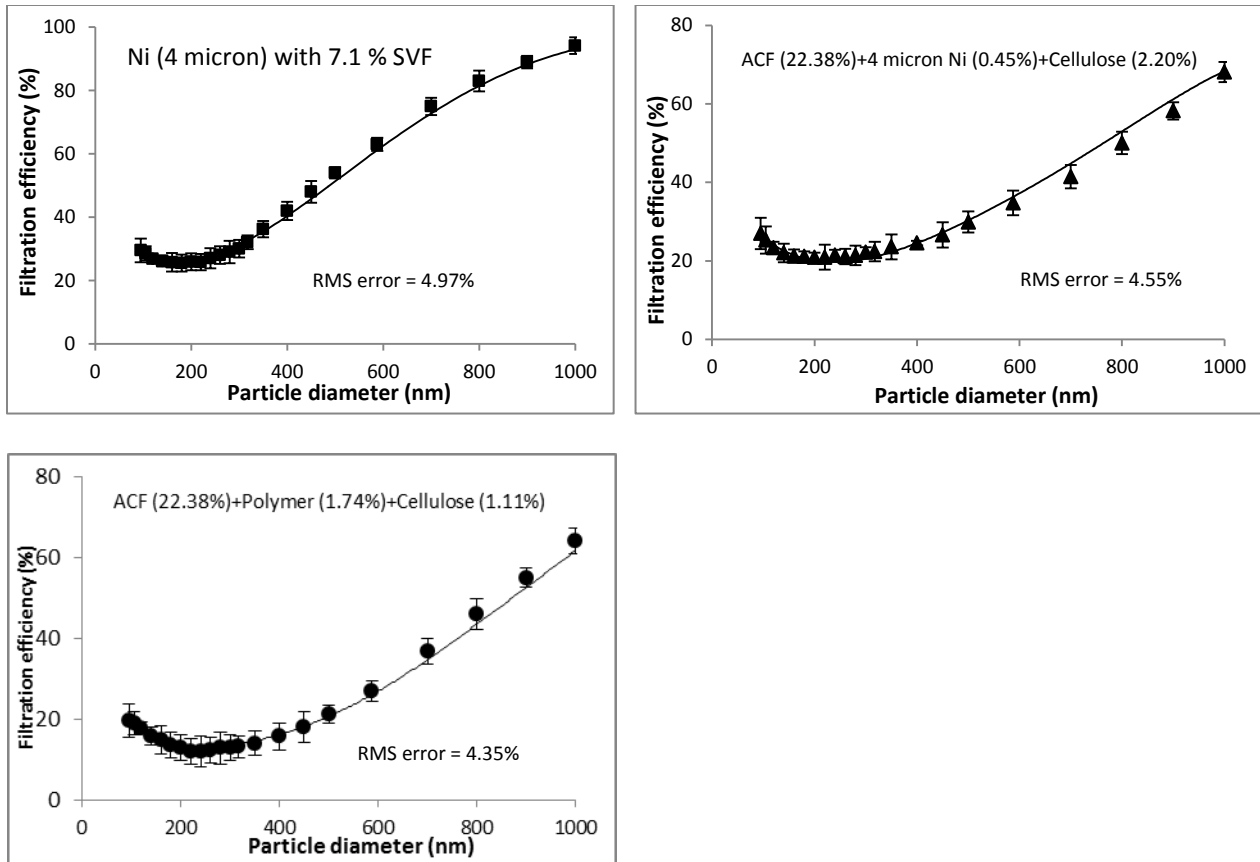


Figure IV-4 Filtration efficiency model fitting results of different composite media (with RMS errors)

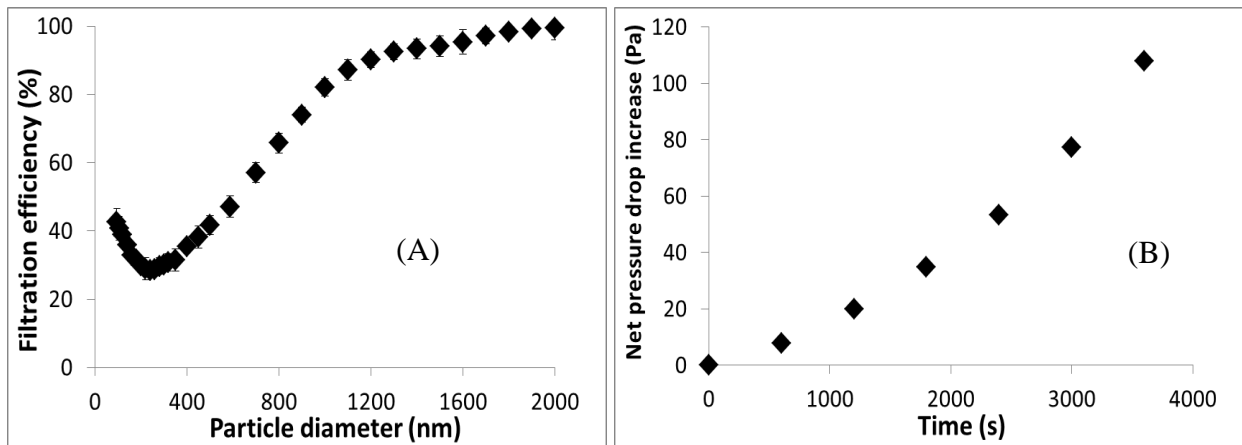
From Figure IV-4 and RMS errors above, we can find that after modification, efficiency models could fit the experimental data very well with RMS error less than 5%. Therefore, modified filtration efficiency models can be effectively applied to estimate efficiency of various materials and their composites.

IV.3.4 Particles loading analysis

Particles loading performance is another significant parameter that needs to be evaluated for filtration performance and it is strongly related to filter media lifetime, which is highly essential during filter media design [IV.15-16]. Higher loading capacity results in longer useful

life time and increasing life of filter media is the most crucial element in reducing filtration costs [IV.17-18]. Thus, it is highly essential to investigate this parameter during filter media design.

Particles loading curve is usually used in this study, which is nominal increase of pressure drop across the media vs total mass of deposited particles onto the media [IV.19-20]. In order to achieve this curve, filtration efficiency tests and pressure drop measurements were both conducted. During salt particles loading, pressure drop of filter media increased gradually with time and the value was recorded within a certain time range. According to filtration efficiency and inlet salt particle concentration, the number of salt particles entrapped by the filter during 1 min can be calculated and as well as the total number of particles during that certain time range. Since the particle diameter is known, the mass of total particles loaded by the filter can be achieved afterwards. This whole estimation process has been shown in Figure IV-5, (A) to (D).



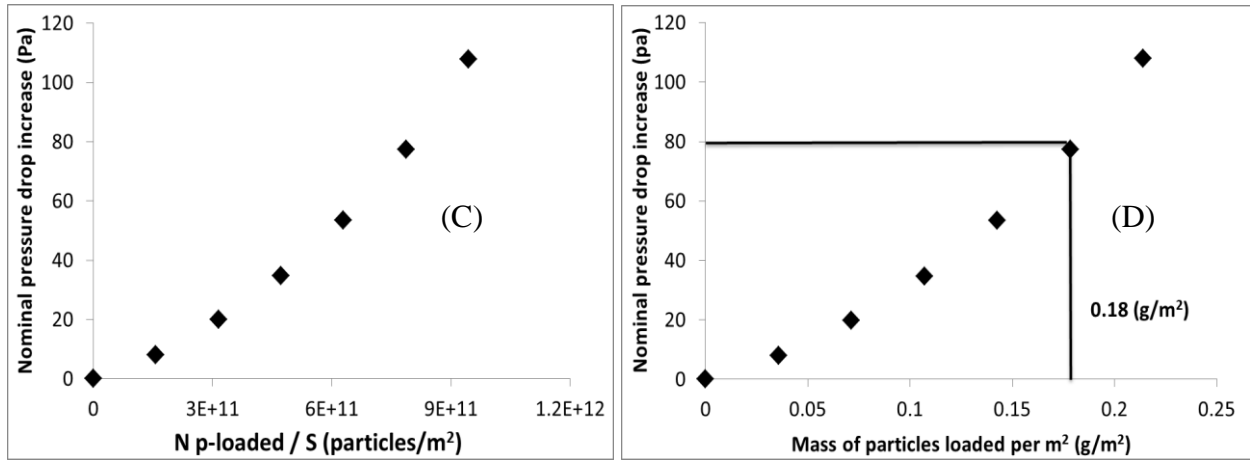


Figure IV-5 Particles loading estimation process

However, salt particles in different diameters have various shapes, like sphere, cube or agglomerate. Thus, estimations of mass of particles for different particle sizes are different, which can be seen from Equation IV.16 to Equation IV.19. In this work, salt particles are considered as spheres, cubes and agglomerates for diameter smaller than 200nm, between 200 and 800 nm and larger than 800 nm, respectively. As for agglomerates, they can be estimated as spheres with shape factor of 1.4 [IV.21].

$$Mass_{<200nm} = N_{<200nm} \times \pi / 6 \times (D)^3 \times \rho \quad (\text{Eq IV.16})$$

$$Mass_{200-800nm} = N_{200-800nm} \times (D)^3 \times \rho \quad (\text{Eq IV.17})$$

$$Mass_{>800nm} = N_{>800nm} \times \pi / 6 \times (1.4D)^3 \times \rho \quad (\text{Eq IV.18})$$

$$Mass_{Total} = Mass_{<200nm} + Mass_{200-800nm} + Mass_{>800nm} \quad (\text{Eq IV.19})$$

Since mass of deposited particles onto filter media and increase of pressure drop were both known, salt particles loading curve for all filter media tested were able to be plotted. In order to verify if this estimation method is correct, different sample media were tested and the calculation results were compared with the experimental data obtained from analytical balance. In Figure IV-6, lines stand for the estimation result and dots stand for the experimental data. As can be observed,

for all various sample media, estimation results are able to fit with experimental data quite well. To demonstrate how well the two results match each other, Root Mean Square (RMS) errors [IV.8] were calculated and are shown in Table IV-9. It shows that RMS errors are all less than 5%, which suggests that the estimation method for mass of deposited particles onto the filter media is correct.

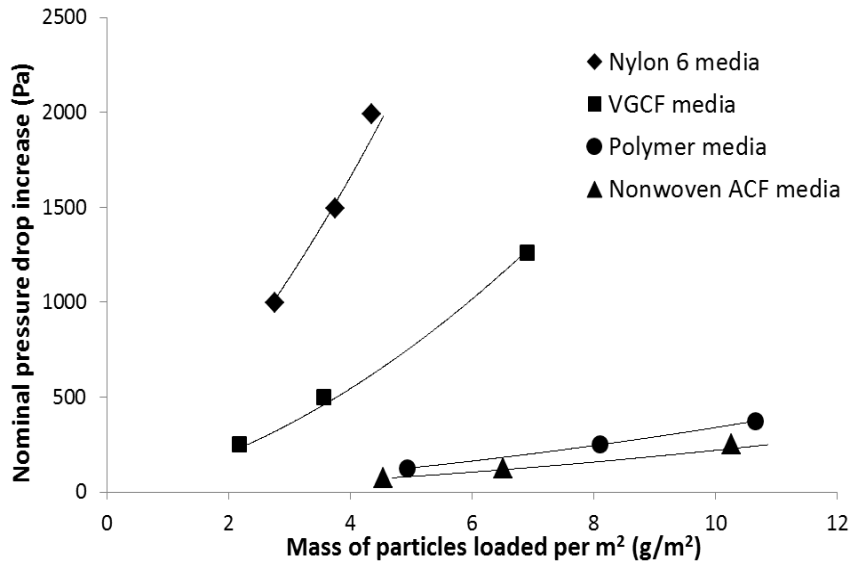


Figure IV-6 Comparison of nominal increase of pressure drop with respect to deposited mass of salt particles per media area between experimental data and calculation result (Data reported at face velocity of 50 cm/s)

Table IV-9 Calculated RMS errors of various filter media

	RMS error
Nonwoven ACF media	4.37%
Polymer media	2.45%
VGCF media	4.81%
Nylon 6 media	3.03%

IV.4 Conclusion

In this part of work, theoretical analysis, including pressure drop across filter media, filtration efficiency and particles loading capacity for salt particles filtration using various filter

media were demonstrated. For pressure drop analysis, porous media permeability (PMP) model was further modified according to different types of fiber material. Shape factors (Φ) were calculated empirically and constants A from laminar flow region and constants B from turbulent flow region were determined experimentally by fitting the data into the PMP equation. In terms of filtration efficiency analysis, three popular models of filtration mechanisms, including Brownian diffusion, interception and inertial impaction, were applied to estimate particles removal efficiency of various filter media. In the last part, salt particles loading performance was investigated as well. A new estimation method of particles loading capacity was proposed according to different ranges of particle size. All of the estimation results above were compared with experiment results and they match each other very well with RMS errors less than 5%. Therefore, all the estimation models, pressure drop, filtration efficiency and particles loading capacity could be effectively applied in the future work.

IV.5 References

- [IV.1] Majchrzak, R., Cole, T. and Cervi, M. (1998). U.S. Navy Sea Salt Particle Removal Systems, Carderock Division Naval Surface Warfare Center.
- [IV.2] Karwa, A. N. (2012). Aerosol Filtration Performance of Novel 3-Dimensional Nonwoven Composites, in Department of Chemical Engineering, Auburn University.
- [IV.3] Karwa, A. N. and Tatarchuk, B. J. (2012b). Aerosol filtration enhancement using carbon nanostructures synthesized within a sintered nickel microfibrinous matrix. *Separation and Purification Technology* 87:84-94.
- [IV.4] ASHRAE 52.2 (1992). Method of Testing General Ventilation Air-cleaning Devices Used for Removal Efficiency by Particle Size, American National Standard, Atlanta, GA, USA.
- [IV.5] Fisk, W. J., Faulkner, D., Palonen, J. and Seppanen, O. (2002). Performance and Costs of Particle Air Filtration Technologies. *Indoor Air* 12:223-234.
- [IV.6] Bird, R. B., Stewart, W. E. and Lightfoot, E. N. (2007). *Transport Phenomena*. J. Wiley.
- [IV.7] Harris, D., Cahela, D. and Tatarchuk, B.J. (2001). Wet layup and sintering of metal-containing microfibrinous composites for chemical processing opportunities. *Composites part A: Applied Science and Manufacturing* 32:1117-1126.
- [IV.8] Cahela, D. and Tatarchuk, B.J. (2001). Permeability of sintered microfibrinous composites for heterogeneous catalysis and other chemical processing opportunities. *Catalysis Today* 69:33-39.
- [IV.9] Karwa, A. N. and Tatarchuk, B. J. (2012a). Pressure drop and aerosol filtration efficiency of microfibrinous entrapped catalyst and sorbent media: Semi-empirical models. *Separation and Purification Technology* 86:55-63.
- [IV.10] Spurny, K. R. (1998). *Advances in Aerosol Filtration*. Lewis.

- [IV.11] Matteson, M. J. and Orr, C. (1987). *Filtration: Principles and Practices*. Marcel Dekker, Inc.
- [IV.12] Hinds, W. C. (1998). *Aerosol technology: Properties, Behavior, And Measurement of Airborne Particles*. John Wiley & Sons, Inc.
- [IV.13] Payet, S., Boulaud, D., Madelaine, G. and Renoux, A. (1992). Penetration and Pressure-drop of A HEPA Filter During Loading with Submicron Liquid Particles. *Journal of Aerosol Science* 23:723-735.
- [IV.14] Brown, R. C. (1993). *Air Filtration: An Integrated Approach to the Theory and Application of Fibrous Filters*. Pergamon Press.
- [IV.15] National Air Filtration Association (2007). *NAFA Guide to Air Filtration*. National Air Filtration Association, Virginia Beach, VA 23471.
- [IV.16] Stenhouse, J.I.T. and Trottier, R. (1991). The Loading of Fibrous Filters with Submicron Particles. *Journal of Aerosol Science* 22:777-780.
- [IV.17] Novick, V.J., Monson, P.R. and Ellison, P.E. (1992). The effect of solid particle mass loading on the pressure drop of HEPA filters. *Journal of Aerosol Science* 23:657-665.
- [IV.18] Lebedev, M.N. and Kirsch, A.A. (1995). Pressure drop of loaded fibrous filters. *Journal of Aerosol Science* 26:S735-S736.
- [IV.19] Walsh, D.C. (1996). Recent advances in the understanding of fibrous filter behavior under solid particle load. *Filtration and Separation* 33:501-506.
- [IV.20] Leibold, H. and Wilhelm, J.G. (1991). Investigation into the penetration and pressure drop of HEPA filter media during loading with submicron particle aerosols at high concentrations. *Journal of Aerosol Science* 22:S773-S776.

[IV.21] Zelenyuk, A., Cai, Y. and Imre, D. (2006). From Agglomerates of Spheres to Irregularly Shaped Particles: Determination of Dynamic Shape Factors from Measurements of Mobility and Vacuum Aerodynamic Diameters. *Aerosol Science and Technology* 40: 197-217

Chapter V Study of sea salt particles (SSP) filtration using various nonwoven filter media

V.1 Introduction

Currently, solid oxide fuel cells (SOFCs) are being considered to be applied on-board ships as power source due to the high efficiency and low waste emission. However, during the sea environment, air contains large amount of salt particles, which are generated mainly from wind stresses over whitecaps or from either the wake or the bow spray by ship itself. These sea salt particles could cause severe degradation of fuel cells performance [V.1-2]. Therefore, removal of them before flowing into cathode side of fuel cell systems is an essential problem that needs to be solved. In the past decades, there has been a lot of achievement in aerosol filtration studies, such as particle flow patterns through filter media and different models for particle filtration mechanisms [V.3]. But they didn't focus on one particular particle, like sea salt and filtration performance of different filter media as well. In this part of work, various filter media were tested for sea salt particles filtration in order to evaluate their performance, including particles removal efficiency, pressure drop and particles loading capacity. Moreover, effect of relative humidity (RH) on hydrophobic media was demonstrated since RH is another significant parameter that could affect salt particles filtration.

These filter media are composed of a three dimensional network of sinter-locked micron size fibers and nano size fibers. Great applicability of particulates removal with low pressure drop have been shown and these filter media could be used as support structure for carbon and

polymer nanofibers, which are able to significantly enhance the strength for sea salt particles filtration application [V.4-6].

V.2 Experimental

V.2.1 Materials

Four different types of materials are used in this part of study, which are bi-component polyester fiber from KOSA, Nickle fiber (alloy Ni-200) with length of 3-6 mm from Intramicon Inc (Auburn, AL), Activated carbon fiber with length of 3 mm from TOYOBO, Japan, Vapor grown carbon nanofiber (VGCF) (PR-19-XT-PS) from Pyrograf Products, Inc and cellulose, respectively. The details are shown in Table V-1.

Table V-1 Details of different fiber materials

	Density (g/cm³)	Diameter (micron)
Nickle	8.7	4 and 8
Polymer	1.125	13
VGCF	1.6	~150 nm
ACF-25	0.35	7-8
Cellulose	1.78	~20

V.2.2 Nonwoven media preparation (wet-laid method)

Filter media manufacturing process is different for different fibers due to their various properties. Overall, there are mainly three steps, pre-form preparation, pre-oxidation and sintering.

Pre-form preparation

As for polymer, they were dispersed in water using a blender. 1 ml Cruwik-SYN was added to improve the dispersion of the suspension of polymer fibers in water. Nickle fibers were dispersed in water with high viscosity, which was increased by the addition of 0.75% (w/w) hydroxyethyl cellulose (HEC). 2-3 ml 0.1N sodium hydroxide (NaOH) was used to enhance the hydrolysis of HEC in the suspension. 20% (w/w) cellulose was added as pre-binder of the pre-

form [V.4]. For VGCF filter media, VGCF were dispersed using water in a blender at a very high rate in order to completely separate them due to the strong Van der Waals force. Then, the VGCF suspension was mixed with polymer fiber suspension. As for activated carbon fiber, they were dispersed in water with other different materials to create a nonwoven composite media, like nickel, polymer and cellulose. In the end, the liquid suspension was transferred to a 6.25 inch diameter TAPPI hand-sheet former to create preforms of media. The preforms were then removed and dried at 40-70 °C to get rid of water.

Pre-oxidation

This step is optional and mainly to eliminate cellulose from nickel preforms by oxidation in air diluted with nitrogen at ~400 °C. And the structure of the preforms without cellulose is extremely weak and needs further sintering. As for polymer media and activated carbon fiber media, this step can be skipped because polymer fiber could be melted by air and activated carbon fiber could be oxidized by air at such high temperature.

Sintering

The preforms obtained from first step and pre-oxidized from second step were sintered at different temperatures due to different properties of fibers. The purpose of sintering is to further increase the bonding between fibers and make media more strong and robust. For metal fibers, like nickel, the preforms were sintered at 950 °C using 5-10% hydrogen in nitrogen for 40 min [V.7]. Polymer fibers were usually sintered at 140-170 °C in air. In terms of activated carbon fiber composite, the sintering temperature varied depending on the other type of material combined.

After all the steps, samples of media that need to be tested were punched out from the final form of media using a steel circular punch. Each sample was about 2.1 inch in diameter. In order to increase the packing fraction of media, samples could be compressed to some extent.

V.2.3 Experimental setup

Filtration efficiency and pressure drop were measured using the setup in Figure V-1. Compressed air was passed through silica gel desiccant to get rid of moisture and HEPA filter to eliminate contaminants in the air stream. There are three main streams in the whole setup. First one is nebulizing air stream to generate aerosols from salt solution. 15% (w/w) sodium chloride (NaCl) solution was used in the nebulizer. A mass flow controller (MFC) was applied to control the flow rate of nebulizing air stream at around 1.2-1.5 LPM. A polydispersed aerosol nebulizer was selected after trying several different ones in order to get constant performance all the time. After the nebulizer, the wet sodium chloride particles were passed through diffusion dryer to remove the moisture of the particles. Diffusion dryer (DD 250) from Air Techniques International (ATI) was used due to its large flow rate and simple operation. Since the particles have some static charges due to aerosolizing, an aerosol neutralizer body (Model-9000) from Brechtel manufacturing, Inc and two Polonium-210 strips (from NRD, LLC) were used to neutralize the particle charges into Boltzman equilibrium. The second air stream was passed through a large glass bubbler with deionized water to obtain saturated air (100% RH) and the third air stream was used to control the RH of the mixed air stream by varying the flow rate ratio of these two air streams. Then, the mixture of all three streams went into the main filter section, which is composed of a stainless steel pipe (1 inch ID) and flanges since particles don't attach to the walls of stainless steel pipe. The media sample was placed between two flanges with foam gaskets for sealing purpose.

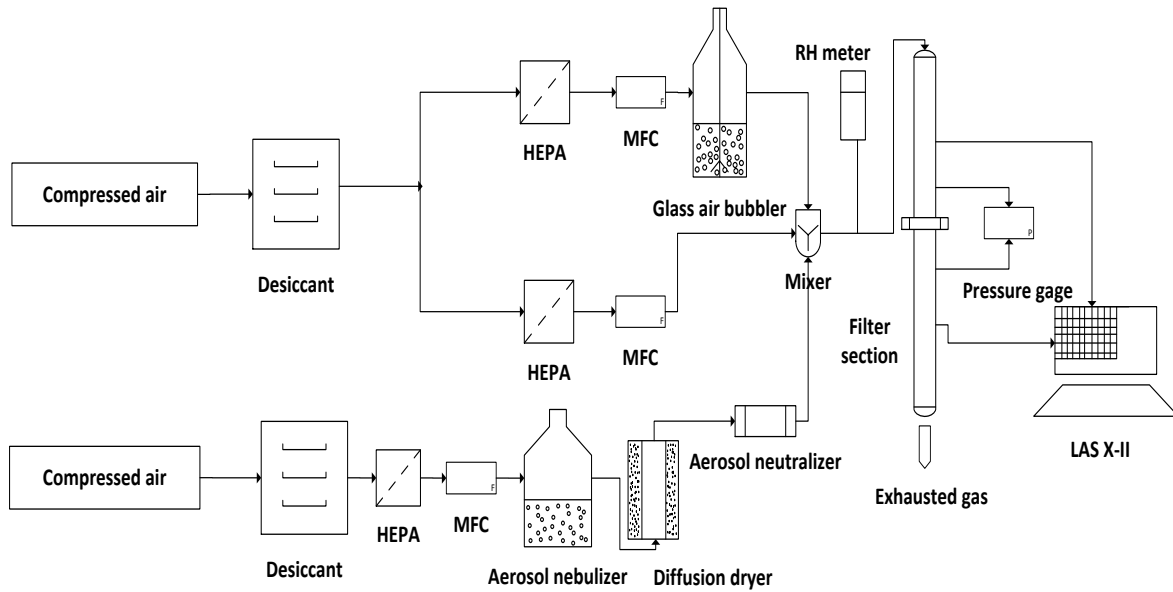


Figure V-1 Experimental setup for filtration efficiency, particles loading capacity and pressure drop test

The pressure drop across the filter media was measured using a pressure transducer from Omega at different air flow rates. As for the filtration efficiency, a particle counter named Laser Aerosol Spectrometer (LAS-XII) from TSI was applied for all the filtration tests in this part of work. This spectrometer can detect particles from 90 to 7500 nm in diameter within 99 channels. The sample flow rate can be varied from 10 sccm to 100 sccm, during which 50 sccm was selected for all the tests. In this work, face velocity for all tests were 0.5 m/s unless notified otherwise. The concentration of the particles was around 73,000 per 50 cc of air with 1460 particles per cc of air. According to the particle size distribution obtained, the median particle diameter is around 284 nm with geometric standard deviation (GSD) of 6.18. For each test, 5 to 10 samples for both upstream and downstream were carried out with 1 min each. Then, average efficiency was calculated using formula below [V.8]:

$$E = \frac{n_{up} - n_{down}}{n_{up}} \times 100\% \quad (\text{Eq V.1})$$

Error bars with 95% confidence interval was also calculated using Excel 2010 and shown in the results. The figure below shows the schematic of the experimental setup.

V.3 Discussions and results

V.3.1 VGCF enhanced microfibrinous filter media

Currently, nanofiber nonwoven media have various application such as particles filtration [V.9-12], coalescence filtration [V.13-14] and high flux ultrafiltration membranes [V.15]. The nanofibers with regard to nonwoven media are typically defined as fibers with diameter less than 500 nm. Electrospinning and melt-blown are two mostly applied technologies to produce nanofiber nonwoven media. However, these two methods can only produce two dimensional media that are lack of strength and very fragile, which is not ideal for sea salt particles filtration. Therefore, three dimensional nanofiber entrapped nonwoven media using wet-laid method is brought up.

VGCF, which stands for vapor grown carbon nanofiber, is nano-scale fiber with diameter around 150 nm and used in this part of work. It is because that the scalability of the process/technology is an important factor to be considered for any application involving nanomaterials in order to harness the potential of ‘nano’ for engineering applications. Therefore, the use of commercially available VGCF in the manufacturing of nanofiber nonwoven composite (nano-nonwoven) is an attractive option for a scalable process.

VGCF could be distributed into nonwoven polymer fiber substrate to make a nano-scale filter media, which is able to enhance its filtration performance for salt particles. Four sample media in different VGCF compositions were made and tested for salt particle filtration performance. The details of the samples are shown in Table V-2:

Table V-2 Thickness, VGCF and polymer volume fraction of fibers of four different media tested

	Thickness (mm)	Mass of VGCF (g)	Volume fraction of VGCF (%)	Volume fraction of polymer (%)
Media 1	0.70	0	0	20.89
Media 2	1.30	0.3	0.79	11.25
Media 3	~1.30	0.5	1.31	10.99
Media 4	~1.30	0.7	1.86	11.00

The filtration efficiency of this nanofiber nonwoven media was tested at 50 cm/s face velocity and dry air (2% RH), which is shown in Figure V-2 (A):

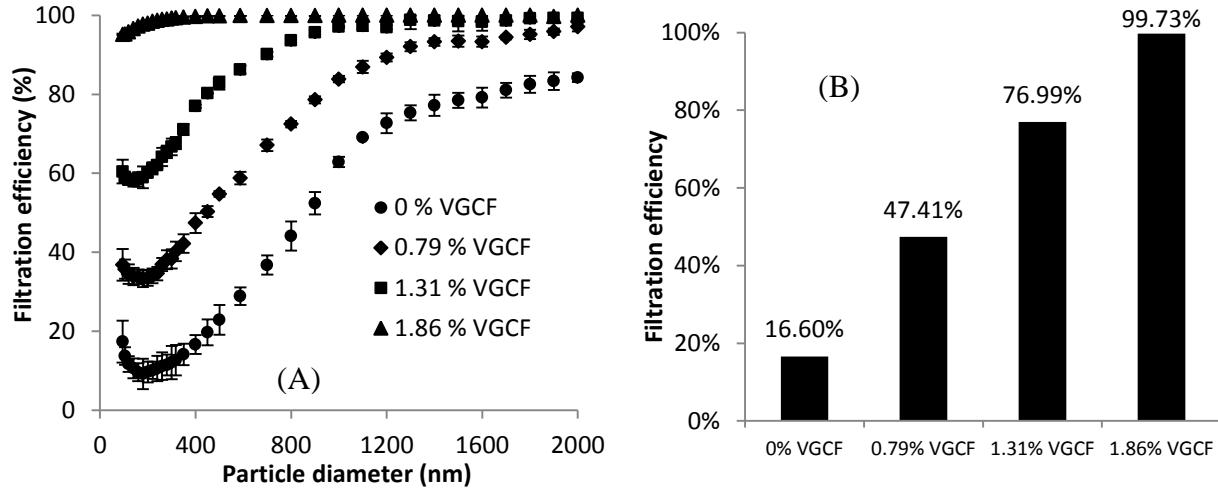


Figure V-2 (A) Filtration efficiency curves of VGCF nonwoven media at different compositions, (B) Filtration efficiency of 400 nm particle using different VGCF composition media (Data reported at face velocity of 50 cm/s)

As shown in Figure V-2 (A), we can see that efficiency increased significantly with VGCF fraction, which is due to much smaller pore diameter after entrapping VGCF. Figure V-2 (B) shows the filtration efficiency of four nanofiber nonwoven media samples using 400 nm particle as an example. It can be seen that efficiency increased significantly from 16.6 % to 99.7%.

Figure V-3 shows the pressure drop curves of four VGCF media in different composition and Table V-3 shows pressure drop at 50 cm/s of four different VGCF nonwoven media:

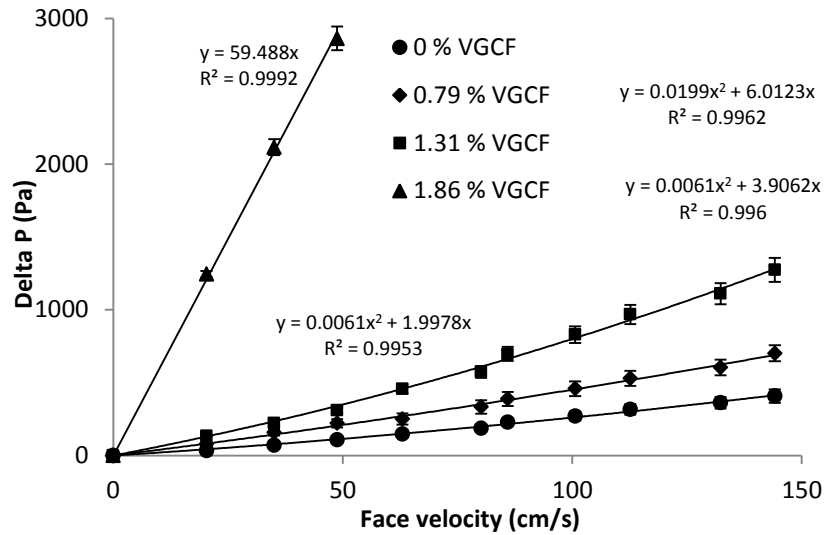


Figure V-3 Pressure drop curves of VGCF nonwoven media in different composition

Table V-3 Pressure drop at 50 cm/s of four different VGCF nonwoven media

	Pressure drop (Pa) at 50 cm/s
0 % VGCF	116
0.79 % VGCF	220
1.31 % VGCF	321
1.86 % VGCF	2980

As can be seen in Figure V-3, the pressure drop curves indicate that higher VGCF volume fraction leads to higher pressure drop across the nonwoven composite media and pressure drop has a huge increase for 1.86 % VGCF, which can be seen from Table V-3. Besides, pressure drop curves show linear with low face velocity and quadratic relationship with high face velocity, which is due to the compression of composite media at high face velocities. According to the pressure drop curves and Darcy's law, permeabilities of VGCF entrapped polymer media were calculated and shown in Table V-4. When VGCF is below 1.31%, the permeability doesn't

decrease much due to slip flow on nanofiber surface. As for 1.86% VGCF, permeability is almost 10 times lower compared to 1.31% VGCF and the reason is that several nanofiber clumps were connected to form a nanofiber bridge on the polymer media surface and therefore significantly resisted air flow passing through it. Thus, a huge difference exists between VGCF fraction of 1.31% and 1.86%. Figure V-4 shows the SEM images of different fractions of VGCF entrapped nonwoven polymer media.

$$\Delta P = AV + BV^2 \quad (\text{Eq V.2})$$

$$A = \frac{\mu L}{K_m} \quad (\text{Eq V.3})$$

Table V-4 Permeability of media at different VGCF fractions

	Permeability (mm ²)
0% VGCF	6.4E-05
0.79% VGCF	6.1E-05
1.31% VGCF	4.0E-05
1.86% VGCF	4.1E-06

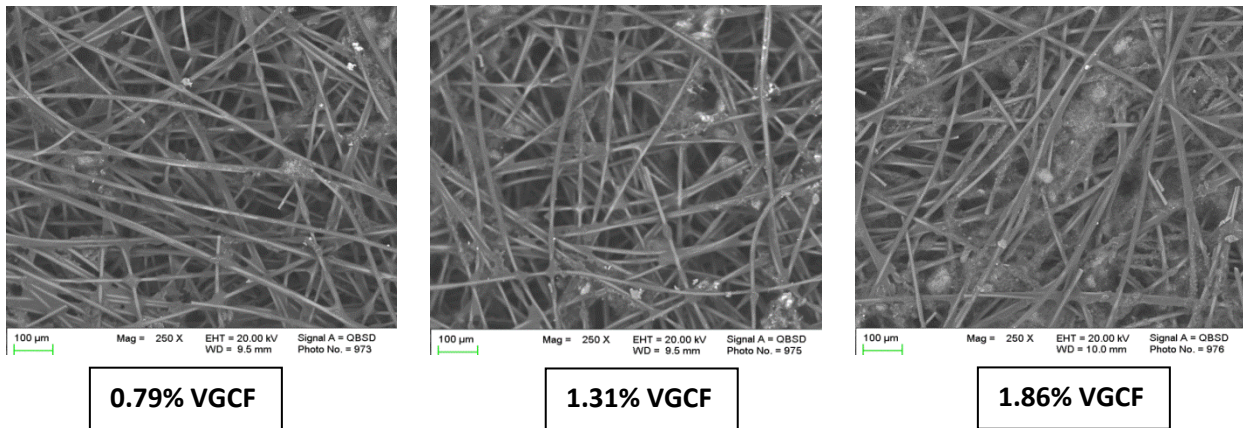


Figure V-4 SEM images of VGCF entrapped polymer media in different VGCF fractions

Moreover, in order to determine if VGCF could enhance the overall filter performance, quality factor (QF) has to be calculated and the results are shown in Figure V-5:

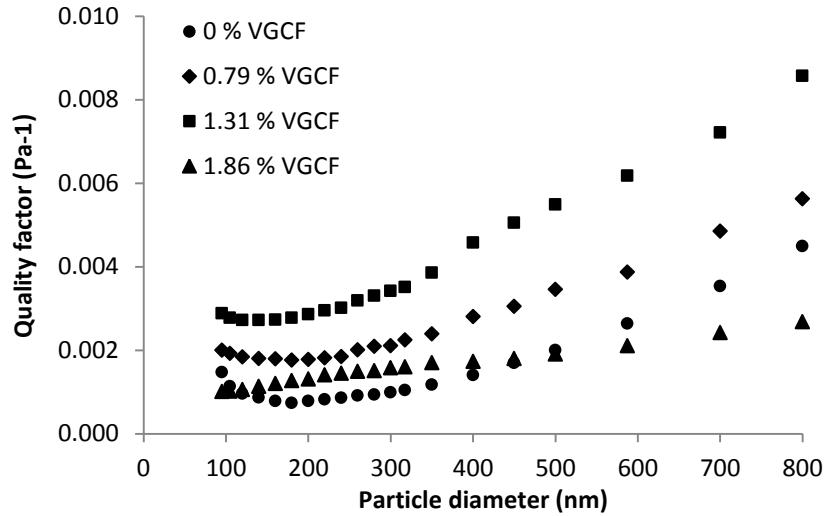


Figure V-5 Comparison of quality factor of different VGCF nonwoven media (Data reported at face velocity of 50 cm/s)

Figure V-5 demonstrates that filtration performance doesn't increase all the way with VGCF volume fraction. From 0 % to 1.31 % VGCF, QF has significant improvement. The reason is that the increase of filtration efficiency has compensated the increase of pressure drop for VGCF from 0 % to 1.31 %. However, when VGCF continued to increase to 1.86 %, QF decreases and for some particle sizes, QF was even lower than 0 % VGCF. This is because the pressure drop increases almost 10 times and the huge increase of pressure drop negated the effect of filtration efficiency improvement. Therefore, there is an optimal point of VGCF fraction that has the largest quality factor. And for this bi-component polyester fiber media, best VGCF fraction should be around 1.31 %. Overall, from Table V-5, we can see that after entrap VGCF, filtration performance for salt particle is enhanced. They can be concluded into three reasons. The first reason is because of the nano-scale fiber diameter. Secondly, it is due to the change of conventional non-slip flow to slip flow, resulting in less air flow resistance [V.16]. The Knudsen number is usually applied to describe the importance of molecular movements of air molecules at the fiber surface to the overall flow field. The Knudsen number is defined as:

$$Kn = \frac{\lambda}{r_f} \quad (\text{Eq V.4})$$

Where λ is the gas mean free path and r_f is the radius of the fiber. When Kn is greater than 0.1, we can generally consider it slip flow. Since the mean free path for air is about 0.066 microns, fibers with diameters smaller than 0.5 microns should be considered to have significant slip flow effect. In the slip flow, the air velocity at the fiber surface can be considered to be non-zero, which leads to smaller air drag force on fibers compared to non-slip flow. Due to the smaller drag force, slip flow has lower pressure drop. Thirdly, slip flow makes air flowing much closer to fiber surface, which could lead to more particles traveling near the fiber, resulting in higher filtration efficiencies [V.17]. Thus, nanofibers could improve filtration efficiency without significantly increase pressure drop. And what can be concluded is that after entrapping VGCF into nonwoven polymer media, filtration efficiency is improved without a significant increase of pressure drop across the filter media.

Table V-5 Average quality factor of four different VGCF nonwoven media

	Average quality factor (Pa⁻¹)
0% VGCF	0.00146
0.79% VGCF	0.00256
1.31% VGCF	0.00399
1.86% VGCF	0.00157

V.3.2 Carbon nanotube (CNT) enhanced nonwoven filter media

Carbon nanotubes (CNT) have been increasingly applied in environmental applications because of their significantly smaller fiber diameter, high surface area and adsorption capability [V.18]. CNTs are allotropes of carbon with a cylindrical nanostructure. Nanotubes are categorized as single-walled nanotubes (SWNTs) and multi-walled nanotubes (MWNTs), which have been constructed with length-to-diameter ratio of up to 28,000,000:1. Carbon nanotubes

share many similarities with carbon nanofibers. They are produced using the same techniques, are both hollow and their diameter sizes are at the nano-scale level. When it comes to the differences, their size, morphology, processing techniques are prices vary from each other. The diameter of the fibers of CNT ranges from 1 to 30 nm. However, carbon nanofibers come with diameters of 100 to 200 nm, which are much larger than nanotubes [V.19].

In this work, MWNTs, which are provided by Nano Tech Labs Inc, were used and tested for nonwoven filtration media performance. Due to the greater magnitude of Van der Waals force caused by their significantly smaller diameters, the filter media fabrication is more difficult and complicated. Thus, special dispersion method is needed. Sonication is chosen here to effectively disperse carbon nanotubes by using ultrasonic bath from Fisher Scientific. Different amounts of MWNTs were dispersed in water using sonication for 20 to 40 mins. The dispersion was then filtered by a vacuum pump onto the substrate, which is nonwoven polymer media manufactured previously. The filters coated by carbon nanotube were dried in oven at 70°C to 100°C for one hour [V.18, V.20-21].

After all the steps above, fabricated CNT filters (Table III-6) were tested at two different face velocities, 10 cm/s and 50 cm/s, during dry air condition (2-3% RH). The filtration efficiency results were shown in Figure V-6.

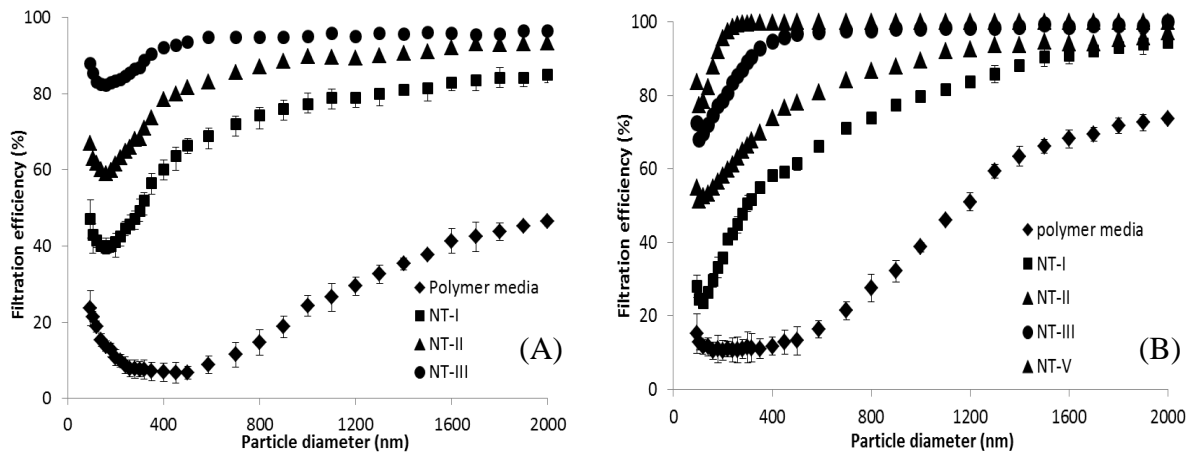


Figure V-6 Filtration efficiency curves of CNT filters at different face velocities: A) 10 cm/s and B) 50 cm/s

Table V-6 Weight and coverage of carbon nanotubes used for different CNT filter media

	Weight of CNT added (g)	Coverage of CNT (mg/cm²)
NT-I	0.001	0.068
NT-II	0.003	0.205
NT-III	0.005	0.341
NT-IV	0.010	0.684
NT-V	0.020	1.367
Polymer media	0.000	0.000

Figure V-6 indicates that higher coverage of carbon nanotube leads to greater filtration efficiency, which is due to effect of much smaller diameter size (nano-scale). For particles between 100 to 400 nm (MPPS), filters coated with CNT have a significant improvement of collection efficiency. Take 400 nm as an example. For polymer media without coated with carbon nanotube, the efficiency is only 6.87%. When coated with CNT, even for the lowest coverage, the efficiency increases to 60.19%, which is almost 55% higher. For filter coated with largest coverage of CNT, the efficiency for 400 nm particle goes up to 96.89%. However, after coated with CNT, the pressure drop of filters increased as well. Table V-7 and Figure V-7 below show the overall filtration efficiency, pressure drop and calculated quality factor for CNT filters with different coverage tested at 10 cm/s face velocity.

Table V-7 Experimental results of different CNT coverage filter media

	Thickness (mm)	Filtration efficiency for d_p=400 nm (%)	Pressure drop at 10cm/s (Pa)	Quality factor for d_p=400 nm (Pa⁻¹)
NT-I	0.70	60.19	261.45	0.00352
NT-II	0.70	78.48	547.80	0.00280
NT-III	0.75	92.18	996.08	0.00256
NT-IV	0.80	96.89	1887.33	0.00184
Polymer media-I	0.70	6.87	34.86	0.00204
Polymer media-II	6.89	55.48	323.70	0.00249

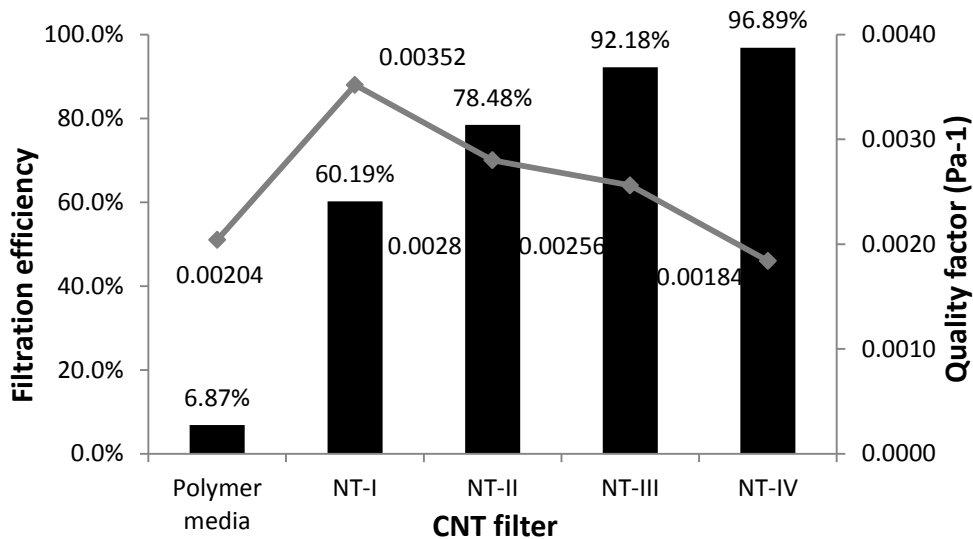


Figure V-7 Comparison results of filtration efficiency and quality factors for different coverage CNT filter media (Data reported at face velocity of 50 cm/s)

As shown in Figure V-7 and Table V-7, even if the pressure drop increased for filters coated with carbon nanotube, the quality factor of CNT filters are still higher compared to polymer media filter. The reason for this is carbon nanotubes could significantly improve particles collection efficiency without causing large increase of pressure drop due to the slip-flow of air stream. With the higher CNT coverage, quality factor decreased because the higher pressure drop negated the effect of the increase of filtration efficiency. When CNT coverage goes up to 0.684 mg/cm², the quality factor is even smaller compared to polymer media filter due to extremely increased pressure drop. But overall, after coating carbon nanotubes on nonwoven polymer media filter, the filtration performance is significantly enhanced. In addition, since filtration efficiency usually increases with pressure drop, in order to eliminate the effect of pressure drop, a series of ten nonwoven polymer media, which has total pressure drop that is equivalent to carbon nanotube coated filter (NT-I) were also tested at the same air conditions. As shown in the

Table, the quality factor of the series of polymer media is smaller compared to other carbon nanotube coated filter, including NT-I, which indicates that the observed difference in filter efficiency can be directly attributed to the novel properties of carbon nanotube.

Since it can be seen from Figure that NT-I has the largest quality factor compared to other CNT coated filters, different series of NT-I filters were tested as well for further understanding. The results are shown in Figure V-8 and Table V-8.

Table V-8 Experimental results of different layers of NT-I filter media

	Thickness (mm)	Filtration efficiency for $d_p=400\text{nm}$ (%)	Pressure drop at 10cm/s (Pa)	Quality factor for $d_p=400\text{nm}$ (Pa^{-1})
NT-I	0.7	60.19	261.45	0.00352
2 layers of NT-I	1.4	88.67	512.90	0.00425
3 layers of NT-I	2.1	95.48	747.24	0.00414
4 layers of NT-I	2.8	97.63	958.65	0.00391

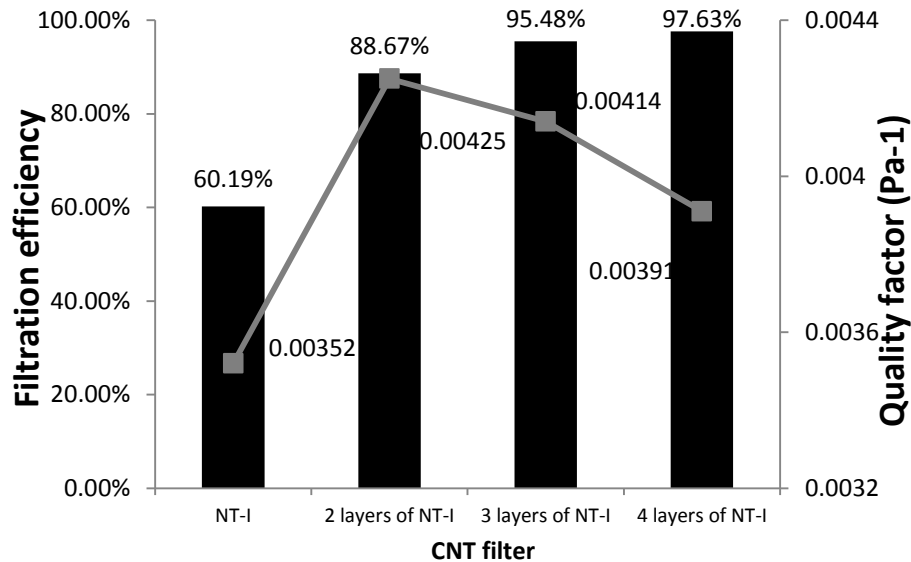


Figure V-8 Comparison results of filtration efficiency and quality factors for different layers of NT-I filter media (Data reported at face velocity of 50 cm/s)

As shown in Figure V-8 and Table V-8, all different series of NT-I filters showed much greater quality factors than only one layer of NT-I, which indicates they have significantly better filtration performance for salt particles. The reason might be due to the higher filter thickness

after stack several layers together without significantly increased pressure drop. Each layer of media could be considered as a single filter to remove salt particles. However, the filter performance didn't improve with the increasing of layers of filter series. It is because that the filtration efficiency didn't increase much compared to the increase of pressure drop, which negated the filtration efficiency effect. Thus, there is a maximum count of layers that shows best filtration performance for salt particles. What is shown in Figure V-8 indicates that 2 layers of NT-I filter gives the best performance due to significantly improved filtration efficiency. In a word, what we can conclude is that carbon nanotube can be applied to nonwoven filter media in order to enhance the air particles filtration performance.

However, economic factor is also very significant when it is considered to be applied in real circumstances. Thus, the estimation of total cost of carbon nanofiber (VGCF) and carbon nanotube (CNT) are calculated and the results are shown in Table V-9. In the calculation, coverage of both two nano-materials is based on an overall filter efficiency of 80% and weight of material needed is calculated on commercial 24'' by 24'' flat filter. From the results, what can be seen is that for each commercial flat filter, cost of carbon nanofiber is much less than carbon nanotube. Therefore, carbon nanofiber is much more economical compared to carbon nanotube when they are considered to be applied in salt particles filtration.

Table V-9 Comparison of cost of VGCF and CNT needed for commercial filter

	Coverage of materials (mg/cm ²)	Cost (\$ per g)	Weight of nano-materials needed (g)	Total cost (\$)
Carbon nanofiber (VGCF)	2.747	0.39	10.25	4.0
Carbon nanotube (CNT)	0.137	20	0.505	10.1

V.3.3 Particles loading performance of various nonwoven filter media

Particles loading capacity is a very important parameter that needs to be considered for evaluation of filtration performance [V.22]. With salt particles deposited into the filter media, filtration performance may change gradually, including both filtration efficiency and pressure drop across the media. Therefore, loading of particles should be investigated as well. Particles loading capacity is defined as the quantity of contaminant filter media can trap and hold before the maximum allowable back pressure or pressure drop is reached. Particles loading capacity is strongly related to life time of filter media, which is a significant character during filter media design [V.23]. Higher particles loading capacity results in longer useful life time and increasing the life time of filter media is the most crucial element in reducing filtration costs. However, filter media with larger particles loading capacity always have lower particles removal efficiency. Therefore, an optimization can be developed according to both particles loading capacity and filtration efficiency.

Particles loading curve is used in this part of study as well and it is the nominal increase of pressure drop across the media vs total mass of deposited particles into the media. In order to achieve this curve, filtration efficiency tests and pressure drop measurements were both conducted. During salt particles loading process, pressure drop of media increased gradually with time and the value was recorded every 5 mins. According to filtration efficiency and inlet salt particle concentration, the number of salt particles entrapped by the filter media during 1 min can be calculated and as well as the total number of particles during 5 mins. The estimation method of mass of salt particles loaded is same to the one used in Chapter II [V.24-25].

Five different filter media were tested for salt particles loading capacity at same air conditions and the details of filter media are listed in Table V-10. Nylon 6 media is a commercial polymer nanofiber media manufactured by electrospinning technology. As shown in Figure V-9,

three different sections of curves exist, which indicates that they belong to three different categories of filtration. Three curves including two ACF filter media and polymer media are at the bottom section, which means they have lowest increase of pressure drop at same deposited mass of particles compared to other tested filter media. After entrapping VGCF into the polymer substrate, what can be seen is that the increase of pressure drop for the same mass loading becomes much higher. This can be explained by the addition of carbon nanofiber. Since nanofibers are able to collect and capture much more particles according to the various filtration mechanisms, the pressure drop across the filter media increases much faster compared to micro-scale filter media.

Table V-10 Details of five various nonwoven filter media

	Thickness (mm)	SVF of activated carbon fiber (% , cal.)	SVF of polyester fiber (% , cal.)	SVF of cellulose (% , cal.)	Voidage (% , cal.)
Nonwoven ACF-I	3.8	16.50	2.57	N/A	80.93
Nonwoven ACF-IV	3.4	18.44	2.87	1.09	77.60

	Thickness (mm)	Mass of VGCF (g)	Volume fraction of VGCF (%)	Volume fraction of polymer (%)	Voidage (% , cal.)
Polymer media	0.70	0	0	20.89	79.11
VGCF media	~1.30	0.5	1.31	10.99	87.70

Meanwhile, Nylon 6 media has shown the highest increase of pressure drop with same mass loading compared to all the other filter media tested. The reason is that Nylon 6 media belongs to surface filter media instead of depth filter media like other tested filter media. The difference between surface and depth filter media is that depth filter media has two filtration processes involved and only one for surface filter media. As for depth filter media, when air stream flows through, salt particles may be deposited inside the media first. And till the fibers inside the media cannot capture any particle, the particles may be further captured on the surface of media until the cake is formed. However for the surface filter media, when filtration starts, most of the particles are deposited on the surface of media immediately until cake is formed. Therefore, surface filter media

is much faster to be fully loaded by particles than depth filter media and due to this fact, surface media shows lower particles loading capacity and shorter filter media life time.

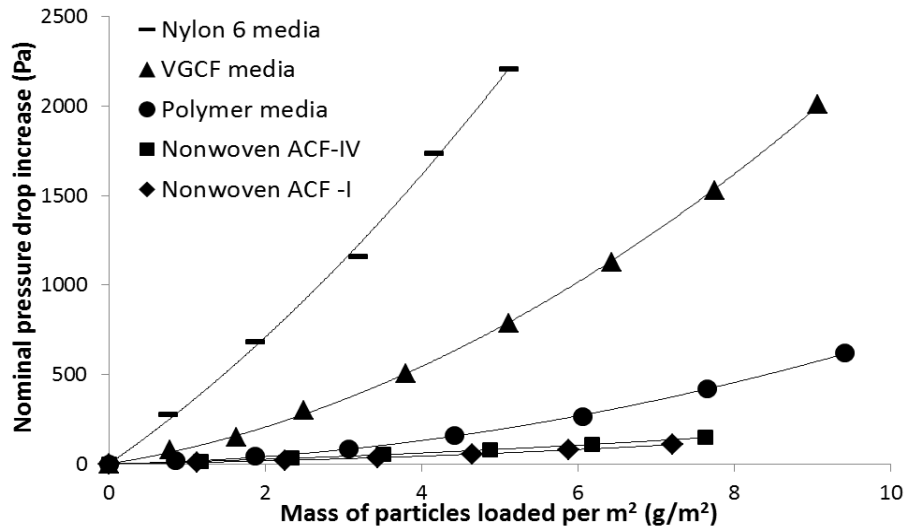


Figure V-9 Nominal increase of pressure drop with respect to deposited mass of salt particles for five various nonwoven filter media (Data reported for face velocity of 50 cm/s)

With particles loaded by the filter media, both pressure drop across the media and filtration efficiency are increased gradually. In order to investigate the evolution of the increase and judge if the filter media is good on the performance and suitable for real applications, a new term, quality factor (QF) [V.26-27] is defined to measure of whether an increase in pressure drop due to particles loading is warranted by the increase in filtration efficiency. It is calculated as the ratio of fractional capture per unit thickness to the pressure drop per unit thickness [V.28-29].

$$QF = \frac{\gamma}{\Delta P / t} = \frac{\gamma t}{\Delta P} = \frac{\ln(1/P)}{\Delta P} = -\frac{\ln(1-E)}{\Delta P} \quad (\text{Eq V.5})$$

According to the equation, what can be seen is larger of filtration efficiency and smaller of pressure drop leads to higher quality factor, which also suggests better performance of filter media. And from the equation, filtration efficiency plays a more significant role compared to pressure drop because of the logarithm.

Evolution of quality factor of various tested filter media with particles loading is calculated and presented in Figure. As shown in Figure V-10, Nylon 6 media has the largest initial quality factor compared to all other studied filter media, which is due to the nano layer on the surface of the filter media. At the beginning of the process when filter media is clean, Nylon 6 media is able to show highest filtration efficiency and largest pressure drop as well. However, according to the definition of quality factor, filtration efficiency is more dominant than pressure drop and therefore, the increase in filtration efficiency compensates the effect of increase in pressure drop for Nylon 6 media. When particles are loaded gradually, pressure drop across the media increases significantly due to the cake formation on the surface of media and thus, quality factor decreases with particles loaded. This suggests that the sudden increase in pressure drop negates the effect of increase in filtration efficiency with particles loaded. For polymer media entrapped with carbon nanofiber, evolution of quality factor has shown similar trend as Nylon 6 media due to the effect of nanofiber added. But due to the depth filtration, quality factor decreases slower compared to Nylon 6 filter media.

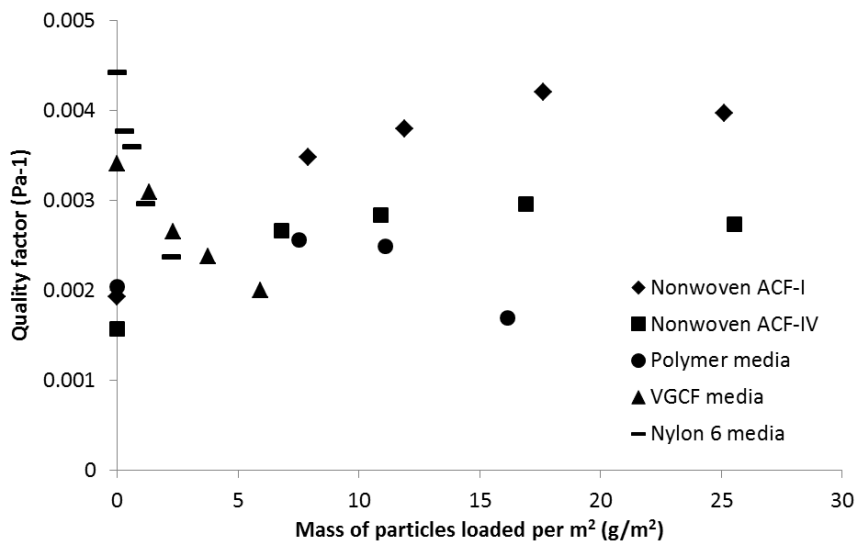


Figure V-10 Quality factor (cal.) with respect to deposited mass of salt particles for five various nonwoven filter media (Data reported for face velocity of 50 cm/s)

As for other three tested media, although they have much lower initial quality factors than other two nano-scale filter media, they have shown significantly higher quality factors when salt particles are loaded gradually. This can be explained by the fact that they have two filtration processes involved, depth and surface filtration, which is able to have much smaller increase of pressure drop at same mass of particles loaded. And it is consistent with what can be observed in previous particles loading curves. Moreover, since no nanofiber is added into the media, pressure drop increases much slower than nano-scale filter media. Therefore, what can be concluded is that nano-scale filter media including surface filter media have better filtration performance at the beginning but the performances decrease with particles loaded gradually. To the contrary, Micro-scale filter media including depth filter media have higher filtration performance when particles are loaded which also suggests that they are more suitable for applications that need longer filter lifetime with less replacements.

In order to further compare particles loading performance of various filter media, particles loading capacity and filter media lifetime were achieved as well. Assuming 4 inch water (996 Pa) is the maximum pressure drop that filter media can reach, the maximum mass of salt particles loaded can be calculated. Since the experimental salt particles concentration is 105 times larger than real concentration within ocean environment [V.2], the time for the filter media to reach the maximum pressure drop when they are applied to real sea environment should be 105 times longer. Moreover, with an average run time of 8 hours per day, the lifetime of these five different filter media are able to be estimated. As shown in Table V-11, two nonwoven ACF media and polymer media have much longer useful lifetime and higher particles loading capacity compared to VGCF and Nylon 6 media, which is consistent with the previous discussion that depth filter media and micro-scale filter media are superior at particles loading performance. Nylon 6 media has shown

the smallest capacity and shortest filter media lifetime, which indicates that surface filter media is not suitable for particles loading application.

Table V-11 Comparisons of particles loading capacity and filter media life time among various nonwoven filter media

	Initial pressure drop (Pa)	Final pressure drop (Pa)	Particles loading capacity (g/m²)	Filter media life time (Days)
Nonwoven ACF-I	280	996	21.52	40
Nonwoven ACF-IV	471	996	17.47	31
Polymer media	119	996	11.36	17
VGCF media	362	996	4.43	5
Nylon 6 media	425	996	1.65	2

V.3.4 Comparison of compressor parasitic power among various nonwoven filter media

In addition to particles loading capacity, compressor parasitic power is one of the major concerns as well because it is strongly related to SOFC system final power output, which demonstrates the performance and energy efficiency of SOFC. Usually, the lower filter pressure drop is, the less compressor parasitic power and the higher SOFC power output will be. The same equation as in Chapter II is applied in this part of work to estimate the compressor parasitic power, which is shown below:

$$P_B = \frac{\gamma}{\gamma - 1} \frac{0.371T_a}{\eta} q_o \left[\left(\frac{p_b}{p_a} \right)^{\frac{\gamma-1}{\gamma}} - 1 \right] \quad (\text{Eq V.6})$$

Where,

P_B is the power output (kW)

γ is the heat capacity ratio (1.4 for air)

T_a is the temperature of the gas entering the compressor (293 K)

p_a is the compressor inlet pressure, which depends on the pressure drop across the filter before the compressor

p_b is the compressor exit pressure, which is also inlet pressure of SOFC

η is the compressor efficiency (0.8)

q_o is the volume of gas compressed evaluated at 293 K and 1 atm pressure (m^3/s)

SOFC's performance needs to be assessed for the full pressure drop range of cathode air filter over its life, not just when the filter is new. Filter pressure drop will increase over the lifetime of the filter. If a filter is selected only based on the initial pressure drop, then the filter engineer can be expect a lower SOFC performance over the life of the filter or to be frequently changing filters in order to maintain the lower pressure drop required for normal SOFC performance. Therefore, it is very important to investigate compressor parasitic power when particles are loaded gradually. Estimation conditions and estimation results are listed in Table V-12 and Figure V-11, respectively.

Table V-12 Compressor parasitic power estimation conditions

Temperature (K)	293 (Room temperature)
Air flow rate (ft^3/min)	~395
Inlet salt particle concentration (ppmw)	4.0
Stoichiometric ratio (λ)	2
Average voltage (V_c)	0.6
SOFC power output (KW)	~190
SOFC inlet pressure (inch water)	814 (2 atm)

As shown in Figure V-11, five curves can be divided into two separate groups according to different trends. Nylon 6, VGCF media and polymer media have higher increase of compressor parasitic power than other two nonwoven ACF media due to the greater pressure drop increase

when particles are loaded, which can be explained by various fiber structure and fiber diameter. Among all tested media, Nylon 6 and VGCF have shown highest compressor parasitic power due to the nano-scale fiber in the media, which leads to lowest SOFC power output. Moreover, during three micro-scale media, two nonwoven ACF media have demonstrated larger compressor parasitic power than polymer media at initial particles loading stage. But when particles are loaded gradually, compressor parasitic power of polymer media is increasing significantly and exceeds that of nonwoven ACF media, which indicates that SOFC power output is lowering and SOFC system performance is decreasing. Therefore, what can be concluded is that in order to have best SOFC performance, nano-scale media is not a good option. To the contrary, nonwoven ACF filter media is potentially able to be more suitable for long term application, such as sea salt particles filtration.

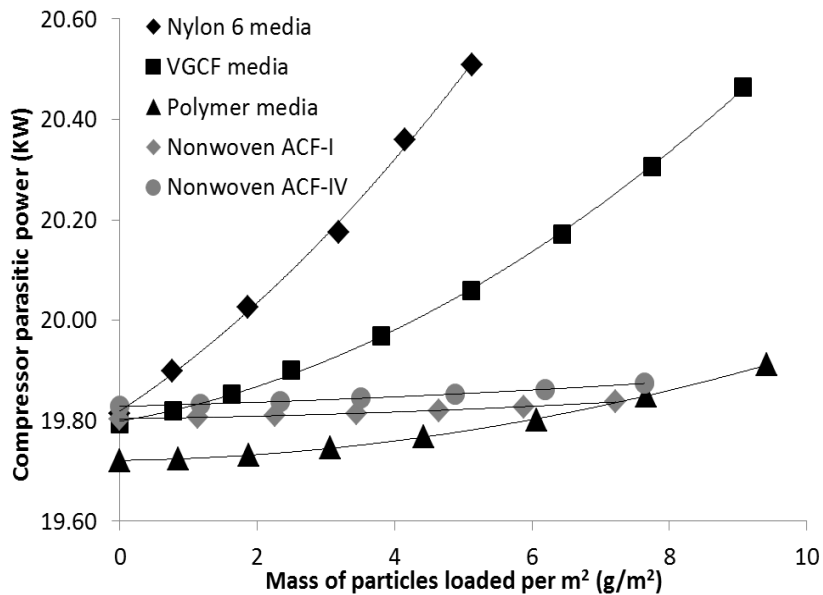


Figure V-11 Comparison of compressor parasitic power among various nonwoven filter media (nano and micro scale) (Data reported for face velocity of 50 cm/s)

V.3.5 Effect of relative humidity (RH) on hydrophobic filter media performance for salt particles

Relative humidity (RH) is an important air property that needs to be investigated for particulates filtration, especially for salt particles during ocean environment. Since relative humidity is extremely higher in the sea, the effect of RH on filtration for salt particles cannot be ignored [V.30-32]. RH is the ratio of the partial pressure of water vapor in an air-water mixture to the saturated vapor pressure of water at a prescribed temperature. It is potentially able to affect the filtration performance of filter media, including both pressure drop and filtration efficiency. Sodium chloride (NaCl) particles belong to hydrophilic particles with deliquescent point of 75% and when RH is above it, particles become saturated as liquid particles (droplets). Therefore, in order to fully understand the RH effect on filtration performance, three RHs (0%, 30%, 50%) below the deliquescent point and one RH (80%) above the deliquescent point were selected for this relative humidity study.

V.3.4.1 Nickel fiber media

As for nickel fiber (metal fiber), it belongs to hydrophobic material. Two nickel media samples were tested at four different RHs with 50 cm/s face velocity. Measured media thickness, solid volume fraction and voidage calculated based on thickness are shown in Table V-13.

Table V-13 Characteristics of two sample media tested

	Diameter	Mass of Ni	Thickness	SVF	Voidage
Ni-Media 1	8 micron	15 g	0.8 mm	7.09 %	92.91 %
Ni-Media 2	8 micron	10 g	0.6 mm	6.30 %	93.70 %

The experimental results for the two samples are shown in Figure V-12 (A) and (B).

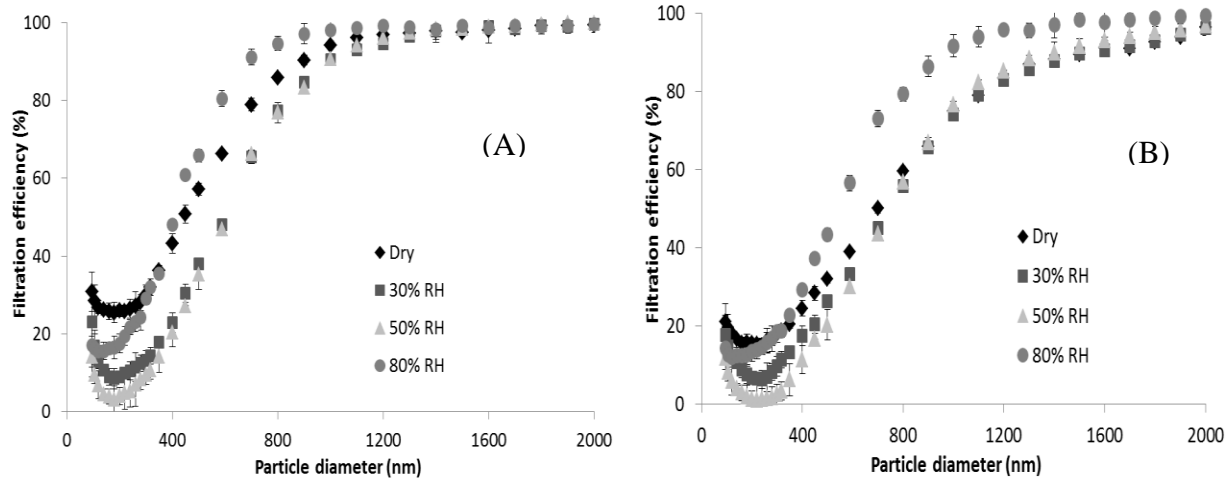


Figure V-12 Filtration efficiency curves of Ni-Media 1 (A), Ni-Media 2 (B) at different relative humidities (RHs) (Data reported for face velocity of 50 cm/s)

As shown in Figure V-12, below sodium chloride deliquescent point, increasing RH could significantly decrease the filtration efficiency for most particle sizes (smaller than 1400 nm). The reason for this might be that water collects on the fiber surface and the droplets occupy the space making some fibers unavailable for collection of particles when increasing the relative humidity. When RH goes up to 80 %, the trend is different since the filtration mechanism could change for droplets. For small particles (less than 400 nm), filtration efficiency is decreased a little bit and for large particles, efficiency is significantly improved compared to dry condition. The reason for this case is firstly because the salt particles are in form of wet particles at that high RH and they can start filling up interstitial spaces between the fibers, which causes less particles passing through the filter media [V.33]. Second reason is due to almost twice bigger particle size of salt at 80% RH, which makes filtration efficiency higher. But for very small particles, the slight efficiency decrease may be because smaller particles are much more difficult to become droplets compared to larger particles, which causes some smaller salt particles to remain as dry particles and at the same time due to space occupied by water droplets, the filtration efficiency of small

particles is decreased compared to dry air condition. However, the efficiency for small particles at 80% RH is still higher than that at 30% and 50%. Figure V- 13 shows the filtration efficiency of both two nickel media samples at four different RHs, taking 200 nm particle size as an example.

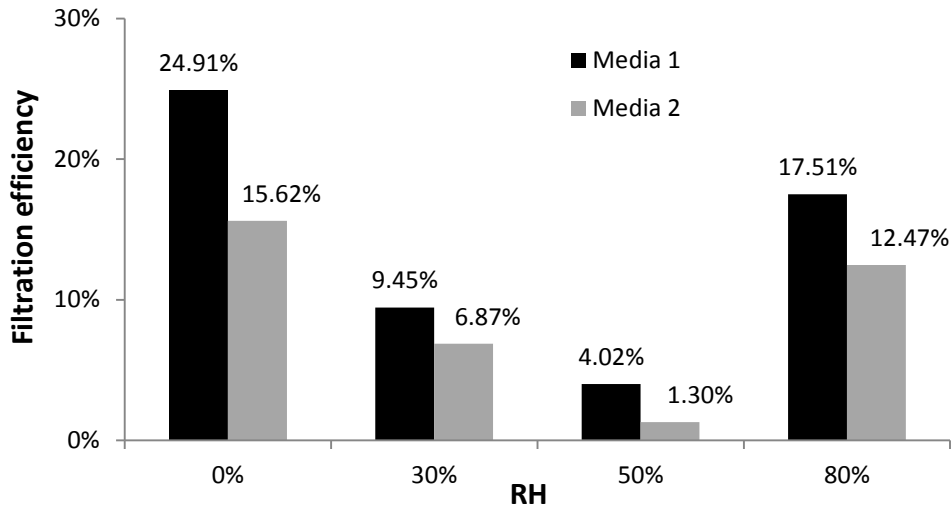


Figure V-13 Filtration efficiency of 200 nm particle of two tested nickel media at various RHs (Data reported at face velocity of 50 cm/s)

V.3.4.2 Polymer fiber media

Polymer fiber used in this work is bi-component polyester fiber, which is hydrophobic in nature and easy for drying. As for polymer fiber media, two different types of experiments were carried out for RH effect study. First one is the same as nickel fiber discussed previously, passing different RH air stream through the filter media. The second one is to keep the filter media in humid air stream for several hours and then tested the filtration efficiency by passing dry air through. The results are shown in Figure V-14 (A) and (B).

Table V-14 Details of polymer sample media tested

	Fiber diameter	Thickness	SVF	Voidage
Polymer fiber	13 micron	1.1 mm	22.16 %	77.84%

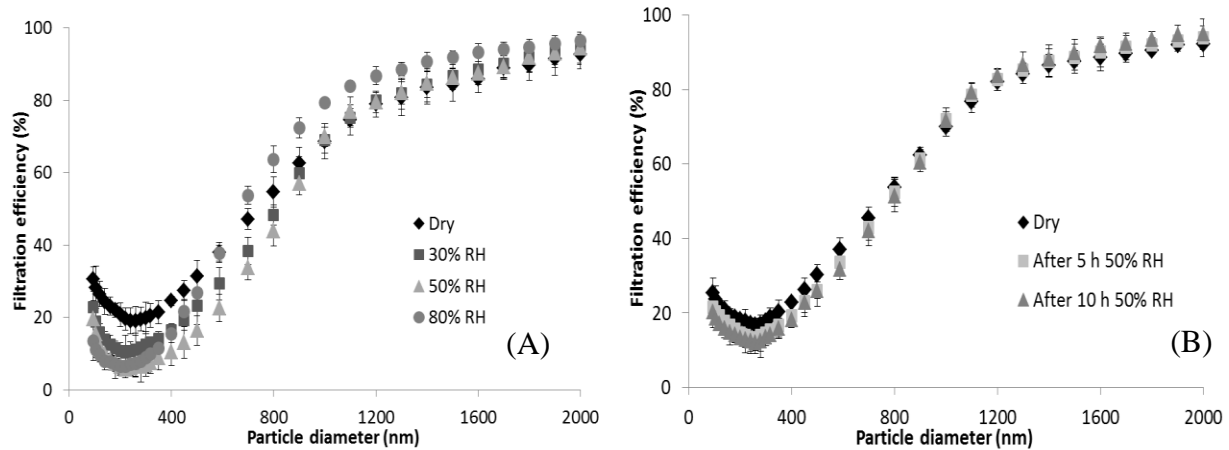


Figure V-14 (A) Filtration efficiency curves of polymer media at various RHs, (B) Filtration efficiency curves of polymer media after RH pretreatment (Data reported for face velocity of 50 cm/s)

As shown in Figure V-14 (A), polymer fiber media has the same trends as Ni fiber media. Below deliquescent point of sodium chloride, higher relative humidity leads to much lower filtration efficiency, which is due to the occupation of fiber space by water droplets. The efficiency decreased from 19.93% to 6.93% when RH increased to 50%, using 300 nm particle as an example.

When RH increased to 80% (above deliquescent point), the filtration efficiency got improved for large particles (> 500 nm) due to the phase change from solid particles to liquid droplets, and for smaller particles, the efficiency decreased due to the same reason as 30% RH and 50% RH, which is caused by less interstitial fiber spaces for particles collection.

Second experiment results are shown in Figure V-14 (B). As can be seen, after 5 h and 10 h pretreatment in humid air condition, filtration efficiency decreased a little for particles smaller than 1000 nm compared to polymer media without pre-treatment. However, the decrease is much less than the first experiment, which is directly passing through humid air [V.34]. Using 300 nm particle as an example, the decrease is about 3-5 % for second case and 13 % for first case.

Figure V-15 shows the comparison of filtration efficiency decrease under different circumstances. Therefore, what we can conclude is that humid air condition could decrease polymer media filtration efficiency for most particle sizes and directly passing through humid air has more significant effect compared to pre-treatment in humid air for hours.

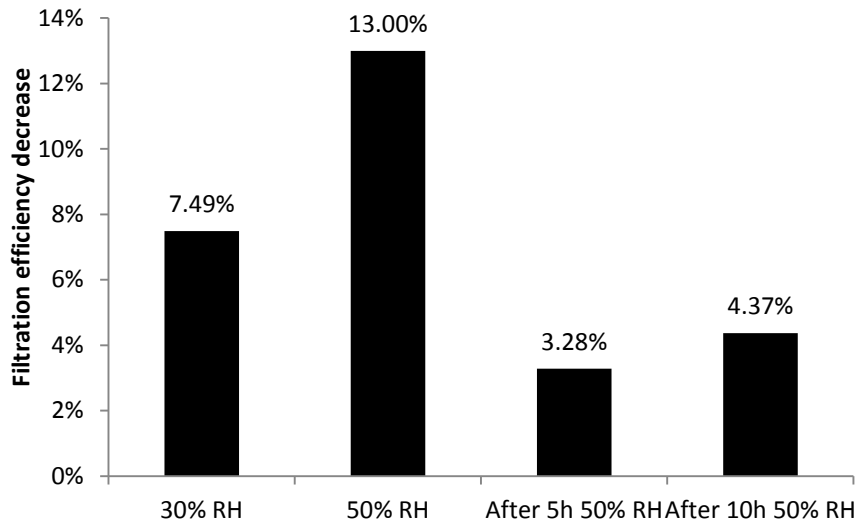


Figure V-15 Filtration efficiency degradation under different RHs and pretreatments (Data reported at face velocity of 50 cm/s)

Thus, from the experiment results above, two different types of hydrophobic material, nickel fiber and polymer fiber, could both be affected by relative humidity (RH) in air stream for sea salt particles filtration, which indicates RH is an important factor that needs to be evaluated during filter media design, especially for sea salt particles.

V.4 Conclusion

In this part of work, nonwoven filter media is the main concern for sea salt particles filtration study. Various nonwoven filter media were tested and evaluated according to their filtration performance, including pressure drop across the filter media, filtration efficiency and particles loading capacity. A new type of three dimensional nonwoven media, vapor grown

carbon nanofiber (VGCF) enhanced polymer media, was manufactured using wet-laid method and the filtration performance was tested. The results have shown that after distributing VGCF into polymer media, both filtration efficiency and pressure drop were increased due to the nano-scale fiber diameter. But the increase of pressure drop was not significant compared to the increase of filtration efficiency because of the slip-flow on nanofiber surface. Thus, the overall quality factor of polymer media with VGCF was much higher, which indicated that adding VGCF into nonwoven polymer media is able to enhance the filtration performance for salt particles. Besides, there is an optimum point of VGCF fraction existed, which could lead to maximum media filtration performance.

Moreover, several different nonwoven filter media were compared in terms of particles loading performance, including VGCF entrapped polymer media, activated carbon fiber media and Nylon 6 media, which is a polymer nanofiber media. From the experiment results, surface filter media, such as media substrate covered by a layer of Nylon 6 nanofiber, has shown much higher initial filtration performance. But it also gives smaller particles loading capacity and higher increase of pressure drop compared to other depth filter media. Evolution of quality factor has also revealed that surface filter media became much worse to remove particles when particles were loaded gradually which can be attributed to the cake formation on the filter media surface. For depth filter media, such as VGCF media, both particles loading capacity and evolution of quality have shown severe degradations after entrapping carbon nanofiber. This revealed that although nanofiber could enhance initial filtration performance, it had deleterious effect on long term particles loading performance because of the nano-scale diameter. Therefore, what can be concluded is that if initial filtration performance is the main concern, nanofiber media could be

much better and more suitable. However, if during certain applications, long term filtration performance is more important, thus depth filter media could be considered as a better choice.

This part of work also shows that relative humidity (RH) has significant effect on filtration performance of hydrophobic filter media for sea salt particles. Below 75% RH, deliquescent point of sodium chloride, higher RH could decrease filtration efficiency due to the occupation of fiber space by water droplets. High relative humidity (80% RH) can cause a decrease in filtration efficiency for small particles by diffusion but an increase in filtration efficiency for large particles by inertial impaction.

V.5 References:

- [V.1] Wilcox, M., Baldwin, R., Hernandez, A. G. and Brun, K. (April 2010). Guideline for Gas Turbine Inlet Air Filtration Systems Gas Machinery Research Council Southwest Research Institute.
- [V.2] Majchrzak, R., Cole, T. and Cervi, M. (1998). U.S. Navy Sea Salt Particle Removal Systems, Carderock Division Naval Surface Warfare Center.
- [V.3] Payet, S., Boulaud, D., Madelaine, G. and Renoux, A. (1992). Penetration and Pressure-drop of A HEPA Filter During Loading with Submicron Liquid Particles. *Journal of Aerosol Science* 23:723-735.
- [V.4] Karwa, A. N. (2012). Aerosol Filtration Performance of Novel 3-Dimensional Nonwoven Composites, in Department of Chemical Engineering, Auburn University.
- [V.5] Kim, G. T., Ahn, Y. C. and Lee, J. K. (2008). Characteristic of Nylon 6 Nanofiber for Removing Ultra Fine Particles. *Korean J. Chem. Eng* 25:368-372.
- [V.6] Park, H. S. and Park, Y. O. (2005). Filtration Properties of electrospun Ultrafine Fiber Webs. *Korean J. Chem. Eng* 22:165-172.
- [V.7] Karwa, A. N. and Tatarchuk, B. J. (2012b). Aerosol filtration enhancement using carbon nanostructures synthesized within a sintered nickel microfibrinous matrix. *Separation and Purification Technology* 87:84-94.
- [V.8] ASHRAE 52.2 (1992). Method of Testing General Ventilation Air-cleaning Devices Used for Removal Efficiency by Particle Size, American National Standard, Atlanta, GA, USA.
- [V.9] K. Kosmider and J. Scott (2002). Polymeric nanofibres exhibit an enhanced air filtration performance, *Filtr.+Sep.* 39:20-22.

- [V.10] Q. Zhang, J. Welch, H. Park, C.-Y. Wu, W. Sigmund, J.C.M. Marijnissen (2010). Improvement in nanofiber filtration by multiple thin layers of nanofiber mats, *J. Aerosol Sci.* 41:230-236.
- [V.11] A. Podgorski, A. Balazy, L. Gradon (2006). Application of nanofibers to improve the filtration efficiency of the most penetrating aerosol particles in fibrous filters, *Chem. Eng. Sci.* 61:6804-6815.
- [V.12] F. Dotti, A. Varesano, A. Montarsolo, A. Aluigi, C. Tonin, G. Mazzuchetti (2007). Electrospun porous mats for high efficiency filtration, *J. Ind. Text.* 37:151-162.
- [V.13] C. Shin, G.G. Chase, D.H. Reneker (2005). Recycled expanded polystyrene nanofibers applied in filter media, *Colloid Surface A* 262:211-215.
- [V.14] M.G. Hajra, K. Mehta, G.G. Chase (2003). Effects of humidity, temperature, and nanofibers on drop coalescence in glass fiber media, *Sep. Pur. Tech.* 30:79-88.
- [V.15] K. Yoon, K. Kim, X. Wang, D. Fang, B.S. Hsiao, B. Chu (2006). High flux ultrafiltration membranes based on electrospun nanofibrous PAN scaffolds and chitosan coating, *Polymer* 47:2434-2441.
- [V.16] Bazargan, A. M., Keyanpour-rad, M., Hesari, F. A. and Ganji, M. E. (2011). A study on the microfiltration behavior of self-supporting electrospun nanofibrous membrane in water using an optical particle counter. *Desalination* 265:148-152.
- [V.17] Grafe, T. H. and Graham, K. M. (2003). Nanofiber Webs from Electrospinning, in *Nonwovens in Filtration- Fifth International Conference, Stuttgart, Germany.*
- [V.18] Viswanathan, G., Kane, D. B. and Lipowicz, P. J. (2004). High efficiency fine particulate filtration using carbon nanotube coatings. *Advanced Materials* 16:2045.
- [V.19] AZoNano (2013). Comparative Study of Carbon Nanotubes and Carbon Nanofibers.

- [V.20] Guan, T. J. and Yao, M. S. (2010). Use of carbon nanotube filter in removing bioaerosols. *Journal of Aerosol Science* 41: 611-620.
- [V.21] Brady-Estevez, A. S., Kang, S. and Elimelech, M. (2008). A single-walled-carbon-nanotube filter for removal of viral and bacterial pathogens. *Small* 4: 481-484.
- [V.22] National Air Filtration Association (2007). *NAFA Guide to Air Filtration*. National Air Filtration Association, Virginia Beach, VA 23471.
- [V.23] Stenhouse, J.I.T. and Trottier, R. (1991). The Loading of Fibrous Filters with Submicron Particles. *Journal of Aerosol Science* 22:777-780.
- [V.24] Zelenyuk, A., Cai, Y. and Imre, D. (2006). From Agglomerates of Spheres to Irregularly Shaped Particles: Determination of Dynamic Shape Factors from Measurements of Mobility and Vacuum Aerodynamic Diameters. *Aerosol Science and Technology* 40: 197-217.
- [V.25] Thomas, D., Penicot, P., Contal, P., Leclerc, D. and Vendel, J. (2001). Clogging of fibrous filters by solid aerosol particles –Experimental and modeling study. *Chemical Engineering Science* 56:3549-3561.
- [V.26] Hinds, W. C. (1998). *Aerosol technology: Properties, Behavior, And Measurement of Airborne Particles*. John Wiley & Sons, Inc.
- [V.27] Moelter, W. and Fissan, H. (1998). Quality assurance of glass fiber filter media, in: Spurny, K. R. (Ed.). *Advances in Aerosol Filtration*. Lewis, 259-282.
- [V.28] Moelter, W. and Fissan, H. (1997). Structure of a high efficiency glass fiber filter medium. *Aerosol Science and Technology* 27:447-461.
- [V.29] Brown, R. C. (1993). Macroscopic behavior of filters, in: *Air Filtration - An Integrated Approach to the Theory and Application of Fibrous Filters*. Pergamon Press, 1-11.

- [V.30] Miguel, A. F. (2003). Effect of air humidity on the evolution of permeability and performance of a fibrous filter during loading with hygroscopic and non-hygroscopic particles. *Journal of Aerosol Science* 34:783-799.
- [V.31] Gupta, A., Novick, V. J., Biswas, P. and Monson, P. R. (1993). EFFECT OF HUMIDITY AND PARTICLE HYGROSCOPICITY ON THE MASS LOADING CAPACITY OF HIGH-EFFICIENCY PARTICULATE AIR (HEPA) FILTERS. *Aerosol Science and Technology* 19:94-107.
- [V.32] Newnum, J. D. (December 2010). The Effects of Relative Humidity on Respirator Performance, in *Occupational and Environmental Health*, University of Iowa.
- [V.33] Ranade, M.B. (1987). Adhesion and removal of fine particles on surfaces. *Aerosol Science and Technology* 7:161-176.
- [V.34] Moyer, E. S. and Stevens, G. A. (1989). "Worst Case" Aerosol Testing Parameters: II. Efficiency Dependence of Commercial Respirator Filters on Humidity Pretreatment. *American Industrial Hygiene Association* 50:265-270.

Chapter VI Conclusions and Recommendations for Future Work

VI.1 Conclusions

The studies in this dissertation have demonstrated, for the first time, the filtration performance of single pleated filter (24'' by 24'') in different configurations, including pleat counts and filter depths. Filtration efficiency, pressure drop across the filter, particles loading capacity and compressor parasitic power were all investigated in order to achieve the optimum filter performance. Moreover, a novel filter packaging configuration, MESA, which is developed by Center for Microfibrous Materials Manufacturing (CM³) in Auburn University has shown significantly superior filtration performance than single filters. For both particles loading capacity and compressor parasitic power, MESAs have shown better performances, which is able to increase filter lifetime and SOFC power output simultaneously. Therefore, MESAs have shown great potential to be applied in real filtration circumstances, like sea salt particles (SSP) filtration for on-board SOFC systems.

Filter media is another important parameter that is investigated in this dissertation. After comparisons between nonwoven and woven activated carbon fiber (ACF) filter media, nonwoven ACF media has shown much higher filtration performance for salt particles, including longer useful lifetime and lower air flow resistance, which indicates they are more suitable and economical when used as filter media. A class of uniform three dimensional nonwoven polymer filter media entrapped with carbon nanofiber was developed as depth media to be used for salt

particles filtration. Experiment results have shown higher filtration efficiency and lower pressure drop of this type of media, which is good for particulates filtration. But lower particles loading capacity and shorter useful lifetime makes it unsuitable as particles filter media because of greater costs. Thus, depending on the different filtration requirements, this three dimensional nanofiber distributed nonwoven polymer media has some potential to be applied when initial filtration performance is the major concern.

During the ocean environment, relative humidity (RH) is very significant and cannot be ignored. Effect of relative humidity (RH) in this dissertation has shown that RH could affect filtration performance of different filter media. Hydrophobic material is able to decrease the filtration efficiency and hydrophilic media could enhance the filtration efficiency due to the pore structures. Therefore, in order to improve the removal of sea salt particles for on-board SOFCs, hydrophilic material, such as activated carbon fiber (ACF) media, could be considered to replace those hydrophobic media.

Semi-empirical models have been developed and modified for estimating the pressure drop across the filter media, particle removal efficiency and particles loading capacity, which were verified very accurate with experimental data. This part of work has resulted in a powerful tool to predict the filtration performance of all various filter media, which is quite significant during future filtration study.

VI.2 Recommendations for Future work

On board SOFCs are widely being considered to be applied as power source due to the high energy efficiency and power output, which is driving the cathode air filtration market growing faster, especially sea salt particles filtration. Two main aspects exist in filtration study, one is

filter packaging design and the other one is filter media design. The recommendation for future work centers on filter media design, which has great potential to have further development.

VI.2.1 Carbon nanofiber synthesized within woven ACF filter media via CCVD method

From experimental results achieved in this dissertation, what we can conclude is that nanofiber entrapped filter media is able to increase salt particles removal efficiency. However, at the same time, pressure drop across the filter media increases as well, which leads to shorter filter media life time and higher compressor parasitic power. Meanwhile, it has been shown that nonwoven filter media have better filtration performance compared to woven filter media, including particles removal efficiency, pressure drop and particles loading capacity, which is due to the homogeneous pore structure. Therefore, in order to enhance filtration efficiency without large increase of pressure drop and transform woven media into nonwoven media at the same time, carbon nanofiber synthesis with woven activated carbon fiber (ACF) media can be a new approach. By this method, filtration efficiency could be improved due to smaller (carbon nanofiber) fiber diameter and slip flow on nanofiber surface without increasing pressure drop. Moreover, changing from inhomogeneous pore structure (woven) into homogeneous structure (nonwoven) leads to higher particles loading capacity and longer filter media life time. The unique mechanical, thermal and electrical properties combined with chemical inertness and a high surface area make carbon nanofibers a very attractive material for an increasing number of applications, including reinforcement in media composites and air particulate filters.

For most of the applications, it is desirable to grow the carbon nanofibers directly onto the substrate with good adhesion. Therefore, catalytic chemical vapor deposition (CCVD) is applied in this work since it allows the direct growth of carbon nanofiber on a surface. CCVD method is a chemical process used to produce high-purity, high performance solid materials, like carbon nanofiber. Gas-phase hydrocarbon molecules are decomposed at high temperature and carbon is

deposited in the presence of a transition metal catalyst on a substrate where subsequent growth of the fiber around the catalyst particles occurs. In general, CVD process contains separate stages, including gas decomposition, carbon deposition, nanofiber growth and purification. The synthesized carbon nanofiber diameter depends on the catalyst size. Usually, acetylene, ethylene, methane are the most commonly used hydrocarbon gases and iron, nickel, cobalt are used as catalysts. Woven activated carbon fiber (ACF) media is selected as substrate in this work because of its highly porous structure (high surface area and pore volume), which can make catalyst preparation process easier and better (uniform dispersion of catalyst on substrate).

VI.2.2 VGCF entrapped nonwoven ACF filter media via ultra-sonication

As discussed previously in this dissertation, nonwoven filter media have significantly higher filtration performance compared to woven filter media due to the homogeneous pore structure. VGCF (carbon nanofiber) can enhance filter media performance because of the nano-scale fiber diameter and not extremely increased pressure drop due to air slip flow. Meanwhile, due to the highly porous structure of activated carbon fiber, they belong to hydrophilic material which is able to absorb water into the pores. During the high relative humidity (RH) environment, such as ocean environment, ACF can entrap and capture much more particles compared to other hydrophobic material due to the increased capillary tension between particles and fiber pores. Therefore, according to the experimental results achieved, a novel type of filter material can be developed by combining VGCF and nonwoven ACF media together. Besides, due to the nano-scale diameter of VGCFs and strong Van Der Waals force between fibers, the dispersion of VGCF clumps is very important to the filtration performance of filter media and via ultra-sonication, VGCF could be dispersed more completely in water and then is able to distributed into nonwoven ACF media more evenly, which leads to higher filtration performance for salt particles.

VI.2.3 CFD (Computational fluid dynamics) modeling of filtration performance of pleated filters

Since the pleat geometry can significantly affect the filtration performance of filter, including filtration efficiency, pressure drop and particles loading capacity, CFD (computational fluid dynamics) can be applied to simulate the air flow with challenging particles into the pleated filters and calculate filtration efficiency and pressure drop of filters in various pleat geometries. Moreover, CFD is very efficient in modeling particles deposition of filters, which could be used to measure particles loading capacity and useful lifetime of filters. Usually, fluent code from CFD is applied to model the air flow pattern in pleated filters.

Appendix : Nomenclature

E = Filtration efficiency

E_{Σ} = Total single fiber collection efficiency

α = Fiber packing fraction

t = Filter media thickness

R = Fiber radius

E_D = Diffusion efficiency

E_R = Interception efficiency

E_I = Inertial impaction efficiency

Stk = Stokes number

Ku = Kuwabara number

Kn_f = Knudsen number

Pe = Peclet number

D = coefficient of Brownian diffusion

λ = gas mean free path

d_p = Particle diameter

d_f = fiber diameter

U = Face velocity of air stream

ΔP = Pressure drop

A, B = Darcy's constants

K_G = Coefficient of grating

K_C = Coefficient of contraction

K_E = Coefficient of expansion

K_P = Coefficient of pleat

K_S = Coefficient of slot

QF = Quality factor

A = Filter media area

M = Mass of particles loaded

μ = Air viscosity

v = Air velocity

ρ = Gas density (Kg/m^3)

Φ = Shape factor of fiber

θ = Flow path angle

L = Filter media thickness

C_f = Coefficient of friction

C_D = Coefficient of drag

C_{FD} = Coefficient of form drag

c = Fiber solid fraction

T = Temperature (K)

$\tau = (2+c)/c$

$X_{fd} = (1-c)^2/12c$

RMS = Root mean square

P_B = Power output (kW)

Γ = Heat capacity ratio (1.4 for air)

T_a = Temperature of the gas entering the compressor (293 K)

p_a = Compressor inlet pressure

p_b = Compressor exit pressure

η = Compressor efficiency (0.8)

q_o = Volume of gas compressed evaluated at 293 K and 1 atm pressure (m^3/s)

K_m = Media permeability (mm^2)